UCSF
UC San Francisco Electronic Theses and Dissertations

Title
Coordinate synthesis and export of lipid virulence factors in Mycobacterium tuberculosis

Permalink
https://escholarship.org/uc/item/1q59q1dq

Author
Jain, Madhulika

Publication Date
2006

Peer reviewed|Thesis/dissertation

eScholarship.org Powered by the California Digital Library
University of California

Coordinate Synthesis and Export of Lipid Virulence Factors in *M. tuberculosis*

by

Madhulika Jain

DISSERTATION

Submitted in partial satisfaction of the requirements for the degree of

DOCTOR OF PHILOSOPHY

in

Biochemistry and Molecular Biology

in the

GRADUATE DIVISION

of the

UNIVERSITY OF CALIFORNIA, SAN FRANCISCO

[redacted]

Date University Librarian

Degree Conferred: ....

copyright

Madhulika Jain

2006

ACKNOWLEDGEMENTS

I thank Jeff for guiding me and sharing his enthusiasm for science with me every day for the last few years. I've learned a tremendous number of techniques during my time in the Cox Lab thanks to Jeff's intrepid intellectual leadership. Jeff's scientific creativity is limitless and I am deeply grateful to him for guiding me in becoming a strong and independent scientist. I also want to thank Jeff for the hours, days and weeks that he spent writing my papers with me. I thank Jeff for his support in all my endeavors both in graduate school and outside. In this, Jeff is joined by Karen, his wife, who has supported the lab strongly ever since its inception.

I deeply thank my thesis committee members, Sandy Johnson, Anita Sil, and Carol Gross. They devoted time, energy, and great thought to my project, my development as a graduate student, and at the end towards my post-doctoral job search. I took all their suggestions very seriously, and have benefitted greatly from their vision. They truly represent all that is best about the Tetrad graduate program.

I especially want to thank Anita Sil who is a pillar of the pathogenesis community at UCSF – her lab and our lab have had joint group meetings for years and she not only advised me as a part of my thesis committee, but also every month at group meetings, and forums such as pathogenesis research talks.

I also want to thank Hiten Madhani for advising me on my projects as well as during the review process for my papers. His generous help and advice in all matters have contributed significantly to my development as a scientist.

I am especially indebted to Sarah Stanley for being my friend and supporting me through all the ups and downs of graduate school. Sarah is an extremely talented experimentalist and I benefitted greatly from her advice and thoughtfulness in all of my projects. I thank Scott Converse, Jason Macgurn and Sridharan Raghavan for their help, insight and wonderful humor. I thank Justin Skoble for advising me and for devoting tremendous energy towards my scientific development.

The second half of my graduate career was the result of a very fruitful collaboration with Christopher Petzold and Mike Leavell in Julie Leary's lab at UC Davis and Joseph Mougous and Mike Schelle in Carolyn Bertozzi's lab at UC Berkeley. I deeply thank all my collaborators for helping me learn new techniques and for their advice on my projects.

I can never thank my classmate Maria Enquist-Newman enough for all her encouragement and support throughout graduate school, for reading drafts of every proposal and paper I wrote, and for listening to an endless number of practice talks. I have also been extremely lucky to have Brian Margolin, Cecile de la Cruz and Dan Levy as my cheering squad in all my efforts – they provided critical feedback on my projects and at countless practice talks.

I was very fortunate to have the support of the Howard Hughes Medical Foundation for my graduate research. Their financial support greatly facilitated my graduate career.

I would like to thank my parents, Uma and Amitabh, for supporting me throughout graduate school and making every endeavor as easy for me as they could.

I want to thank Ben, my husband, best friend, and soulmate, who makes me extremely happy and has supported me in more ways than I thought possible.

The text of Chapter 2 is largely a reprint of the material as it appears in "Interaction between polyketide synthase and transporter suggests coupled synthesis and export of virulence lipid in *M. tuberculosis*" Jain, M., Cox, J.S. PLoS Pathogens September 2005; 1(1):e2.

ABSTRACT

Coordinate Synthesis and Export of Lipid Virulence Factors in *M. tuberculosis*

Madhulika Jain

Mycobacterium tuberculosis is a highly successful human pathogen and is estimated to infect 2 billion people worldwide, resulting in about 2 million deaths per year. *M. tuberculosis* synthesizes and secretes a wide array of lipid virulence factors that are central to its pathogenesis. Several of these lipids are associated with the cell wall and are surface-exposed. These surface-exposed polyketide lipids are important in modulating the host immune system as well as for protection from host radicals. The overall goal of the work presented here is to better understand the synthesis, export and regulation of these virulence lipids. The first part of this thesis describes the coordinate synthesis and transport of a critical surface-exposed lipid virulence factor, phthiocerol dimycocerosate (PDIM). PDIM is synthesized by a large number of enzymes including PpsE and transported to the cell wall via MmpL7. We show that PpsE interacts with MmpL7 suggesting coupled synthesis and export of PDIM. We propose that the synthesis and transport proteins form a complex that promotes efficient lipid export. The second part of this thesis describes a novel mechanism in which virulence polyketide synthesis is regulated by metabolite availability. Using a powerful mass spectrometric approach that simultaneously monitors hundreds of lipids, we found that the production of two lipid virulence factors, PDIM and sulfolipid-1 (SL-1), are coupled and co-regulated by the concentration of a common metabolite, methyl malonyl CoA. Consistent with this view, increased levels of methyl malonyl CoA led to increased abundance and mass of both

PDIM and SL-1. Furthermore, perturbation of methyl malonyl CoA metabolism led to attenuation of the bacteria in mice. *M. tuberculosis* likely grows on host lipids during infection suggesting that methyl malonyl CoA production by the bacteria is high in vivo due to either increased flux through the citric acid cycle or the catabolism of odd-chain fatty acids. Interestingly, PDIM is produced in high mass forms during infection suggesting that, indeed, high levels of methyl malonyl CoA exist in vivo. We propose that growth of *M. tuberculosis* on fatty acids during infection leads to increased flux of methyl malonyl CoA through lipid biosynthetic pathways, resulting in increased virulence lipid synthesis during infection.

Jeffery S. Cox November 1, 2006

TABLE OF CONTENTS

Chapter 1

Introduction.. 1

Chapter 2

Interaction between polyketide synthase and transporter suggests coupled synthesis and export of virulence lipid in *M. tuberculosis*....................... 7

Chapter 3

Lipidomics reveals post-transcriptional control of *M. tuberculosis* virulence lipid synthesis via direct metabolic coupling... 58

Chapter 4

Conclusions and Perspectives... 125

References.. 132

LIST OF FIGURES AND TABLES

Chapter 2

Figure 1 26
Figure 2 29
Figure 3 32
Figure 4 36
Figure 5 40
Figure 6 43
Figure 7 47
Figure 8 49
Figure 9 53
Table 1 55
Table 2 57

Chapter 3

Figure 1 81
Figure 2 84
Figure 3 88
Figure 4 90
Figure 5 94
Figure 6 98
Figure 7 104
Figure 8 111
Figure 9 113
Figure 10 115
Figure 11 117
Figure 12 121
Table 1 124

Chapter 1

Introduction

Mycobacterium tuberculosis has an extraordinary ability to resist the immune mechanisms of the host. Tuberculosis remains a tremendous global health burden as it causes over 2 million deaths per year, and it is estimated that approximately one third of the world is infected (McKinney et al., 1998). *M. tuberculosis* is transmitted aerogenically and is engulfed by alveolar macrophages in the terminal air spaces of the lung. From here, the bacteria employ a number of strategies to evade the microbicidal mechanisms of the macrophage and are able to replicate intracellularly and disseminate to other organs of the host.

It has long been appreciated that the mycobacterial cell wall and its associated lipids are likely important for the pathogenesis of *M. tuberculosis* (Brennan and Nikaido, 1995; Glickman and Jacobs, 2001). In addition to a peptidoglycan layer beyond its cell membrane, *M. tuberculosis* has a formidable cell wall comprising arabinogalactan molecules esterified to long chain ($C_{50\text{-}70}$) acids termed mycolic acids (Brennan and Nikaido, 1995). The frontline drug against tuberculosis, isoniazid, inhibits mycolic acid synthesis (Banerjee et al., 1994). Associated with the cell wall are a number of surface-exposed lipids that have historically been implicated in virulence. Genes involved in the synthesis and export of these surface-exposed lipids have recently been shown to be required for growth and virulence in mice, rigorously demonstrating their requirement for *M. tuberculosis* pathogenesis (Camacho et al., 1999; Cox et al., 1999).

Two of these surface-exposed lipids, phthiocerol dimycocerosate (PDIM) and sulfolipid-1 (SL-1), have been extensively studied historically and recently for their role in virulence. Both lipids are synthesized by specialized polyketide synthases that elongate straight chain fatty acids by the stepwise addition of a variety of short acyl chains. PDIM, which consists of two mycocerosic acids esterified to phthiocerol, is the product of two such polyketide synthase systems. Mas synthesizes methyl branched mycocerosic acids through successive additions of methyl malonyl CoA (Azad et al., 1996; Minnikin et al., 2002; Trivedi et al., 2005) while PpsA-E synthesize phthiocerol (Azad et al., 1997). The protein MmpL7 has been shown to be required for the export of PDIM to the outer leaflet of the cell wall (Cox et al., 1999).

A number of PDIM synthesis and export genes were found in a signature tagged transposon mutagenesis (STM) screen for *M. tuberculosis* mutants that are attenuated for virulence (Camacho et al., 1999; Cox et al., 1999). This genetic screen consisted of pooled infections of 48 mutants that were each uniquely identifiable by a DNA tag, permitting the screening of hundreds of mutants in a mouse model. Mutants in several of the genes required for PDIM synthesis and export were subsequently also shown to be attenuated in clonal infections of mice. PDIM has also been shown to be an important component of the cell wall for providing a physical barrier to host-induced damage as well as for altering the immune response of the host. PDIM mutants are more sensitive to SDS, have altered cytokine profiles in macrophages and elicit less reactive nitrogen species (Camacho et al., 2001; Reed et al., 2004; Rousseau et al., 2004).

SL-1 consists of trehalose-2-sulfate esterified to three molecules of phthioceranic or hydroxy-phthioceranic acids and one straight chain fatty acid, palmitate or stearate (Goren, 1970; Goren et al., 1971). Phthioceranic and hydroxy-phthioceranic acids contain multiple methyl branches which are incorporated by the polyketide synthase Pks2 (Sirakova et al., 2001). MmpL8 is also required for the complete synthesis of SL-1 and a biosynthetic precursor, SL_{1278}, accumulates in *mmpL8*⁻ cells (Converse et al., 2003). Furthermore, mutants in MmpL8 are attenuated in a mouse model of infection.

SL-1 has been well studied historically due to a correlation between its presence in the cell wall and virulence (Goren et al., 1974). Surprisingly however, *pks2*⁻ cells which do not make either SL-1 or SL-1278 have wild-type bacterial growth in vivo apparently negating a role for SL-1 in virulence (Converse et al., 2003). One hypothesis to reconcile the disparate *mmpL8*⁻ and *pks2*⁻ phenotypes is that MmpL8 may function to transport an as yet unidentified substrate required for virulence. Alternatively, the attenuated virulence of the *mmpL8*⁻ mutant could also be due to the build-up of SL-1278, as SL-1278 has been shown to be a CD1b ligand and T-cell clones that specifically recognize SL-1278 have been found. SL-1278 specific T-cells are able to recognize *M. tuberculosis* infected cells and kill intracellular bacteria (Gilleron et al., 2004). Virulence studies with an *mmpL8*/*pks2* double knockout would distinguish between these two possibilities. Importantly, however, *pks2*⁻ cells have only been tested for growth in vivo at 6 weeks and virulence or bacterial numbers at late timepoints close to mortality have not been tested in a mouse model of infection. It may be that *pks2*⁻ mutants are indeed attenuated, implying a role for SL-1 in virulence.

The role of MmpL7 in PDIM transport and MmpL8 in SL-1 synthesis prompt speculation that MmpL (mycobacterial membrane protein large) proteins in general may play a role in virulence lipid synthesis and export. Indeed, several of the 13 members of the MmpL family of proteins in *M. tuberculosis* have been implicated in virulence (Domenech et al., 2005). MmpLs are themselves a part of the larger family of RND (resistance, nodulation and division) proteins that have a myriad of functions in other organisms (Tseng et al., 1999). A number of MmpL genes are also genomically organized proximally to lipid synthesis and modification genes lending further support to the idea that MmpLs play a role in lipid synthesis or transport. Indeed, MmpL7 is organized near the PDIM biosynthetic genes in the genome. Genomic organization of MmpL8 has also proven to be significant as MmpL8 is downstream of the gene *pks2*.

Interestingly, there is specificity in MmpL mediated transport. Aside from PDIM export, MmpL7 does not appear to have any other lipid associated defects and secretes other surface-exposed lipids similarly to wild-type. Conversely, other MmpL mutants are able to transport PDIM like wild-type cells (Converse et al., 2003). It is therefore also possible that MmpLs are adapters that interface with a separate lipid export machinery to promote specificity in lipid transport.

A central question in the understanding of surface-exposed virulence lipids is how these lipids are exported to the outer leaflet of the cell wall. In the first part of this thesis, I show that MmpL7 interacts with PpsE, an enzyme required for the synthesis of PDIM and suggest that MmpL7 may act to couple synthesis and secretion of PDIM. Thus, MmpLs may in fact act as scaffolds for the assembly of polyketide synthetic machinery thereby promoting the synthesis and export of their specific lipid substrates.

In the second part of the thesis, I employ a mass-spectrometric approach that simultaneously monitors hundreds of lipid species to identify novel differences in lipid synthesis and export under different conditions. Using this method, we made the interesting discovery that the production of PDIM and SL-1 is coupled and co-regulated by the concentration of the common precursor, methyl malonyl CoA and that this

Chapter 2

Interaction between polyketide synthase and transporter suggests coupled synthesis and export of virulence lipid in *M. tuberculosis*

Abstract

Virulent mycobacteria utilize surface-exposed polyketides to interact with host cells but the mechanism by which these hydrophobic molecules are transported across the cell envelope to the surface of the bacteria is poorly understood. Phthiocerol dimycocerosate (PDIM), a surface-exposed polyketide lipid necessary for *Mycobacterium tuberculosis* virulence, is the product of several polyketide synthases including PpsE. Transport of PDIM requires MmpL7, a member of the MmpL family of RND permeases. Here we show that a domain of MmpL7 biochemically interacts with PpsE, the first report of an interaction between a biosynthetic enzyme and its cognate transporter. Over-expression of the interaction domain of MmpL7 acts as a dominant negative to PDIM synthesis by poisoning the interaction between synthase and transporter. This suggests that MmpL7 acts in complex with the synthesis machinery to efficiently transport PDIM across the cell membrane. Coordination of synthesis and transport may not only be a feature of MmpL-mediated transport in *M. tuberculosis*, but may also represent a general mechanism of polyketide export in many different microorganisms.

Introduction

Mycobacterium tuberculosis, the causative agent of tuberculosis, has an extraordinary ability to resist the bactericidal mechanisms of the human immune system (McKinney et al., 1998). The integrity of the complex mycobacterial cell wall and its associated lipids has long been thought to be important for virulence (Brennan and Nikaido, 1995; Chan et al., 1991; Glickman and Jacobs, 2001; Goren et al., 1974; Ng et al., 2000). This complex lipid metabolism is reflected in the enormous capacity of *M. tuberculosis* for polyketide lipid synthesis as there are at least 24 different polyketide synthases and numerous lipid modification enzymes encoded in its genome (Cole et al., 1998). Recent evidence has shown that surface-exposed polyketides, associated with the outer leaflet of the cell wall, are central to the pathogenesis of *M. tuberculosis* (Camacho et al., 1999; Converse et al., 2003; Cox et al., 1999; Domenech et al., 2004). Genes involved in the synthesis and transport of these polyketides are required for growth and virulence in mice. Furthermore, these lipids have been shown to provide both a direct physical barrier to host induced damage (Camacho et al., 2001) as well as to modulate the immune response to infection by altering cytokine profiles in macrophages (Rao et al., 2005; Reed et al., 2004; Rousseau et al., 2004).

Many of the surface-exposed polyketides in *M. tuberculosis* require active transport from their site of synthesis in the cytoplasmic membrane to the cell surface. Unfortunately, little is known about the mechanism of polyketide secretion. MmpL7, a member of the MmpL (mycobacterial membrane protein large) family of proteins in *M. tuberculosis*, was the first MmpL shown to be required for the transport of a specific polyketide, phthiocerol dimycocerosate (PDIM) to the cell surface (Cox et al., 1999). A number of genes involved in PDIM biogenesis have also been identified (Azad et al., 1997; Azad et al., 1996; Onwueme et al., 2004) and the biosynthetic pathway is shown in a schematic in Figure 1A. The Pps A-E gene products extend straight chain fatty acids to phthiocerol and the Mas enzyme catalyzes the addition of methyl branches to synthesize mycocerosic acids (Azad et al., 1997; Azad et al., 1996; Trivedi et al., 2005). The enzymes FadD26 and FadD28 are thought to be AMP ligases which activate straight chain fatty acids for transfer to the Pps and Mas enzymes (Trivedi et al., 2004). Finally, both MmpL7 and DrrC are required for transport of PDIM to the cell surface (Camacho et al., 1999; Cox et al., 1999). MmpL8, another MmpL family member, has been shown to be required for the biogenesis and transport of sulfolipid (SL-1) (Converse et al., 2003; Domenech et al., 2004). Given the apparent specificity in MmpL-mediated transport, it is likely that the other eleven MmpL proteins encoded by the *M. tuberculosis* genome transport specific lipids that may be involved in bacterial virulence.

MmpLs belong to a broader class of proteins termed RND (resistance, nodulation and cell division) permeases (Tseng et al., 1999). MmpL7, like most RND transporters, is predicted to contain twelve transmembrane (TM) domains with two non-transmembrane domains between TM #1 and #2 (domain 1) and between TM #7 and #8 (domain 2) (Figure 1B). The structure of AcrB, a well studied RND transporter involved in multidrug efflux in *Escherichia coli*, has been determined and its non-transmembrane domains have been localized to the periplasm (Murakami et al., 2002; Yu et al., 2003). AcrB interacts with an outer membrane protein, TolC, to expel a variety of drugs from the cytoplasmic membrane across the entire cell wall (Tikhonova and Zgurskaya, 2004; Touze et al., 2004). Since MmpLs are similar in predicted topology to RND permeases, and are required for the transport of cytoplasmic polyketide substrates, we reasoned that they may also interact with other proteins that are involved in the transport of lipids to the cell surface. To better understand the transport of PDIM to the outer leaflet of the cell wall, we probed for interactors of MmpL7. Surprisingly, we found an interaction between MmpL7-domain 2 and the PDIM synthetic enzyme PpsE that is required for the final step of phthiocerol synthesis. Because PpsE acts in the cytoplasm, where PDIM is synthesized, the interaction suggests that MmpL7-domain 2 is accessible to the cytoplasm. We propose that MmpL7 acts as a scaffold to recruit PDIM synthetic machinery, forming a complex that coordinates lipid synthesis and transport.

Results

Identification of MmpL7-PpsE interaction

To determine the mechanism of PDIM transport to the surface of *M. tuberculosis* bacilli, we first sought to identify components that interact with the two large non-transmembrane domains of MmpL7 using a yeast two-hybrid approach (Figure 1B) (Golemis et al., 1999). We created two "bait" constructs to express either an MmpL7-domain 1 or an MmpL7-domain 2 fusion with the LexA DNA binding protein in yeast. Although MmpL7-domain 1 activated transcription of both the *LEU2* and *lacZ* yeast reporters on its own, MmpL7-domain 2 expression did not auto-activate the reporters (Figure 2A, B) and thus was suitable for screening an *M. tuberculosis* genomic "prey" library for interactors. We identified positive library clones by selecting for growth on media lacking leucine followed by blue-white screening on plates containing X-gal. Out of the 16 million clones screened, we obtained about 2000 positive interactors on media lacking leucine. Out of these 2000 interactors, we tested 1000 by blue-white screening and obtained over 500 positive clones, out of which we sequenced 136. A list of the gene fragments that yielded good sequence and that were also in the correct orientation in the prey plasmid is included in Table 2.

Surprisingly, our screen identified an interaction between MmpL7-domain 2 and a 373 amino acid fragment of PpsE, the enzyme required for the final step of phthiocerol synthesis (Figure 2). A number of reasons suggest that the interaction between MmpL7-domain 2 and PpsE is meaningful. First, PpsE was one of the strongest interactors identified in the screen as judged by blue color on indicator plates as well as quantitative β-galactosidase assays (>100X over controls, Figure 2B). Second, the interaction between MmpL7-domain 2 and PpsE is specific as PpsE did not interact with either LexA alone or with domain 2 of the homologous transporter, MmpL8 (Figure 2A, B). Western blot analysis using anti-LexA antibodies indicated that the MmpL8-domain 2 and MmpL7-domain 2 baits were expressed at equivalent levels (data not shown). Finally, as PpsE is required for the synthesis of PDIM and MmpL7 is required for the transport of PDIM (Cox et al., 1999), the interaction between PpsE and MmpL7 suggested the intriguing possibility that PDIM synthesis and transport are coupled.

To confirm the interaction between MmpL7-domain 2 and PpsE *in vitro* and test its role *in vivo*, we first sought to generate a mutant MmpL7-domain 2 that does not interact with PpsE. We used a reverse yeast two-hybrid approach (Bennett et al., 2004) to identify single amino acid changes in MmpL7-domain 2 that disrupt its interaction with PpsE . We engineered our original MmpL7-domain 2 bait vector to include a C-terminal GFP fusion to easily avoid mutations that resulted in protein truncations. We randomly mutagenized MmpL7-domain 2 using error prone PCR, introduced these constructs into yeast cells bearing the PpsE prey plasmid, and screened for colonies that were both white on X-gal indicator plates and GFP positive. Colonies with the desired phenotype were isolated and the bait plasmids were recovered, re-tested, and sequenced. Interestingly, of the 12 plasmids that contained mutations that led to single amino acid changes in MmpL7-domain 2, 9 clustered in a 50 amino acid region of the protein (Figure 3A). Eight of the mutations led to substitutions with Proline or Glycine which are more likely to be structurally disruptive and possibly lead to global unfolding of the protein. The four remaining mutants, W571R, Y594H, Y594C, and I611S (amino acid numbers correspond to positions in full-length MmpL7) were reconstituted into the original bait vector lacking GFP and assayed for interaction both on X-gal plates and by liquid β-galactosidase assays (Figure 3B). Western blot analysis confirmed that these changes did not lead to differences in protein levels (data not shown). Since the I611S mutation is the most conservative mutation and leads to a large reduction in the interaction with PpsE, this mutant was chosen for subsequent analysis.

MmpL7-domain 2 interacts with PpsE *in vitro*

To independently test the interaction between MmpL7-domain 2 and PpsE identified in the two-hybrid screen, we performed *in vitro* GST pulldown experiments (Figure 3C). Glutathione agarose beads coated with MmpL7-domain 2 GST fusion protein were incubated with lysates from *M. smegmatis* cells expressing full-length, myc tagged PpsE. PpsE interacted with MmpL7-domain 2 coated beads but not with beads containing only GST protein (lanes 2 and 3). Furthermore, the I611S mutation led to drastically reduced binding with PpsE (lane 4). Coomassie staining of proteins eluted from the beads demonstrated that equal amounts of MmpL7-domain 2 and the I611S mutant protein were present during the pulldown (data not shown). Importantly, while the I611S mutation has a large effect on PpsE binding, we consistently observed low-level residual binding both by GST pulldown and yeast two-hybrid assays. Taken together, our results demonstrate that MmpL7-domain 2 can specifically interact with PpsE *in vitro*.

MmpL7-domain 2 inhibits PDIM synthesis *in vivo*

We next sought to determine whether the interaction between MmpL7 and PpsE occurs *in vivo*. Since MmpL7 is an integral membrane protein and PpsE is most likely present in the cytoplasm, we reasoned that MmpL7-domain 2 must be accessible to the cytoplasm in order to interact with PpsE. Over-expression of MmpL7-domain 2 in the cytoplasm would then act as a dominant negative by titrating PpsE away from endogenous full-length MmpL7.

To this end we expressed MmpL7-domain 2 in the cytoplasm of wild-type cells, under the control of the constitutive *groEL2* promoter. To assay PDIM synthesis and transport, we labeled cells with ^{14}C-propionate (which is incorporated into PDIM) and extracted surface-exposed lipids from the cell wall. In this procedure, radioactively labeled cells were resuspended in hexanes and then harvested by centrifugation to yield a supernatant fraction (S) that contained surface-exposed lipids, and a pellet fraction (P) that contained the remaining total lipids associated with the cell. Lipids from both fractions were extracted and separated by thin layer chromatography (TLC) in order to resolve PDIM (Figure 4A). As expected, in wild-type cells PDIM was present in both the pellet and supernatant fractions (lanes 1 and 2) demonstrating that PDIM is both synthesized and transported. In a PDIM synthesis mutant, *fadD28*$^-$, PDIM was absent from both fractions (lanes 3 and 4), whereas in the PDIM transport mutant, *mmpL7*$^-$, PDIM was present only in the pellet fraction (lanes 5 and 6). Interestingly, over-expression of MmpL7-domain 2 in wild-type cells resulted in >98% inhibition of PDIM synthesis (Figure 4A, lanes 7 and 8). Although over-expression of MmpL7-domain 2 did not cause any growth defects (data not shown), it was possible that it had a non-specific effect on lipid synthesis. To confirm that over-expression of MmpL7-domain 2 specifically inhibits PDIM synthesis, we monitored SL-1, which like PDIM also incorporates propionic acid, in the same extracts and observed no differences in SL-1 synthesis or transport (Figure 4A).

The effect on PDIM synthesis was surprising, as *mmpL7*$^-$ cells are still able to synthesize PDIM; thus a simple prediction would have been that a dominant negative form of MmpL7 would inhibit PDIM transport not synthesis. Although the mechanism of the dominant negative effect of domain 2 is unclear, the specific effect of MmpL7-domain 2 on PDIM synthesis, in addition to its specific interaction with PpsE, suggests that MmpL7-domain 2 interacts with PpsE *in vivo*.

To test whether the dominant negative effect of MmpL7-domain 2 on PDIM synthesis is indeed due to its interaction with PpsE, we over-expressed the I611S mutant form that fails to interact with PpsE. The I611S mutation was generated in the MmpL7-domain 2 over-expression construct and introduced into wild-type *M. tuberculosis* cells. Although MmpL7-domain 2 I611S was expressed at similar levels to the wild-type version, it was unable to inhibit PDIM synthesis to the same extent (Figure 4B). PDIM synthesis in this strain was approximately 50% of wild-type, consistent with the severely reduced, but not completely abolished, interaction of the I611S mutant MmpL7-domain 2 with PpsE. This result strongly suggests that MmpL7-domain 2 inhibits PDIM synthesis via direct inhibition of PpsE.

We reasoned that if MmpL7 interacts with PpsE *in vivo* to coordinately synthesize and transport PDIM, then an MmpL7 mutant that does not interact with PpsE may be defective for PDIM transport. To test this we introduced the I611S change in the context of full-length MmpL7 and expressed the wild-type and mutant forms of MmpL7 in an *mmpL7*$^-$ strain. We found that both forms were able to complement the PDIM transport defect (Figure 4C, lanes 8 and 10). We also tested the mutant form of MmpL7 for subtle defects in PDIM transport as well as increased sensitivity to SDS and found no difference between the wild-type and mutant forms of MmpL7 (data not shown). Therefore, although the I611S mutation led to decreased interaction between MmpL7-domain 2 and PpsE in earlier experiments, in the context of full-length protein this mutation alone was not sufficient to decrease MmpL7 activity *in vivo*. Although the reason is unclear, this could be because MmpL7 has multiple interactions with PpsE, and perhaps with other members of the PDIM synthesis and transport machinery, that compensate for this mutation.

Dominant negative effect of MmpL7-domain 2 requires MmpL7

A simple mechanism to account for the dominant-negative effect of MmpL7-domain 2 expression is that the protein interacts directly with PpsE in the cytoplasm in such a way as to render the synthase inactive. Alternatively, because other RND family members act as trimers (Murakami et al., 2002; Yu et al., 2003), it is possible that MmpL7-domain 2 may inhibit PpsE while in a complex with full-length MmpL7. To distinguish between these two possibilities, we tested whether the dominant-negative effect of MmpL7-domain 2 requires the presence of full-length MmpL7. Interestingly, expression of MmpL7-domain 2 in *mmpL7*$^-$ transposon mutant cells failed to inhibit PDIM synthesis (Figure 5A, lane 4). Because the transposon mutant may express fragments of MmpL7, we also created an *M. tuberculosis* strain in which the full *mmpL7* gene was removed (Figure 6). Like the transposon mutant, the Δ*mmpL7* strain was unable to transport PDIM (Figure 6C) and was insensitive to the dominant-negative effect of MmpL7-domain 2 expression (Figure 5A, lanes 5 and 6). Expression of MmpL7-domain 2 was similar in all three strains (Figure 5B, lanes 2-4). Therefore, this data demonstrates that the activity of cytoplasmically expressed MmpL7-domain 2 requires the presence of wild-type MmpL7. Taken together, our results suggest that MmpL7-domain 2 enters into a complex with endogenous MmpL7 that interacts with PpsE, trapping the synthase in an inactive state, thus inhibiting PDIM synthesis.

Sub-cellular localization of MmpL7 and PpsE.

To experimentally determine the sub-celullar localization of MmpL7 we heterologously expressed an HA-tagged version of MmpL7 in *M. smegmatis*. We performed sub-cellular fractionations and analyzed the fractions by SDS-PAGE and western blotting. We found that MmpL7 preferentially localizes to the membrane over the cytoplasm (Figure 7).

We also attempted to determine if PpsE is recruited to the membrane preferentially in *M. smegmatis* cells expressing MmpL7 as compared to cells that were not, but were unable to monitor a difference in membrane-associated levels of PpsE in the presence of absence of MmpL7 (data not shown). In either case, we found PpsE in both the membrane and cytoplasm fractions of the cells.

As a membrane control for MmpL7 we also introduced the membrane protein Snm4 which is required for the secretion of Esat6 (Stanley et al., 2003) along with PpsE into wild-type *M. smegmatis* cells. Curiously, we observed that this strain had significantly smaller membrane pellets as compared to wild-type cells, or wild-type cells expressing MmpL7 and PpsE, suggesting perhaps that expression of Snm4 destabilizes membranes.

Discussion

PDIM, like other polyketide lipids, is a key molecule in the pathogenesis of *M. tuberculosis*. In this study, we have identified a novel interaction between MmpL7, a protein required for PDIM transport, and PpsE, an enzyme required for PDIM synthesis. Over-expression of the interaction domain of MmpL7 causes a drastic defect in PDIM synthesis, suggesting that this domain interacts with PpsE *in vivo* and inhibits its activity. To our knowledge, this is the first report of an interaction between a synthetic enzyme and its cognate transporter. We propose that MmpL7 interacts with the PDIM synthetic machinery to form a complex that coordinately synthesizes and transports PDIM across the cell membrane (Figure 9).

Interestingly, the dominant negative effect of domain 2 on PDIM synthesis is dependent upon the presence of full-length MmpL7. This strongly suggests that domain 2 incorporates into a complex with endogenous MmpL7 and exerts its effect only in this context. Like AcrB, an RND transporter in *E. coli* (Murakami et al., 2002; Yu et al., 2003), MmpL7 may normally act as a trimer or a higher order oligomer, and a hybrid complex of full-length MmpL7 with domain 2 may trap PpsE in an inactive state.

Since MmpL7 is dispensable for PDIM production it is curious that expression of domain 2 inhibits PDIM synthesis. We propose a simple model to reconcile this paradox. In a stepwise process of efficiently coordinating PDIM synthesis and export, MmpL7 may possess both inhibitory and activating activity on PDIM synthesis. For example, domain 2 may act to inhibit PpsE activity until the entire PDIM synthesis-transport complex is assembled, at which point the inhibition is relieved. Thus, MmpL7-domain 2 may exert its dominant negative effect by stabilizing the inhibitory state of this complex. In the absence of MmpL7, however, there is no inhibition or activation of PDIM synthesis, therefore PDIM synthesis is unaffected. This model would also explain why the I611S mutation, when reconstituted into full-length MmpL7, has no apparent effect. If the isoleucine residue is important for inhibition of PpsE then the I611S mutation would not necessarily lead to a defect in PDIM synthesis or transport.

Since MmpL7 and AcrB share the defining features of RND transporters, it is tempting to draw parallels between the two proteins. Both contain twelve putative transmembrane helices with non-transmembrane loops between TM #1 and #2, and TM #7 and #8. In the crystal structure of AcrB, the non-transmembrane domains are predicted to be periplasmic (Murakami et al., 2002; Yu et al., 2003) and the transmembrane domains form a central cavity that is accessible to the cytoplasm. Transmembrane prediction algorithms (TMPred, TMHMM) suggest that the non-transmembrane domains of MmpL7 are also periplasmic although no experimental data exists to validate this prediction. Since the interaction domain of MmpL7 lies between TM #7 and #8, in order to interact with PpsE, it must be accessible to the cytoplasm. There are a number of ways in which this could occur. First, like the glutamate transporter, EAAT1 (Seal and Amara, 1998), the interaction domain of MmpL7 may be reentrant through the membrane and thus interact with PpsE. Alternatively, the PpsE protein may access the extracellular portion of MmpL7 via a central pore created by the MmpL7 transmembrane domains. Finally, since MmpLs and AcrB are distantly related members of the RND permease family, the structure of MmpL7 may differ from AcrB and the orientation of MmpL7 in the membrane may be such that domain 2 is located in the cytoplasm. Indeed, there are examples of evolutionarily-related transporters with opposite membrane topology (Saier, 2003).

Since there is specificity in MmpL-mediated transport, it is attractive to speculate that this specificity may be in part due to the interaction with the cognate transporter. There is evidence in both *E. coli* and *Pseudomonas aeruginosa* that when both the non-transmembrane regions of two different RND permeases with different drug efflux specificities are swapped, that the respective drug specificities are also switched (Elkins and Nikaido, 2002; Tikhonova et al., 2002). We constructed analogous chimeras between MmpL7 and MmpL8; although these hybrids were expressed, they were non-functional (Figure 8). Despite the negative result, this suggests that portions other than domains 1 and 2 are required for MmpL function.

Given the results presented here, we propose that MmpL proteins act not only as transporters but also as scaffolds to couple polyketide synthesis and secretion. This model may also provide a framework to explain the role of two other RND-family transporters in polyketide synthesis. In *M. tuberculosis, mmpL8*$^-$ mutants are defective for SL-1 synthesis and accumulate a partially lipidated precursor SL_{1278} (Converse et al., 2003). Originally, we proposed that MmpL8 may transport SL_{1278} across the cell membrane where subsequent enzymatic steps would convert it to mature SL-1. However, in light of the interaction between MmpL7 and PpsE, it is now tempting to speculate that MmpL8 may similarly recruit a biosynthetic enzyme required to complete the synthesis of SL-1 prior to transport. Likewise, an RND transporter in *S. coelicolor*, ActII-ORF3, is also involved in the biogenesis of a polyketide, γ-actinorhodin (Bystrykh et al., 1996). Therefore, the coupling of polyketide synthesis and transport via interactions between synthases and cognate transporters may represent a general mechanism utilized by RND-family members to efficiently export complex polyketides. This paradigm is reminiscent of protein secretion where newly synthesized polypeptides are co-translationally translocated across the membrane (Keenan et al., 2001). Coupling of synthesis and transport may be energetically favorable while promoting specificity and directionality in transport processes.

Materials and Methods

Strains and Plasmids. *M. tuberculosis* cells (Erdman strain) were cultured in 7H9 medium supplemented with 10% OADC, 0.5% glycerol and 0.1% Tween-80, or on 7H10 solid agar medium with the same supplements except for Tween-80 (Cox et al., 1999). Kanamycin (20 μg ml^{-1}) and hygromycin (50 μg ml^{-1}) were used where necessary. All strains and plasmids used in this study are described in Table 1.

Construction of *M. tuberculosis* knockout strain. The Δ*mmpL7* (MJM39) mutant strain was created by homologous recombination using specialized transducing phage phMJ1 (Glickman et al., 2000). This deletion replaced all 2763 bp of *mmpL7* with a hygromycin resistance cassette and correct replacement of the gene was confirmed by Southern Blot analysis (Figure 6).

Yeast Two-Hybrid. The yeast two-hybrid screen was performed as described (Golemis et al., 1999) and expression of bait proteins in yeast was confirmed by Western blotting using antibodies against LexA (kind gift of R. Brent). Bait constructs using MmpL7-domain 2 and MmpL8-domain 2 were created by PCR amplification and insertion into pEG202. The prey library was constructed using random Erdman genomic DNA fragments inserted into pjsc401. Positive interactors were selected on media lacking leucine and then screened by blue-white screening on agar plates containing 5-bromo-4-chloro-3-indolyl β-D-galactoside (X-gal). β-galactosidase activity was assayed in yeast cells permeabilized with chloroform and sodium dodecyl sulfate as previously described (Guarente and Ptashne, 1981). For reverse two-hybrid, error prone PCR was performed using Taq polymerase, 100 ng of the bait plasmid containing *mmpL7-domain 2* (pMJ2) as the PCR template, and 18 cycles of amplification with an annealing temperature of 72°C. Mutagenesis rate under these conditions was ~1 mutation per kilobase. Yeast homologous recombination (with 80 base-pairs of overlap) was used to introduce the mutant MmpL7-domain 2 PCR product into the bait vector. GFP screening was performed visually by fluorescence microscopy.

GST Pull-down Binding Assays. Recombinant MmpL7-domain 2-GST, MmpL7-domain 2-I611S-GST and GST alone were expressed in *E. coli* strain DH5α by growing a 500 mL culture to mid log phase at 32°C and inducing with 1mM IPTG for 30 minutes. Cells were centrifuged and resuspended in 10mL of 50 mM Tris, 1 mM EDTA, 150 mM NaCl, 1 mM PMSF, 1 mM DTT. A tiny amount of lysozyme was added and the cells were lysed by sonication three times for 1 min (with 1 min rest on ice in between) at maximum power. 1 mL of 10% Triton (for a final concentration of 1% Triton) was added to the lysed cells and the whole mixture was incubated at 4°C for an hour. Lysates were cleared by centrifugation at 12,000 g and incubated with 500 μL glutathione agarose beads (G 4510, Sigma, St. Louis, MO, 400 mg beads were first resuspended in PBS and washed 3x. Final resuspension of 10 mL PBS yields a 50% slurry for storage) at 4°C overnight. Beads were washed four times with 10 mL of PBS, 1 mM EDTA, and 0.5% Triton X-100, and then stored as a 50% slurry in 50 mM Tris, 1 mM EDTA, 500 mM NaCl, 20% glycerol, 0.5% Triton X-100. PpsE-myc was expressed in *Mycobacterium smegmatis* and lysates were prepared by bead beating 3x cells obtained from a 250 mL log phase culture into 500 μL binding buffer (20 mM Tris, 1 mM EDTA, 150 mM NaCl, 1 mM PMSF, 1mM DTT). Lysates were incubated with 50 μL of protein coated beads overnight at 4°C, washed quickly three times in 1 mL binding buffer and resuspended in 30 μL SDS sample buffer. Samples were boiled to elute all proteins off the beads and the entire sample was loaded and resolved on a 7.5% SDS-PAGE gel. PpsE-myc was detected by Western blotting using 9E10 monoclonal antibodies (kind gift of J. M. Bishop).

Biochemical Analysis of PDIM and SL-1. *M. tuberculosis* cultures (50 mL) were labeled with ^{14}C-propionate (7.5 μL of 1 mCi/mL), which is incorporated into both

PDIM and SL-1, for 16 hours. Cells were centrifuged at 3000 rpm on a Beckman tabletop centrifuge (rotor GH 3.8) and surface-exposed lipids were extracted by resuspending the cell pellet in 1 mL hexanes and gently sonicating at 25% for 1.5 min (Converse et al., 2003). Cells were centrifuged again as above to yield a hexanes fraction and a pellet fraction containing the remainder lipids. Lipids from both fractions were extracted by the Bligh-Dyer method (Bligh and Dyer, 1959). For 0.5 mL of cell pellet fraction, 1.5 mL of 2:1 $ChCl_3$:MeOH was added and for 1 mL of hexanes fraction, 3 mL of 2:1 $ChCl_3$:MeOH was added. Samples were mixed by vortexing and then removed from the BSL3. In the BSL2, 0.5 mL of chloroform was added per 0.5 mL of original fraction and samples were mixed thoroughly by vortexing. 0.5 mL of water was then added per 0.5 ml of original fraction, mixed by vortexing, and then centrifuged briefly to separate layers. The lower layer (organic phase) was extracted and transferred to a fresh glass tube and dried down under nitrogen. Samples were resuspended in 100 µL of chloroform and stored at -80°C. Lipids were analyzed by loading 4-8 µL on 10 cm x 10 cm HPTLC plates (Alltech Associates, Deerfield, IL) and separation using either hexanes/ether (9:1) to resolve PDIM or chloroform/methanol/water (60:30:6) to resolve SL-1. Lipids spots on TLC plates were quantified using a phosphorimager.

Protein Preparation and Analysis. *M. tuberculosis* cells were grown into mid-logarithmic phase and harvested by centrifugation. Cell lysates were separated by SDS-PAGE using 12% polyacrylamide gels. Proteins were visualized by immunoblotting using monoclonal antibodies against the hemagglutinin epitope tag (HA.11, Covance, Berkeley, CA). Loading was normalized by total protein and efficiency of transfer was confirmed by Ponceau S staining of the nitrocellulose membrane.

Sub-cellular fractionation of mycobacterial cells. *M. smegmatis* cells expressing MmpL7 were grown to an O.D.600 of 0.8 and spun down. Cell pellets were fractionated as follows. 500 mL cells were grown to late-log phase and harvested by centrifugation. The cell pellet was resuspended in 5 mL PBS containing DNase, RNase, PMSF, and a protease inhibitor cocktail. Cells were broken apart by sonication at maximum power three times for 1 minute each with 1 minute on ice in between. Unbroken cells were removed by centrifugation at 3000g. Cell wall was removed by centrifugation at 27000g twice. The supernatant was subjected to a 100,000g centrifugation for four hours to yield membranes. The resulting membrane pellet was washed in PBS and resuspended in 100 µL 0.01 M ammonium bicarbonate and stored at -80°C. The resulting supernatant, or cytosolic fraction, was also stored at -80°C.

Figure 1. PDIM synthesis and export pathway and topology of MmpL7.

(A) Schematic of the known steps in the PDIM synthesis and transport pathway. PpsA-E and Mas are polyketide synthases that extend fatty acids to phthiocerol and mycocerosic acids respectively (Azad et al., 1997; Azad et al., 1996). These are then esterified to produce phthiocerol dimycocerosate (PDIM). MmpL7 and DrrC are required for the transport of PDIM to the cell surface (Camacho et al., 1999; Cox et al., 1999). R is =O (keto) or $-OCH_3$ (methoxy). **(B)** Predicted membrane topology of MmpL7 indicating the two non-transmembrane domains 1 and 2.

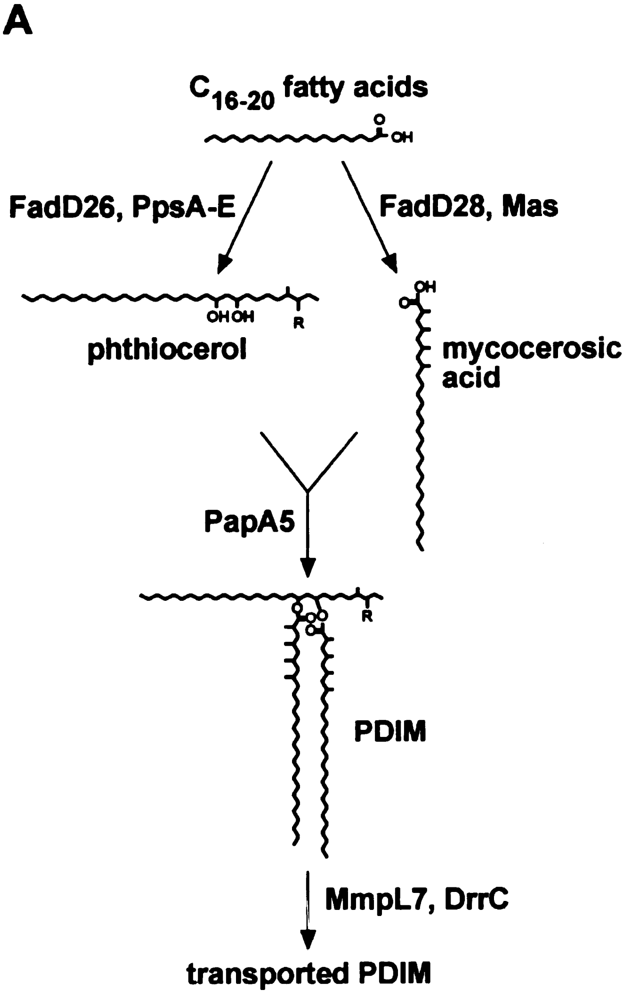
A
C16-20 fatty acids
OH
FadD26, PpsA-E
FadD28, Mas
OH OH
R
phthiocerol
OH
mycocerosic acid
PapA5
R
PDIM
MmpL7, DrrC
transported PDIM

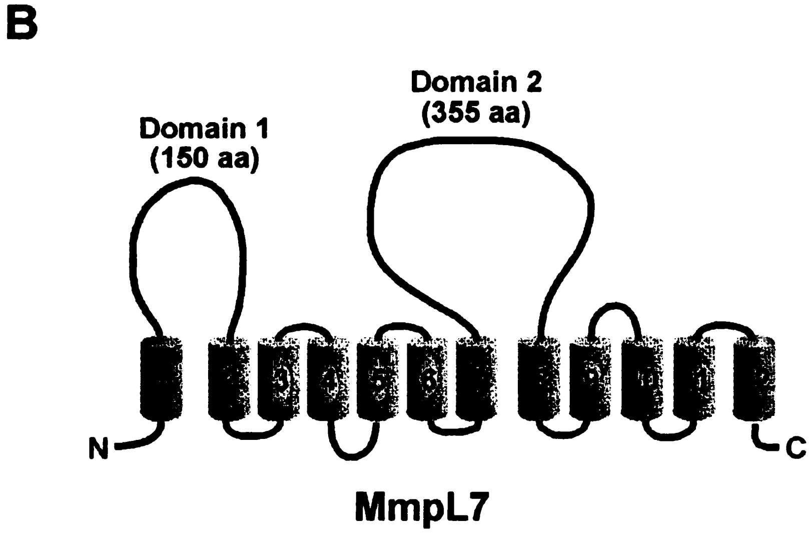
B
Domain 2
(355 aa)
Domain 1
(150 aa)
3
4
5
6
N
C
MmpL7

Figure 2. MmpL7-domain 2 interacts with the PDIM synthesis enzyme, PpsE.

(A) Yeast two-hybrid reporter strains harboring the indicated bait and prey plasmids were streaked onto solid media with or without leucine. Growth on –leucine plates indicate a positive interaction. (MmpL7^{d2}, MmpL7-domain 2; MmpL8^{d2}, MmpL8-domain 2). **(B)** The same strains as in (A) were transferred onto X-gal containing indicator plates (inset) and reporter activity was quantified from liquid cultures using β-galactosidase assays. **(C)** Linear representation of full-length PpsE protein (1488 aa) with the MmpL7 interaction region denoted. Catalytic domains of PpsE are also shown (KS, Ketoacyl Synthase; AT, Acyl Transferase; ACP, Acyl Carrier Protein; CE, Condensing Enzyme).

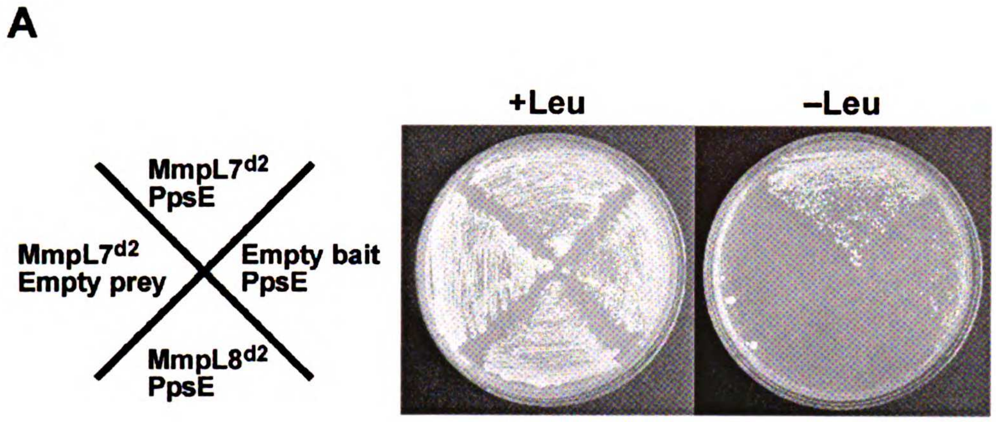
A
+Leu
–Leu
MmpL7^{d2}
PpsE
MmpL7^{d2}
Empty prey
Empty bait
PpsE
MmpL8^{d2}
PpsE

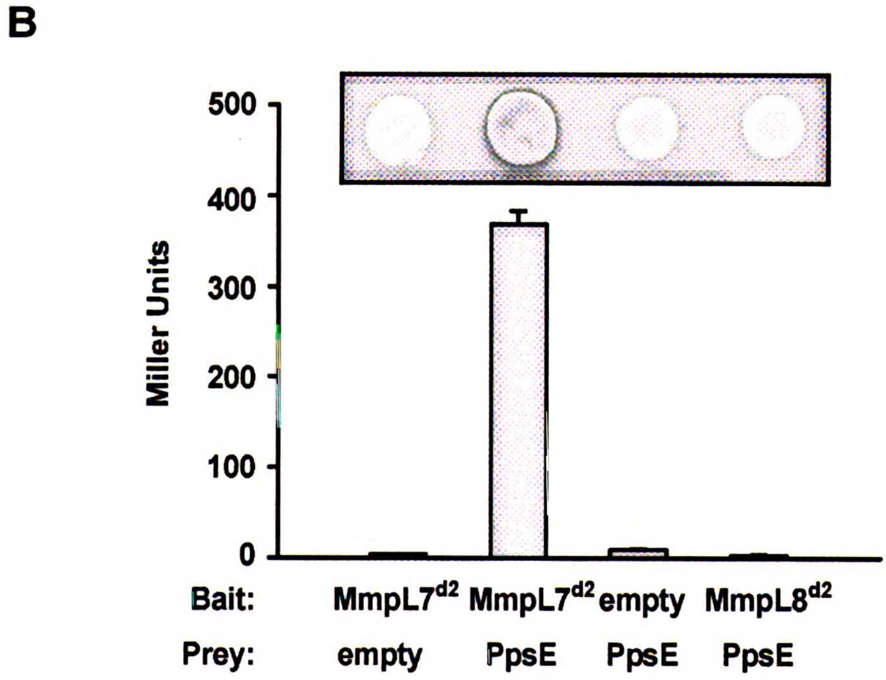
B
Miller Units
500
400
300
200
100
0
Bait:
Prey:
MmpL7^{d2}
empty
MmpL7^{d2}
PpsE
empty
PpsE
MmpL8^{d2}
PpsE

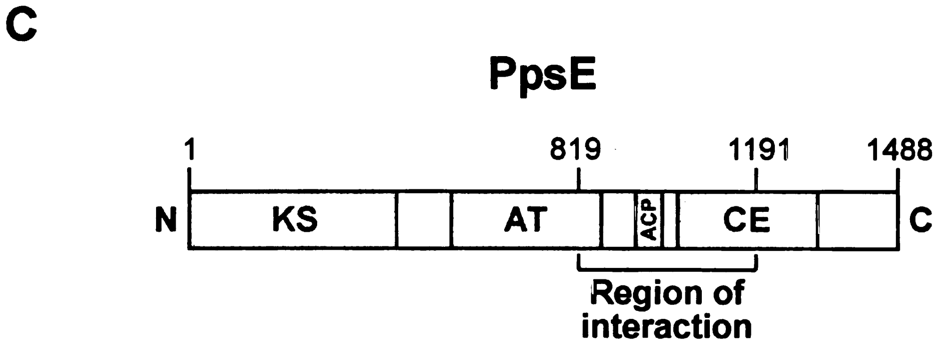
C
PpsE
1
819
1191
1488
N
KS
AT
ACP
CE
C
Region of
interaction

Figure 3. Identification of residues in MmpL7-domain 2 required for PpsE interaction.

(**A**) Twelve MmpL7-domain 2 mutants defective for PpsE binding were isolated in a reverse two-hybrid screen. These amino acid substitutions are displayed on a linear map of MmpL7-domain 2 with changes to amino acids other than proline or glycine in bold. Amino acid numbers correspond to positions in full-length MmpL7. Transmembrane domains 7 and 8 are denoted by hatched bars. (**B**) Yeast strains expressing the PpsE prey construct and various MmpL7-domain 2 bait plasmids were transferred onto X-gal indicator plates (inset) and reporter activity was quantified from liquid cultures by monitoring β-galactosidase activity. (**C**) Beads containing equal amounts of MmpL7-domain 2 and the I611S mutant were incubated with protein extracts containing myc-tagged PpsE and washed. Bound proteins were eluted and separated by SDS-PAGE, and PpsE was visualized by Western blot using anti-myc antibodies. GST coated beads serve as a negative control and 1% of the protein extract added to the pulldown was loaded as a positive control ("input").

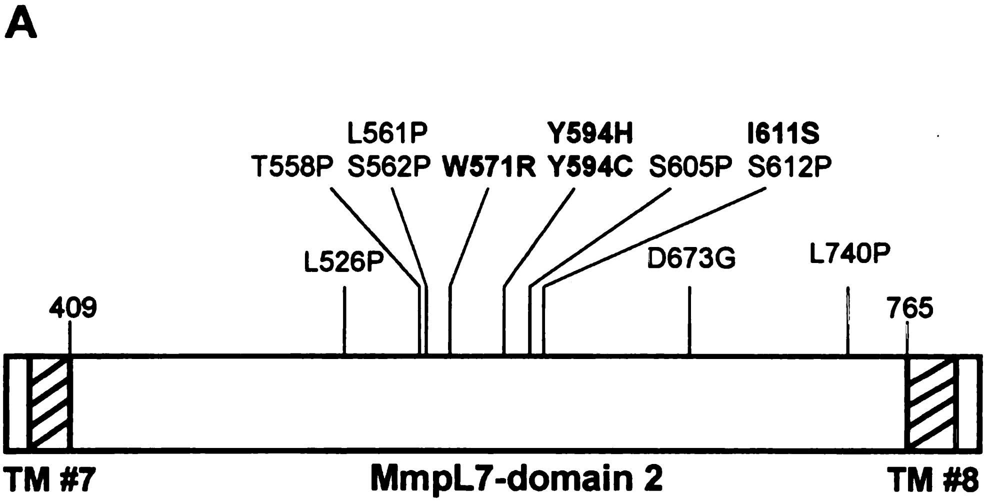
A
L561P
T558P
S562P
W571R
Y594H
Y594C
S605P
I611S
S612P
L526P
D673G
L740P
409
765
TM #7
MmpL7-domain 2
TM #8

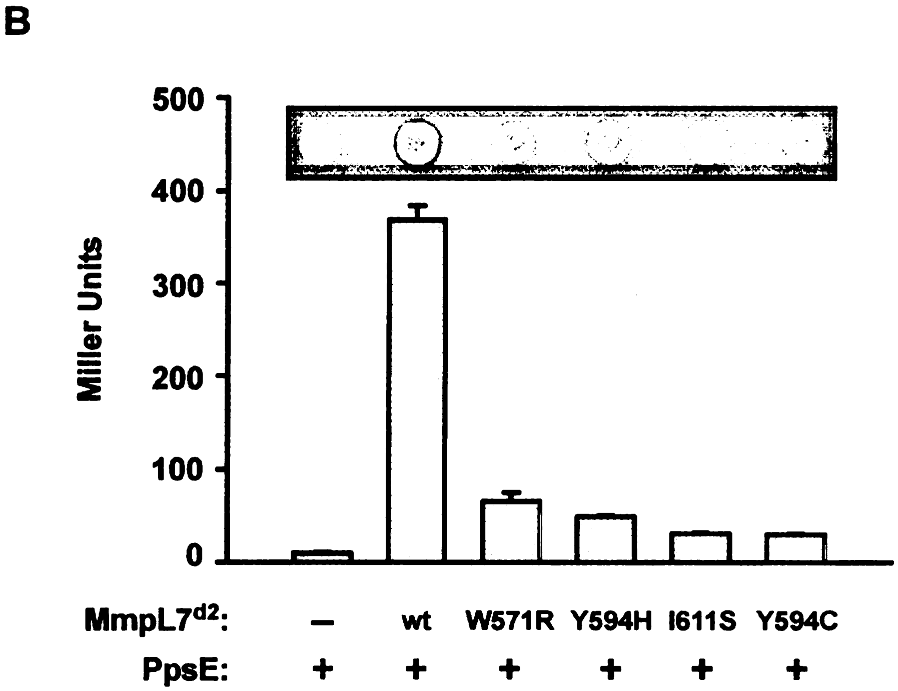
B
500
400
300
200
100
0
Miller Units
MmpL7d2:
—
wt
W571R
Y594H
I611S
Y594C
PpsE:
+
+
+
+
+
+

C

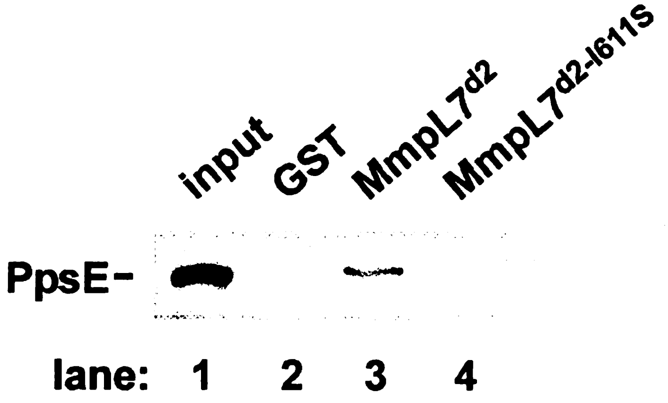
input
GST
MmpL7d2
MmpL7d2-I611S
PpsE-
lane: 1 2 3 4

Figure 4. MmpL7-domain 2 acts as a dominant-negative inhibitor of PDIM synthesis *in vivo.*

(A) The indicated strains carrying either no plasmid (-), control vector (vector), or a plasmid with MmpL7-domain 2 under the control of the constitutive *groEL2* promoter (MmpL7^{d2}) were labeled with ^{14}C-propionate. Surface-exposed lipids (S) were extracted by resuspension in hexanes and cell pellets (P) were harvested by centrifugation. Lipids from both fractions were extracted and separated by TLC under solvent conditions to separate PDIM (upper panel, keto and methoxy forms) and sulfolipid (SL-1, lower panel). **(B)** Top panel: Lipids were extracted as in (A) from pellets of wild-type cells carrying either no plasmid (-), the MmpL7-domain 2 expression plasmid (d2), or the MmpL7-domain 2 expression plasmid with the I611S mutation (d2-I611S). Lower panel: Western blot analysis was performed to confirm equivalent expression of wild-type MmpL7-domain 2 and the I611S mutant by using antibodies against the hemagglutinin (HA) epitope tag. **(C)** Complementation of an *mmpL7*$^{-}$ *M. tuberculosis* strain with the wild-type (*mmpL7*^{wt}) or the I611S mutant *mmpL7* (*mmpL7*^{I611S}). Surface-exposed lipids (S) and lipids associated with the remaining cell pellet (P) were extracted and separated by TLC to resolve PDIM as in (A).

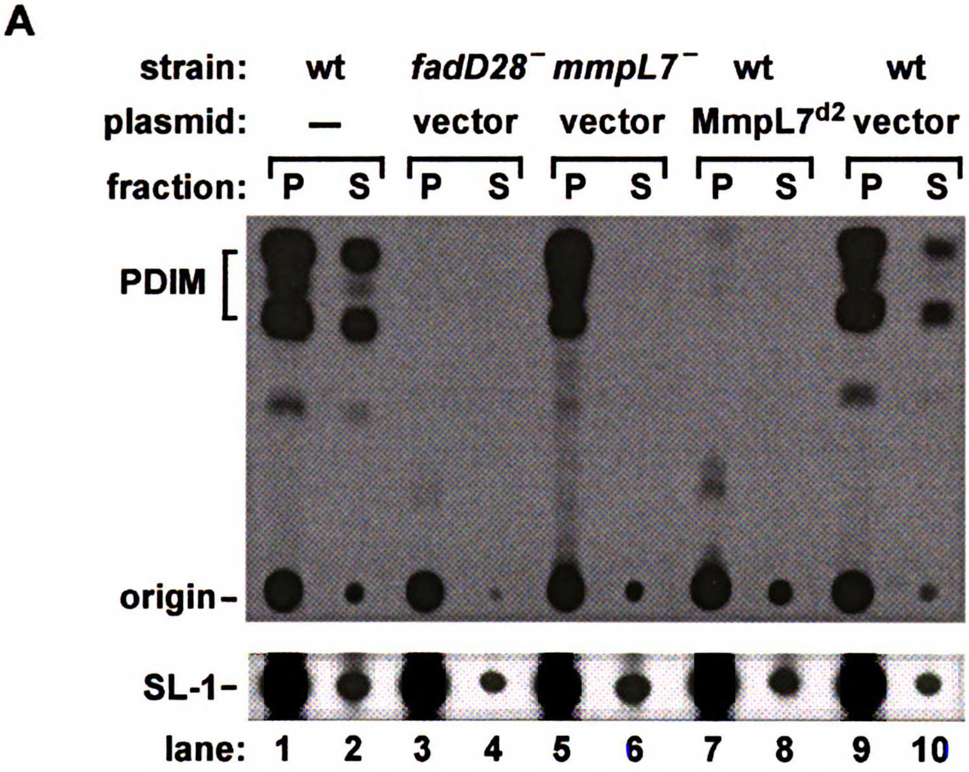
A
strain: wt fadD28$^-$ mmpL7$^-$ wt wt
plasmid: — vector vector MmpL7^{d2} vector
fraction: P S P S P S P S P S
PDIM
origin-
SL-1-
lane: 1 2 3 4 5 6 7 8 9 10

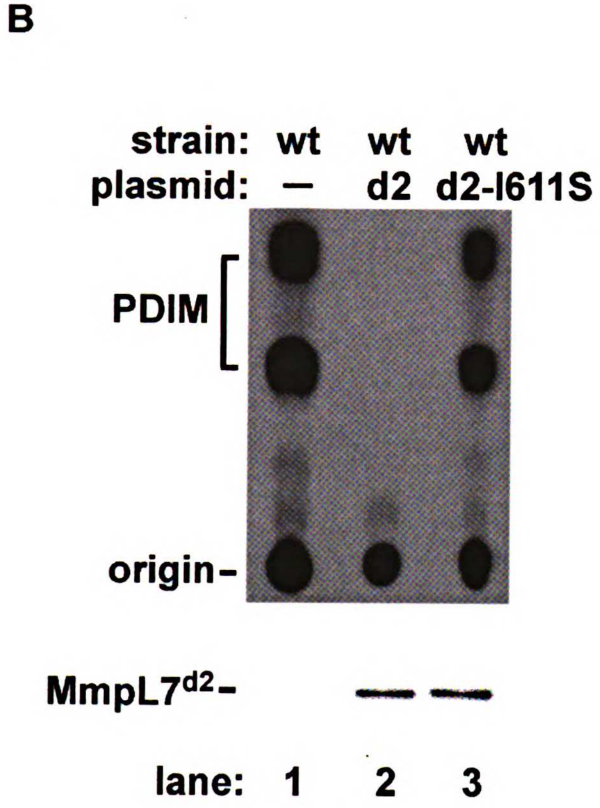
B
strain: wt wt wt
plasmid: — d2 d2-I611S
PDIM
origin-
MmpL7d2-
lane: 1 2 3

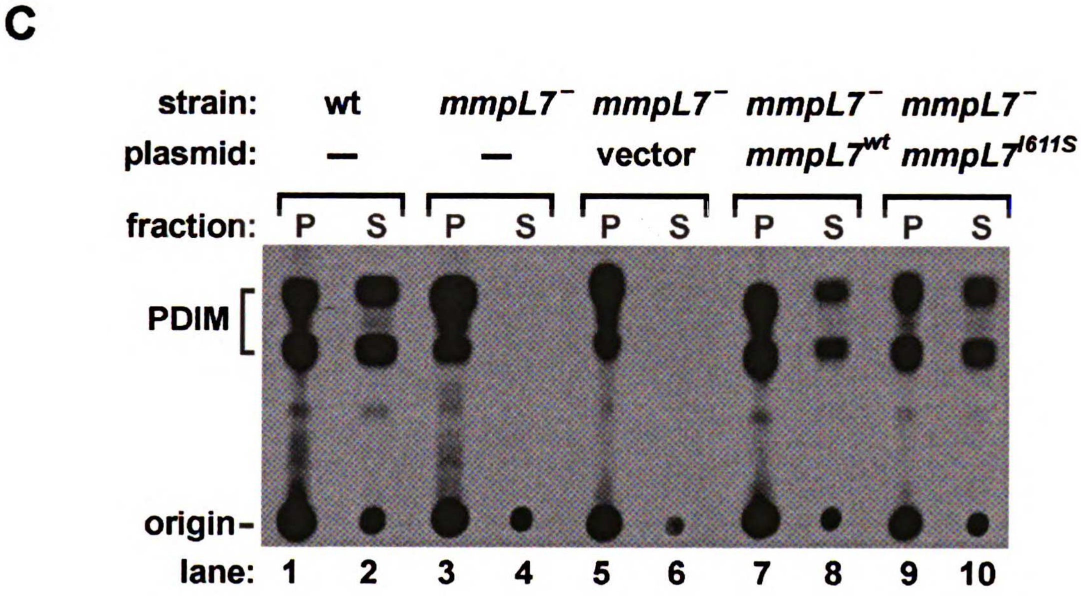
C
strain: wt $mmpL7^{-}$ $mmpL7^{-}$ $mmpL7^{-}$ $mmpL7^{-}$
plasmid: — — vector $mmpL7^{wt}$ $mmpL7^{I611S}$
fraction: P S P S P S P S P S
PDIM
origin-
lane: 1 2 3 4 5 6 7 8 9 10

Figure 5. Dominant negative effect of MmpL7-domain 2 requires the presence of full-length MmpL7.

(A) Wild-type cells, an *mmpL7* transposon mutant (*mmpL7*$^-$), and a complete *mmpL7* knockout (Δ*mmpL7*) carrying either no plasmid (-) or the MmpL7-domain 2 expression construct (+). Labeled lipids were extracted from pellets as described in Figure 4 and separated by TLC to resolve PDIM. **(B)** Western blot of MmpL7-domain 2 showing that it is expressed at equivalent levels in the different *M. tuberculosis* strains.

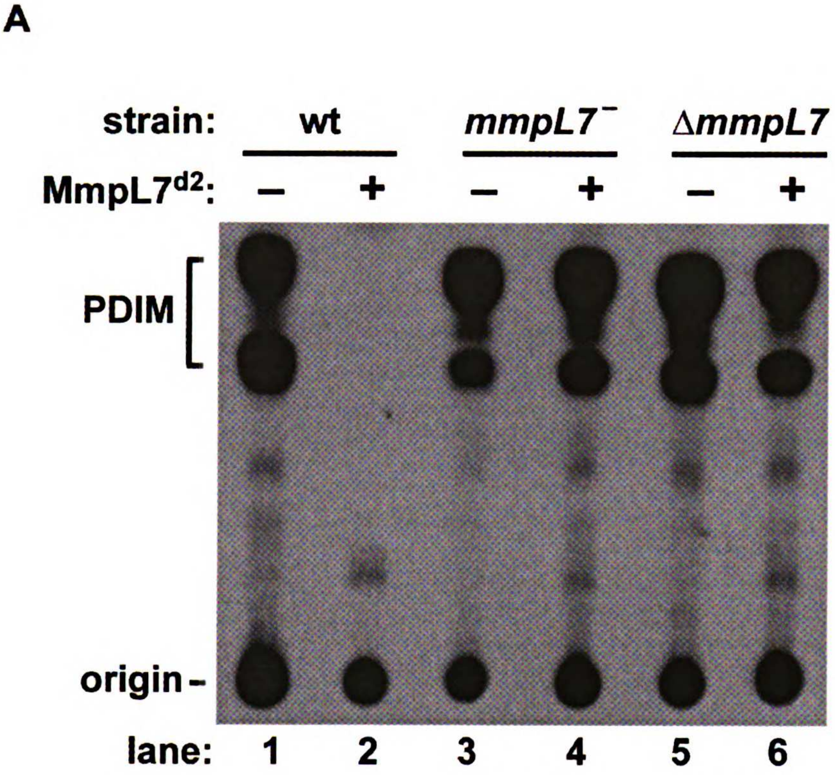
A
strain:
wt
mmpL7⁻
ΔmmpL7
MmpL7d2:
–
+
–
+
–
+
PDIM
origin
lane:
1
2
3
4
5
6

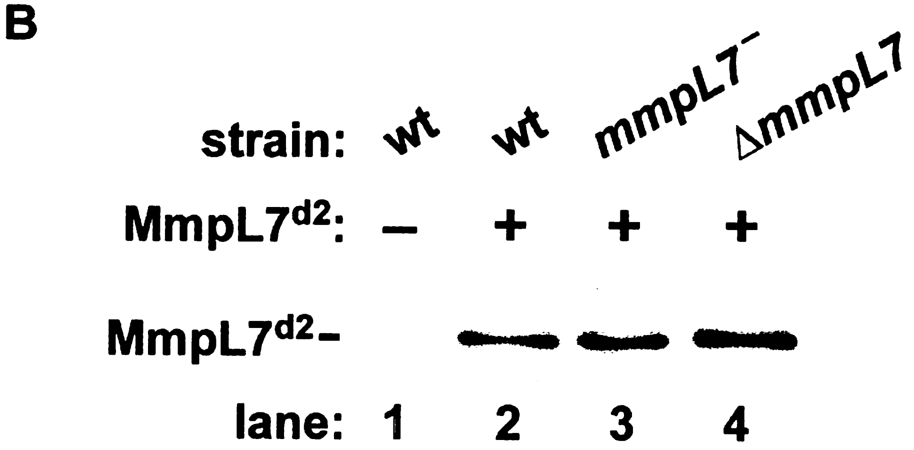
B
strain:
wt
wt
mmpL7⁻
ΔmmpL7
MmpL7d2:
–
+
+
+
MmpL7d2-
lane:
1
2
3
4

Figure 6. Creation of Δ*mmpL7* in *M. tuberculosis* by specialized transduction.

(A) Map of the *mmpL7* region in wild-type and the Δ*mmpL7* mutant showing the restriction sites and probe location for southern blot. Genomic DNA from both wild-type as well as Δ*mmpL7* was digested with *Bam*HI, and the blot was probed with a 1029 bp 5' flank to *mmpL7* revealing a 2636 bp fragment for wild-type and a 4700 bp fragment for the mutant. **(B)** Southern blot of *Bam*HI digested genomic DNA from indicated strains. **(C)** Surface-exposed lipids (S) and lipids associated with the remaining cell pellet (P) were labeled and extracted from wild-type and Δ*mmpL7* cells as described in Figure 4A and then separated by TLC to resolve PDIM.

A

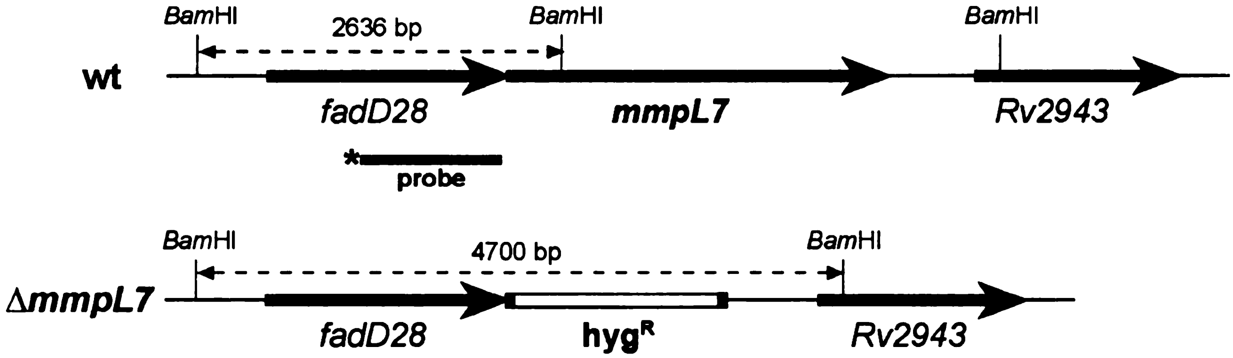
BamHI
2636 bp
BamHI
BamHI
wt
fadD28
mmpL7
Rv2943
*
probe
BamHI
4700 bp
BamHI
ΔmmpL7
fadD28
hygR
Rv2943

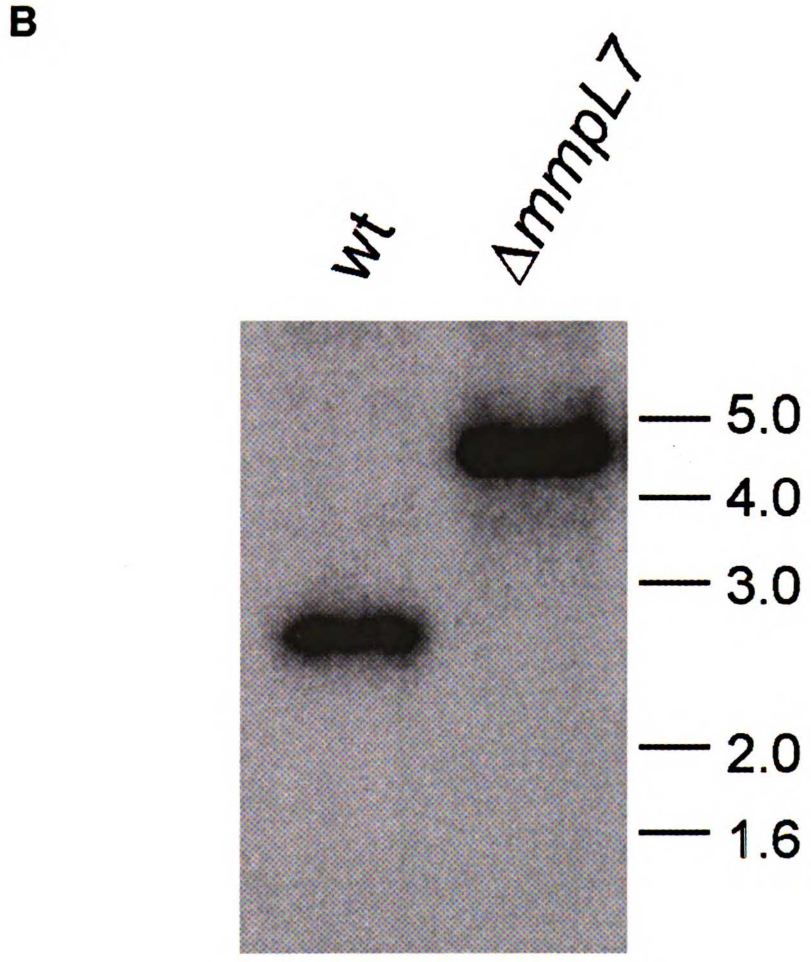
B
wt
ΔmmpL7
5.0
4.0
3.0
2.0
1.6

c

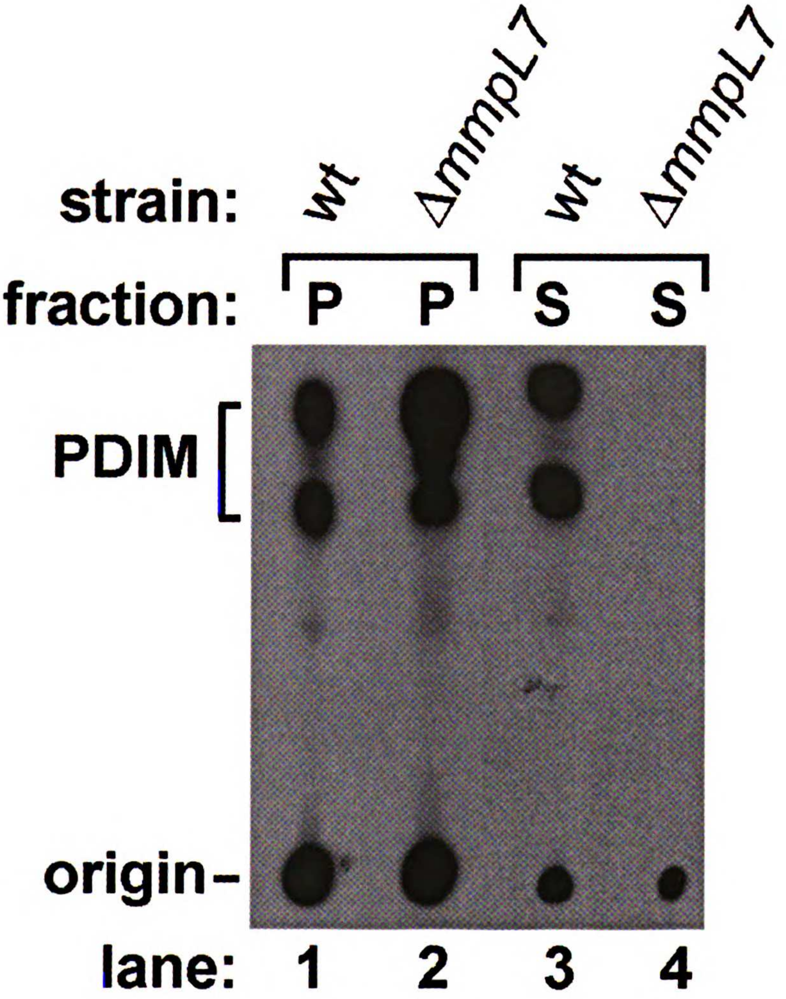
strain:
wt
ΔmmpL7
wt
ΔmmpL7
fraction:
P
P
S
S
PDIM
origin
lane:
1
2
3
4

Figure 7. Membrane localization of MmpL7.

M. smegatis cells expressing HA-tagged MmpL7 from *M. tuberculosis* (+) and cell expressing empty vector (-) were separated into membrane and cytoplasmic fractions as described in the methods. MmpL7 was detected by western blotting using an anti-HA antibody.

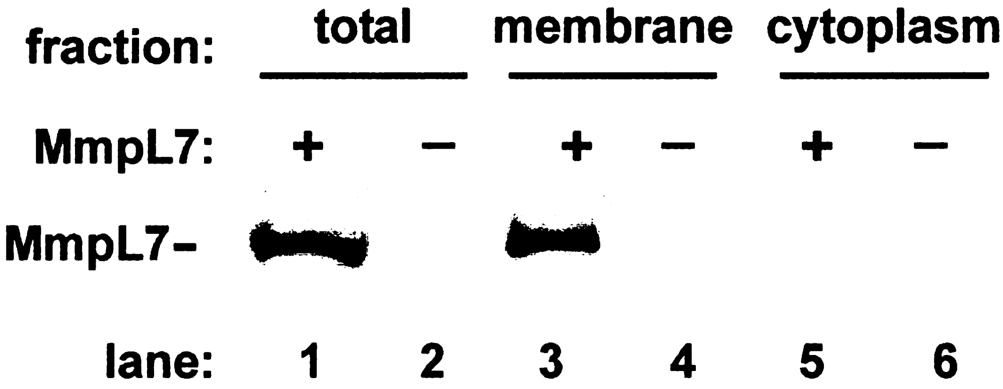
fraction:
total
membrane
cytoplasm
MmpL7:
+
–
+
–
+
–
MmpL7-
lane:
1
2
3
4
5
6

Figure 8. Chimeric analysis of MmpL7 and MmpL8

Expression constructs containing chimeras of MmpL7 and MmpL8 as indicated were introduced into *mmpL7*$^-$ and *mmpL8*$^-$ cells and **(A)** PDIM transport and **(B)** SL-1 synthesis were assessed. **(C)** Chimeric proteins using MmpL7 as a backbone were tagged with 2xHA and their expression was analyzed by western blotting.

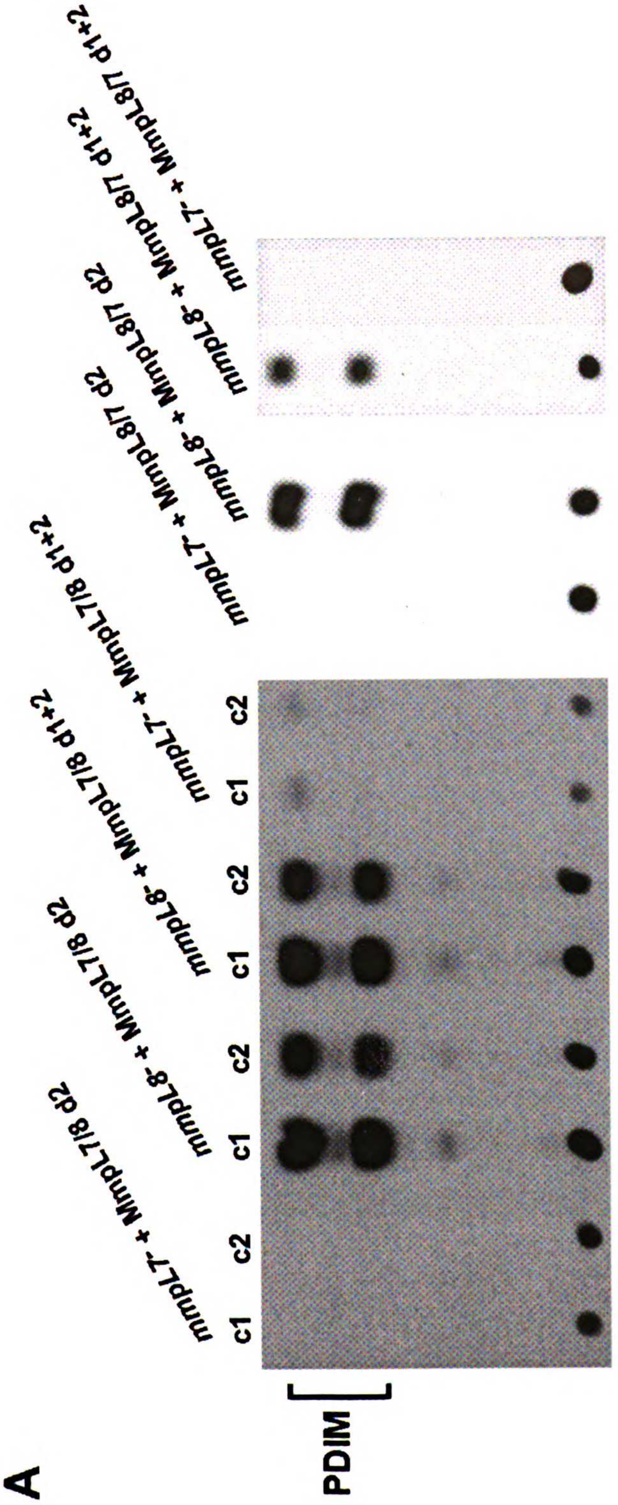
A
PDIM
c1
c2
mmpL7- + MmpL7/8 d2
c1
c2
mmpL8- + MmpL7/8 d2
c1
c2
mmpL8- + MmpL7/8 d1+2
c1
c2
mmpL7- + MmpL7/8 d1+2
mmpL7- + MmpL8/7 d2
mmpL8- + MmpL8/7 d2
mmpL8- + MmpL8/7 d1+2
mmpL7- + MmpL8/7 d1+2

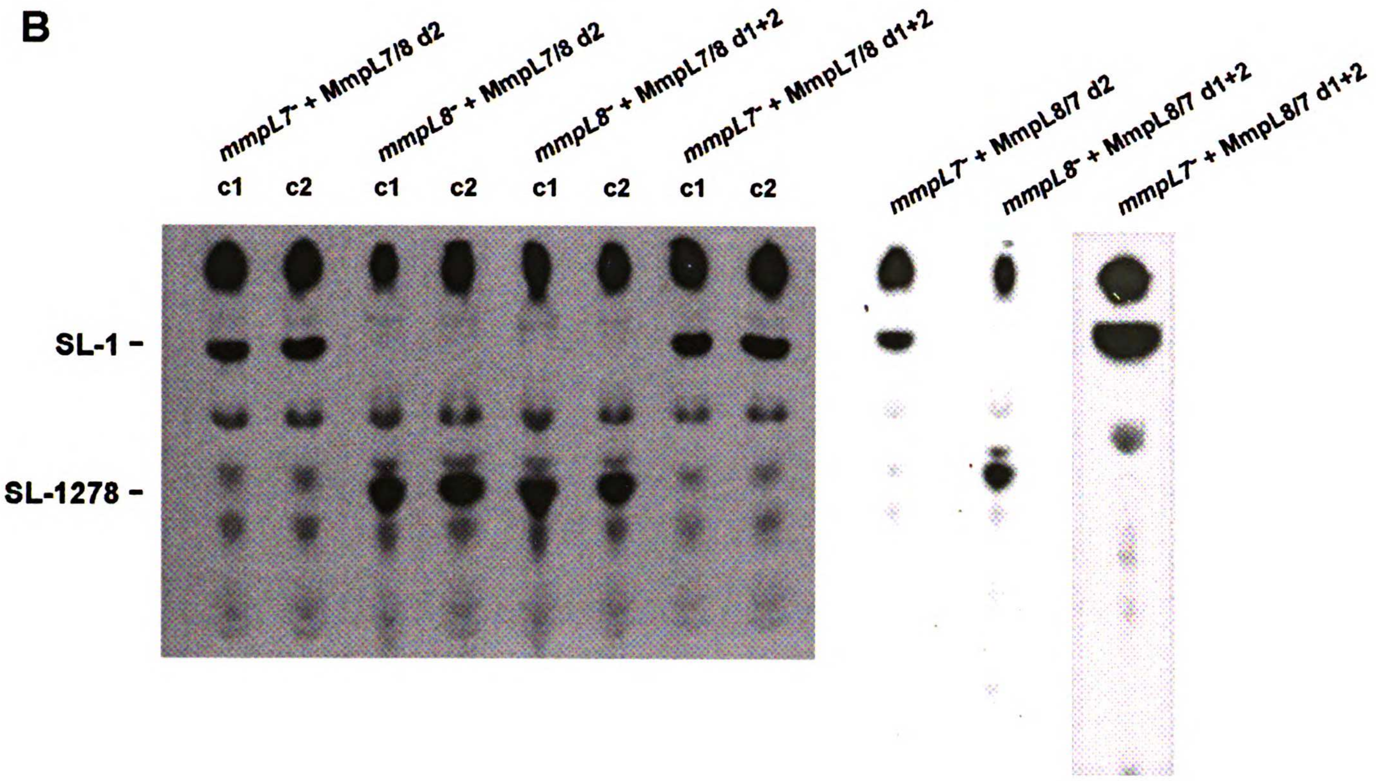
B
mmpL7$^-$ + MmpL7/8 d2
mmpL8$^-$ + MmpL7/8 d2
mmpL8$^-$ + MmpL7/8 d1+2
mmpL7$^-$ + MmpL7/8 d1+2
c1
c2
c1
c2
c1
c2
c1
c2
mmpL7$^-$ + MmpL8/7 d2
mmpL8$^-$ + MmpL8/7 d1+2
mmpL7$^-$ + MmpL8/7 d1+2
SL-1 –
SL-1278 –

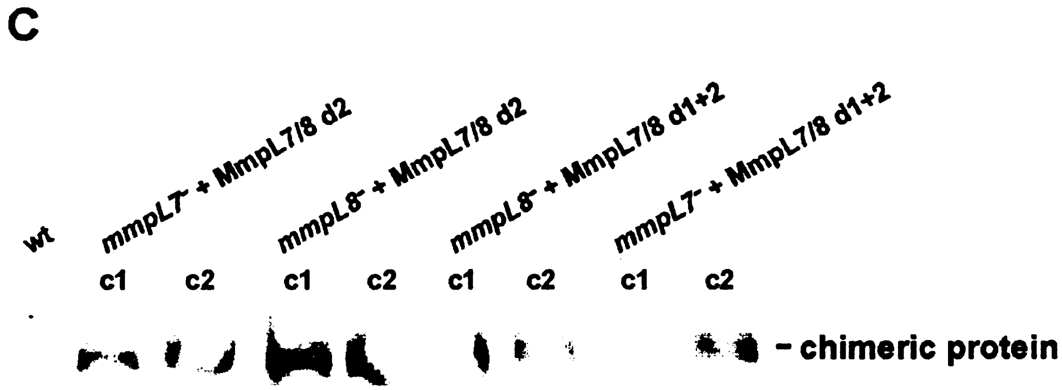
C
wt
mmpL7⁻ + MmpL7/8 d2
mmpL8⁻ + MmpL7/8 d2
mmpL8⁻ + MmpL7/8 d1+2
mmpL7⁻ + MmpL7/8 d1+2
c1
c2
c1
c2
c1
c2
c1
c2
– chimeric protein

Figure 9. Model of PDIM synthesis and transport.

MmpL7 interacts with PpsE, a subunit of the Pps enzyme required for PDIM synthesis. We propose that MmpL7 acts as a scaffold to recruit PDIM synthesis machinery, including Pps and perhaps mycocerosic acid synthase (Mas), leading to coordinate synthesis and transport of PDIM across the cytoplasmic membrane (CM). Whether MmpL7, or other factors, are required for delivery of PDIM through the peptidoglycan (PG) and mycolyl-arabinogalactan (mAG) layers is unclear.

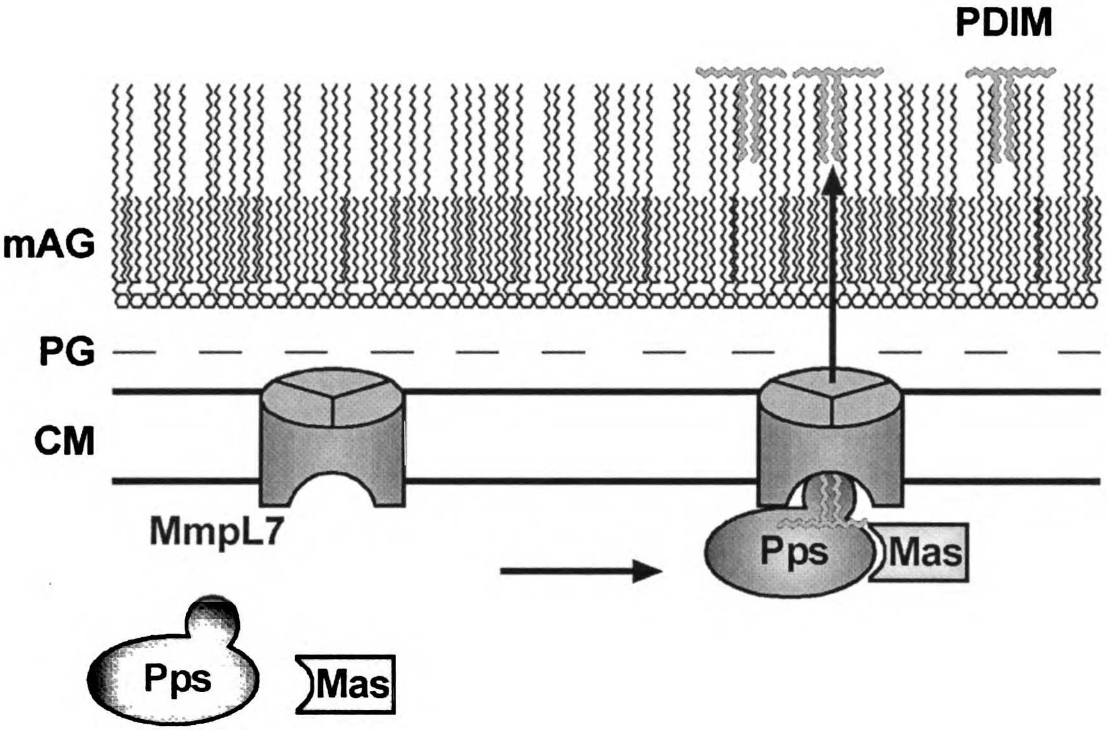
PDIM
mAG
PG
CM
MmpL7
Pps
Mas
Pps
Mas

Table 1. Strains and Plasmids

Strain or Plasmid	Genotype/Description	Source/ref.
M. tuberculosis		
Erdman	wild-type	W. R. Jacobs, Jr.
mc^{2}3106	Erdman *fadD28::*Tn*5370*, Hyg^R	(Cox et al., 1999)
mc^{2}3107	Erdman *mmpL7::*Tn*5370*, Hyg^R	(Cox et al., 1999)
JCM96	mc^{2}3106 + pMV306.kan, Hyg^R, Kan^R	This study
JCM98	mc^{2}3107 + pMV306.kan, Hyg^R, Kan^R	This study
MJM20	Erdman + pMJ35, Kan^R	This study
MJM21	Erdman + pMJ35:2-100, Kan^R	This study
MJM2	Erdman + pMV261.kan, Kan^R	This study
MJM3	Erdman + pMJ10, Kan^R	This study
MJM4	Erdman + pMJ13, Kan^R	This study
MJM22	Erdman + pMJ10:2-100, Kan^R	This study
MJM36	mc^{2}3107 + pMJ35, Kan^R	This study
MJM39	Erdman Δ*mmpL7*, Hyg^R	This study
MJM54	MJM39 + pMJ35, Hyg^R, Kan^R	This study
JCM108	Erdman Δ*mmpL8*, Hyg^R	(Converse et al., 2003)
MJM11	mc^{2}3107 + pMJ33, Hyg^R, Kan^R	This study
MJM12	JCM108 + pMJ33, Hyg^R, Kan^R	This study
MJM29	JCM108 + pMJ55, Hyg^R, Kan^R	This study
MJM35	mc^{2}3107 + pMJ55, Hyg^R, Kan^R	This study
MJM8	mc^{2}3107 + pMJ22, Hyg^R, Kan^R	This study
MJM10	JCM108 + pMJ22, Hyg^R, Kan^R	This study
MJM25	JCM108 + pMJ53, Hyg^R, Kan^R	This study
MJM31	mc^{2}3107 + pMJ53, Hyg^R, Kan^R	This study
Saccharomyces cerevisiae		
W303-1a	*MATa; ura3-1; leu2-3,-112; his3-11,-15; trp1-1; ade2-1; can1-100*	P. Walter
EGY48	*MATα; trp1, his3, ura3, lexAop-LEU2*	R. Brent
Plasmids		
pEG202	LexA bait plasmid, *HIS3*, 2μm	(Golemis et al., 1999)
pSH18-34	8 x *lexA*op-*lacZ* reporter, *URA3*, 2μm	(Golemis et al., 1999)
pJG4-5	*GAL1*prom-*GAL4*$_{AD}$, *TRP1*, 2μm	(Golemis et al., 1999)
pjsc401	pJG4-5 + *Cla*I linker in MCS	(Stanley et al., 2003)
pMJ2	pEG202 + *mmpL7-domain 2*	This study
pMJ3	pjsc401 + *ppsE* (a.a. 819-1191)	This study
pMJ6	pEG202 + *mmpL8-domain 2*	This study
pMJ2:1-51	pEG202 + *mmpL7-domain 2* W571R	This study
pMJ2:2-31	pEG202 + *mmpL7-domain 2* Y594H	This study
pMJ2:2-100	pEG202 + *mmpL7-domain 2* I611S	This study
pMJ2:3-1	pEG202 + *mmpL7-domain 2* Y594C	This study
pMV306.kan	*int, oriE*, Kan^R	W. R. Jacobs, Jr.
pMV261.kan	*oriE*, *oriM*, groEL2 promoter, Kan^R	W. R. Jacobs, Jr.
pMJ13	pMV261.kan + C-terminal in-frame *2xHA* tag, Kan^R	(Converse and Cox, 2005)
pMJ35	pMJ13 + *mmpL7-domain 2*	This study
pMJ35:2-100	pMJ13 + *mmpL7-domain 2* I611S	This study
pMJ10	pMJ13 + *mmpL7* (endogenous promoter)	This study
pMJ10:2-100	pMJ13 + *mmpL7* I611S	This study
pGEX2T	P*tac*, lacI^Q, N-terminal GST, Amp^R	Invitrogen (Carlsbad,

		CA)
pMJ4	pGEX2T + *mmpL7-domain 2*	This study
pMJ74	pGEX2T + *mmpL7-domain 2* I611S	This study
pMJ31	pMV261.kan + C-terminal in-frame *myc* tag, Kan^{R}	(Converse and Cox, 2005)
pMJ32	pMJ31 + *ppsE*	This study
pSEC16	pMV306.kan + *mmpL8* (endogenous promoter), Kan^{R}	(Converse et al., 2003)
pMJ33	pMJ10::*mmpL7/mmpL8* domain 2, Kan^{R}	This study
pMJ55	pMJ10::*mmpL7/mmpL8* domain 1 and 2, Kan^{R}	This study
pMJ22	pSEC16::*mmpL8/mmpL7* domain 2, Kan^{R}	This study
pMJ53	pSEC16::*mmpL8/mmpL7* domain 1 and 2, Kan^{R}	This study

Table 2. Yeast two-hybrid interactors with MmpL7 domain 2

Rv0125, *pepA,* 3x
Rv0176
Rv0352, *dnaJ*
Rv0364, *dedA*
Rv0560c
Rv0610c
Rv0708, *rplP*
Rv0724, *sppA*
Rv0775
Rv0845
Rv0866, *moaE2*
Rv0878c
Rv0928, *pstS3*
Rv0939
Rv0973, *accA2*
Rv1017c, *prsA*
Rv1071c, *echA9*
Rv1184c†
Rv1294, *thrA*
Rv1319c
Rv1328, Rv1329c, *glgP, dinG*
Rv1442, *bisC*
Rv1461
Rv1475c, *acn*
Rv1498A
Rv1596, *nadC*
Rv1623c, *cydA, appC*
Rv1679, *fadE16*
Rv1702c
Rv1756c
Rv1821, *secA*, 2x
Rv1901, *cinA*
Rv1922
Rv1975†
Rv2047c
Rv2112c†
Rv2135c
Rv2151c, *ftsQ*
Rv2223c, *slpD*, 2x
Rv2260, 3x
Rv2467, *pepN*, 5x
Rv2531c, *adi*
Rv2538c, Rv2539c, *aroK, aroB*
Rv2573
Rv2590, *fadD9*
Rv2624c
Rv2649
Rv2672, 2x
Rv2680
Rv2682c, *dxs*
Rv2851c
Rv2935, *ppsE*
Rv2967c, *pca*
Rv3215, *entC*
Rv3238c
Rv3240c
Rv3262
Rv3276c, *purK*
Rv3524
Rv3548c
Rv3627c
Rv3712
Rv3730c
Rv3793, *embC*

† Contains putative signal sequence and does not interact with MmpL8 domain 2 by yeast two-hybrid.

Chapter 3

Lipidomics reveals post-transcriptional control of *M. tuberculosis* virulence lipid synthesis via direct metabolic coupling

Abstract

M. tuberculosis synthesizes specific polyketide lipids to interact with host cells and catabolizes host lipids to grow during infection. We have uncovered a novel mechanism in which virulence polyketide synthesis is regulated by metabolite availability. Using genetics and a mass spectrometric approach that simultaneously monitors hundreds of lipids, we found that the production of two lipid virulence factors, PDIM and SL-1, are coupled and co-regulated by the concentration of a common metabolite, methyl malonyl CoA. Consistent with this view, increased levels of methyl malonyl CoA led to increased abundance and mass of both PDIM and SL-1. Furthermore, perturbation of methyl malonyl CoA metabolism attenuated pathogen replication in mice. Importantly, this mode of regulation is likely operative in vivo as we found that PDIM is produced in high mass forms during infection. We propose that growth of *M. tuberculosis* on fatty acids during infection leads to increased flux of methyl malonyl CoA through lipid biosynthetic pathways, resulting in increased virulence lipid synthesis.

Introduction

Mycobacterium tuberculosis, the causative agent of tuberculosis, produces and secretes a wide array of biologically active polyketide lipids that interact with the host (Brennan and Nikaido, 1995; Cox et al., 1999; Goren et al., 1974). Genes involved in the synthesis and export of surface-exposed lipid virulence factors such as phthiocerol dimycocerosate (PDIM) and sulfolipid-1 (SL-1) are required for bacterial growth and virulence in mice (Camacho et al., 1999; Converse et al., 2003; Cox et al., 1999;

Domenech et al., 2004). Surface-exposed lipids provide protection against host induced damage as well as modulate the immune response to infection (Camacho et al., 2001; Rao et al., 2005; Reed et al., 2004; Rousseau et al., 2004). The interplay between host and pathogen is likely complex as mycobacterial lipids can also serve as antigens recognized by the immune system during infection (de la Salle et al., 2005; Gilleron et al., 2004; Moody et al., 2000; Moody et al., 2000).

Most surface-exposed lipids are synthesized by specialized polyketide synthases that elongate straight chain fatty acids by the stepwise addition of a variety of short acyl chains. PDIM, which consists of two mycocerosic acids esterified to phthiocerol, is the product of two such polyketide synthase systems (Figure 1B). Mas synthesizes methyl branched mycocerosic acids through successive additions of methyl malonyl CoA (Azad et al., 1996; Minnikin et al., 2002; Trivedi et al., 2005) while PpsA-E synthesize phthiocerol (Azad et al., 1997). FadD26 and FadD28 are responsible for activating straight chain fatty acids for transfer to Pps and Mas, respectively (Trivedi et al., 2004). The protein MmpL7 is required for the export of PDIM to the surface (Cox et al., 1999) and interacts with PpsE to coordinate synthesis and transport of PDIM (Jain and Cox, 2005).

SL-1 consists of trehalose-2-sulfate esterified to three molecules of phthioceranic or hydroxy-phthioceranic acids and one straight chain fatty acid, palmitate or stearate (Goren, 1970; Goren et al., 1971) (Figure 1A). Similar to mycocerosic acids, phthioceranic and hydroxy-phthioceranic acids contain multiple methyl branches which are incorporated by the polyketide synthase Pks2 (Sirakova et al., 2001). MmpL8 is also required for the complete synthesis of SL-1 and a biosynthetic precursor, SL_{1278}, accumulates in *mmpL8⁻* cells (Converse et al., 2003) (Figure 1A).

Host lipids are also important for the host-pathogen interaction as they appear to be the primary carbon source for *M. tuberculosis* during infection. Bacteria grown in vivo preferentially metabolize fatty acids over carbohydrates (Segal and Bloch, 1956). The *icl1* and *icl2* genes, which encode enzymes in the anaplerotic glyoxylate cycle in *M. tuberculosis*, are required for growth on lipids as a sole carbon source and are required for growth in vivo (McKinney et al., 2000; Munoz-Elias and McKinney, 2005). Furthermore, *icl1* and *icl2*, along with genes involved in the β-oxidation of fatty acids, are up-regulated in both a macrophage and murine model of *M. tuberculosis* infection (Dubnau et al., 2005; Graham and Clark-Curtiss, 1999; Honer Zu Bentrup et al., 1999; Schnappinger et al., 2003; Sturgill-Koszycki et al., 1997; Timm et al., 2003). These results strongly suggest that *M. tuberculosis* alters its metabolism in order to catabolize host lipids during infection.

In this work we investigated the global lipid profile of *M. tuberculosis* using Fourier Transform Ion Cyclotron Resonance Mass Spectrometry (FT-ICR MS) (Converse et al., 2003; Marshall et al., 1998; Mougous et al., 2002). Although *M. tuberculosis* lipids have been extensively analyzed using a variety of methods including mass spectrometry (Brennan and Nikaido, 1995), this new method has allowed us to rapidly and reproducibly monitor hundreds of lipid species. We discovered that the size and abundance of PDIM and SL-1 are controlled by the availability of a common precursor, and that this regulation occurs during infection. We propose that virulence lipid anabolism is coupled with increased catabolism of host lipids.

Results

Global analysis of *M. tuberculosis* lipids.

To comprehensively analyze lipid regulation, we utilized FT-ICR MS to simultaneously measure the abundance of the high complexity of lipid species in *M. tuberculosis*. We have previously used the high resolution capabilities of FT-ICR MS to analyze individual lipids (Converse et al., 2003; Mougous et al., 2002) but here sought to maximize the number of species we could detect within a crude lipid extract. We directly infused total lipid extracts of *M. tuberculosis* cells grown in log phase into the electrospray ionization source of the mass spectrometer and observed reproducible spectra containing hundreds of unique lipid species in both negative mode (Figure 2A) and positive mode (data not shown). By measuring the peak intensities, FT-ICR MS also allows us to quantify the relative abundance of lipid species between samples.

Accurate mass measurements permitted identification of a number of complex lipid species without the need for standard compounds. For instance, phosphatidylinositol mannosides (PIMs), a group of related glycolipids implicated in *M. tuberculosis* virulence (Alexander et al., 2004), were readily identified in the negative ion mode (Figure 2A). The phosphatidylinositol (PI) linkers esterified with two acyl chains (Ac_2PI, *m/z* 835.5355 for PI esterified to palmitate and oleate, and *m/z* 851.5638 for PI esterified to palmitate and tuberculostearate) were observed within 2 ppm of their theoretical masses (Kolattukudy et al., 1997; Nigou et al., 2003). The dimannose species esterified to three acyl chains (Ac_3PIM_2, *m/z* 1413.8988) and finally the hexamannose species esterified to three acyl chains (Ac_3PIM_6, *m/z* 2062.1079) were also observed and were among the most abundant species in the mass spectra. Likewise, accurate mass measurements permitted identification of peaks corresponding to multiple lipoforms of SL-1 (Figure 2A, m/z 2401.1544 to 2639.3480) and SL_{1278} (Figure 2A, m/z 1277.9394) in negative ion mode, as well as sodiated PDIM ions (Figure 4A, m/z 1318.3012 to 1500.5008) in positive ion mode. Although we observed peaks corresponding to the exact mass of the published structure of SL-1, the major lipoform observed for SL-1 was 2 amu greater than the published structure, as previously reported (Mougous et al., 2002). The mass of this major SL-1 lipoform is consistent with it containing three hydroxy-phthioceranic acids instead of two hydroxy-phthioceranic acids and one phthioceranic acid (for a detailed discussion see Figure 8).

Importantly, we obtained highly reproducible spectra from repeat experiments with *M. tuberculosis* cells grown under the same conditions. This reproducibility allowed us to compare spectra from lipid extracts prepared from cells grown under different conditions in order to identify alterations in the profiles. For example, by harvesting cells at over a time course during growth in culture, we found that the abundance of SL-1 per cell increases with cell density suggesting that SL-1 synthesis is regulated by growth phase (Figure 9).

Increased production of SL-1 in PDIM synthesis mutants.

To validate FT-ICR MS as a method for analyzing lipid changes in *M. tuberculosis*, we analyzed extracts from mutants in the synthesis and transport of the virulence lipids PDIM and SL-1. SL-1 from wild-type cells appeared as a broad set of peaks from m/z 2401.1544 to 2639.3480 corresponding to the known m/z (Figure 1A)

(Goren et al., 1976). These peaks were separated by 14 amu corresponding to differences in the number of CH_2 units present in the four lipid chains of SL-1 (Figure 1A). In *pks2*$^-$ cells, which are unable to synthesize SL-1 (Sirakova et al., 2001), the peaks were completely absent (Figure 2B). In *mmpL8*$^-$ cells, SL-1 peaks were also absent (Figure 2B) but there was a dramatic increase in peaks at m/z 1277.9394 corresponding to SL_{1278} (Figure 2A) (Converse et al., 2003). Likewise, in *fadD26*$^-$, *fadD28*$^-$, *mas*$^-$ and *tesA*$^-$ cells, which are defective in the synthesis of PDIM (Cox et al., 1999), all PDIM peaks were absent (Figure 4A, data not shown).

Surprisingly, in cells defective for PDIM synthesis, we observed greatly increased amounts of SL-1 (Figure 2B). This was unexpected since PDIM synthesis mutants have been well characterized by other methods but these differences were not detected. In addition to being more abundant, SL-1 from PDIM mutants was also of higher average mass as compared to that from wild-type bacteria. The increase in abundance and average mass was specific to SL-1 with the exception of a slight increase in the abundance of unknown species at m/z 1826.73, 1854.77, 1942.89 and 1970.91 (data not shown). We quantified SL-1 abundance and found that, on average, there was a two to three-fold increase in the amount of SL-1 in PDIM synthesis mutants as compared to wild-type (Figure 2C). We also calculated a weighted average mass of SL-1 and found a dramatic shift in the average mass of SL-1 of over 100 amu (Figure 2D).

Since PDIM mutants have altered cell walls (Camacho et al., 2001; Cox et al., 1999), we reasoned that the absence of PDIM may have caused structural changes in the cell wall that were sensed in the bacteria, leading to compensatory changes in SL-1 production. To test this, we determined the lipid profile of *mmpL7*$^-$ cells which can synthesize PDIM but are unable to export it across the cell membrane to the cell wall. Interestingly, SL-1 production in *mmpL7*$^-$ cells is similar to wild type (Figure 2B-D), demonstrating that SL-1 is regulated in direct response to PDIM synthesis and not to perturbations in the cell wall.

Transcriptional regulation does not account for increased SL-1 production in PDIM synthesis mutants.

Since lipid biosynthetic genes in *M. tuberculosis* can be transcriptionally regulated (Makinoshima and Glickman, 2005), we hypothesized that inhibition of PDIM production may lead to transcriptional activation of SL-1 synthesis genes. To test this, we performed microarray experiments to compare the global gene expression program of wild-type, *fadD26*$^-$ and *pks2*$^-$ cells. Cells were grown to log phase, and RNA was extracted and used for microarray analysis using oligonucleotide arrays representing every gene in the *M. tuberculosis* genome. Very few changes were detected in the transcriptional profiles of either mutant as compared to wild type (Figure 10). We performed significance analysis of microarrays (SAM) (Tusher et al., 2001) on data from three repetitions of the experiment and found that *fadD26* was the only mRNA consistently reduced more than three-fold in *fadD26*$^-$ cells as compared to wild type and similarly *pks2* was the only transcript differentially regulated in *pks2*$^-$ cells. The *ppsA-D* transcripts were reduced about three-fold in *fadD26*$^-$ cells indicating a polar effect on downstream genes. Even if we permitted a false discovery rate of higher than 0%, no changes in the transcription of SL-1 synthesis genes could be detected in *fadD26*$^-$ cells.

Therefore, the increased SL-1 production in PDIM synthesis mutants is likely due to post-transcriptional regulation.

Abundance and average mass of SL-1 and PDIM increase with methyl malonyl CoA concentration.

Because both PDIM and SL-1 biosynthetic pathways share a common precursor, methyl malonyl CoA, a simple model is that in the absence of PDIM synthesis, greater amounts of methyl malonyl CoA are now available to the SL-1 biosynthetic pathway leading to increased SL-1 production. This is an attractive model as methyl malonyl CoA is incorporated into methyl branches in both PDIM and SL-1 but is not heavily incorporated into other lipid species, consistent with the specificity observed in the mass spectra. To test whether increased methyl malonyl CoA can lead to increased SL-1 production, we added a direct precursor of methyl malonyl CoA, propionate, to the media of wild-type cells (over the course of three doublings) and monitored SL-1 production by FT-ICR MS. Interestingly, we found that with the addition of increasing amounts of propionate, wild-type cells responded by making two to five-fold more SL-1 (Figure 3A, B). We also observed an increase in average mass of SL-1 of over 100 amu (Figure 3A, C) similar to the PDIM mutants. Likewise, in *mmpL8*$^-$ cells, we observed a two-fold increase in the amount of SL_{1278} and an increase of ~24 amu in the average mass, consistent with the SL-1 result (Figure 11).

We also added propionate to the *mas* mutant to test whether we could further increase the already elevated SL-1 production in these cells. Although there was no significant increase in SL-1 abundance, there was an increase of over 50 amu in the average mass of SL-1 at higher concentrations of propionate (Figure 3A-C). These results indicate that methyl malonyl CoA is limiting during in vitro growth and its availability regulates production of SL-1. While we cannot rule out additional modes of post-transcriptional regulation, these results suggest that increased flux of methyl malonyl CoA in the SL-1 biosynthetic pathway leads to increased SL-1 abundance and average mass.

We next sought to determine if PDIM production was also sensitive to methyl malonyl CoA concentration. Interestingly, *pks2*⁻ and *mmpL8*⁻ cells do not make significantly more PDIM than wild-type (Figure 4A). Since SL-1 is much less abundant than PDIM (unpublished observations), it is possible that inhibition of SL-1 synthesis does not alter the concentration of methyl malonyl CoA enough to affect the synthesis of PDIM. Alternatively, PDIM biosynthetic enzymes such as Mas may be precise and unable to incorporate more methyl branches into PDIM even in the presence of increased methyl malonyl CoA concentrations. However, addition of propionate to cells led to an increase in both abundance and average mass of PDIM (Figure 4B-D) demonstrating that PDIM production increases upon elevated levels of methyl malonyl CoA. Taken together, our results indicate that production of PDIM and SL-1 are metabolically coupled via competition for limiting amounts of methyl malonyl CoA inside the cell.

Increased average mass of PDIM is due to increased chain-length of mycocerosic acids.

To determine the differences between low and high mass forms of PDIM we performed collision induced dissociation (CID) on the different PDIM ions. To simplify analysis of the CID pattern, we selected only the lowest mass peak in a given isotope packet which contains only the pure ^{12}C keto form of PDIM. We thus eliminated peaks corresponding to ^{13}C and ^{2}H incorporation into PDIM, as well as the methoxy form of PDIM. Sodiated PDIM ions corresponding to a mass of 1402 were isolated from wild-type *M. tuberculosis*, and ions corresponding to a mass of 1458 and 1486 were isolated from cells treated with 1 mM propionate. The CID fragmentation patterns are shown in Figure 5 and ions corresponding to sequential loss of the mycocerosic acid moieties are observed in each case. Interestingly, we found that while mycocerosic acids had increased chain length in the higher mass forms of PDIM, the mass of the phthiocerol moiety remained constant. In fact, for all PDIM lipoforms we found that phthiocerol exists as either a C20 form (*m/z* 497 in Figure 5B) or a C22 form (*m/z* 525 in Figure 5A and C), consistent with previous reports and likely due to differences in the fatty acid primers used for elongation (Noll, 1957). The 1402 and 1486 forms of PDIM both contain the same size phthiocerol group (C24), and differ only in the mass of their mycocerosic acids (Figure 5A and C). The two sequential losses of 438 amu in the CID spectrum of the 1402 ion indicate that this PDIM lipoform contains two mycocerosic acids of 438 amu each and similarly the 1486 lipoform contains two mycocerosic acids of 480 amu each. This difference of 42 amu between the mycocerosic acids in the 1402 form and the 1486 form corresponds exactly to the addition of a single propionate molecule. While our study cannot distinguish between the addition of a methyl branched or a straight 3 carbon chain (because they result in the same mass increase), it is extremely likely that the mycocerosic acids in the 1486 form have an additional methyl branch as compared to the 1402 form because methyl malonyl CoA is directly incorporated into PDIM to form methyl branches (Rainwater and Kolattukudy, 1985). Taken together, these data show that increased methyl malonyl CoA is incorporated into mycocerosic acids, resulting in an increase in the average mass of PDIM. These data also suggest that while the Pps enzymes are precise in the number of functional groups they incorporate, Mas is more flexible and is able to incorporate a variable number of methyl branches into mycocerosic acids based on the availability of methyl malonyl CoA.

Perturbations in methyl malonyl CoA regulation lead to altered PDIM and SL-1 production and attenuation in vivo.

Exogenous addition of propionate leads to an increase in methyl malonyl CoA which is directly incorporated into PDIM and SL-1 (Figure 6A). Since propionate addition may lead to other changes in the cell, we tested whether altering endogenous methyl malonyl CoA production in vivo would also lead to changes in PDIM and SL-1 production. Methyl malonyl CoA mutase, encoded by the *mutAB* genes in *M. tuberculosis*, catalyzes the conversion of the citric acid cycle intermediate succinyl CoA to methyl malonyl CoA (Figure 6A) (Ogata et al., 1999) and its over-expression has been used to increase polyketide synthesis in heterologous systems (Dayem et al., 2002). We over-expressed methyl malonyl CoA mutase by placing the *mutAB* genes under the control of the constituitive *groEL2* promoter on an episomal plasmid in wild-type cells. This resulted in a marked increase in the average mass of SL-1 and PDIM but, in contrast with the exogenous addition of propionate, led to a decrease in their total abundance (reduction of 30% for PDIM and 80% for SL-1, Figure 6B-G). Although the reason for this is unclear, it is possible that chronic over-expression of MutAB depletes citric acid cycle intermediates, leading to pleiotropic effects on cell metabolism. However, PDIM and SL-1 production are specifically affected while the rest of the lipid mass-spectrum in MutAB over-expressing cells was similar to wild-type (data not shown). MutAB over-expressing cells also doubled with same kinetics in vitro as wild-type cells carrying the empty vector under kanamycin selection (doubling time of 25 hours, data not shown) showing that MutAB over-expression does not affect cell growth and viability.

Since MutAB over-expressing cells have altered PDIM and SL-1 production, we hypothesized that they would have altered virulence in vivo. Based on the decreased amounts of PDIM and SL-1 we would expect this strain to be attenuated relative to wild-type, although the increased mass of PDIM and SL-1 might have additional unknown effects. We assessed virulence of the MutAB over-expressing strain during a mouse infection by infecting BALB/C mice via the aerosol route with wild-type *M. tuberculosis* cells over-expressing MutAB. We found that during infection bacterial growth of the MutAB over-expressing strain is attenuated ~10-fold compared to wild-type cells and this level of attenuation is similar to that observed for *fadD26*$^-$ cells (Figure 7). Ten mice per group were also monitored for time to death (as determined by 15% weight loss). Wild-type infected mice succumbed to infection earlier than mice infected with the MutAB over-expressing strain (Figure 7E).

If over-expression of MutAB is responsible for attenuated bacterial growth in vivo, then there should be a selective advantage for loss of the *mutAB* over-expressing plasmid. Indeed, we found that while there was virtually no plasmid loss in the wild-type or *fadD26*$^-$ cells carrying the empty vector, there was 90% plasmid loss in the MutAB over-expressing strain in mouse lungs by 6 weeks (Figure 7A). Furthermore, seeding in the liver and spleen of bacteria carrying the MutAB over-expression plasmid was much lower (10 to 100-fold) than bacteria that had lost the plasmid (Figure 7B, C). These data clearly show that the strain over-expressing MutAB is attenuated relative to wild-type cells and that proper regulation of methyl malonyl CoA in the cell is critical for virulence.

PDIM is produced in higher mass forms during infection.

Since *M. tuberculosis* catabolizes fatty acids during infection (Munoz-Elias and McKinney, 2006), a consequent increase in the concentration of citric acid cycle intermediates could lead to increased production of methyl malonyl CoA in vivo via the action of MutAB. If this occurs, we predict that increased methyl malonyl CoA production would lead to increased virulence factor production during infection. To test this idea, we compared the mass distribution of PDIM isolated from bacteria growing within infected tissue with that from bacteria growing in culture. Mice were infected via the aerosol route with a high dose of wild-type *M. tuberculosis* and mouse lungs were harvested three weeks post infection and homogenized. We enriched for *M. tuberculosis* lipids using a differential extraction procedure and monitored PDIM and SL-1 by FT-ICR MS. Although SL-1 levels were below the limit of detection, PDIM was readily observed in infected mouse lungs but absent in uninfected tissue (Figure 7D). This is the first report of *M. tuberculosis* lipids being detected in vivo during infection. Importantly, we found that *M. tuberculosis* produced high mass forms of PDIM in vivo, with an average mass of 1430 amu compared to 1403 amu for PDIM extracted from in vitro grown cells. The increase in mass was similar to wild-type cultures grown in the presence of propionate (Figure 7D), suggesting that this regulation is due to increased concentration of methyl malonyl CoA in vivo.

Increased synthesis of PDIM and SL-1 during growth on odd-chain fatty acids.

The increased mass of PDIM during infection suggests a link between anabolism of virulence polyketides and catabolism of host lipids. Therefore, we grew *M. tuberculosis* in culture on different short-chain fatty acids as a sole carbon source and monitored lipid production. There was no increase in PDIM or SL-1 production upon growth on acetate as compared to glucose, but we observed a significant increase during growth on propionate (Figure 12). Interestingly, we also found a significant increase in mass and abundance of PDIM and SL-1 upon growth on the odd-chain fatty acid valerate, but not on the even-chain fatty acid butyrate (Figure 12). These data suggest that the increased mass of PDIM observed in vivo during infection was due to released propionate from beta-oxidation of odd-chain fatty acids.

Probing for novel lipid substrates of MmpL and Pks proteins.

Due to the breadth of the lipid spectrum observed for *M. tuberculosis* using FT-ICR MS, it is attractive to use this method to discover novel substrates of MmpL and Pks proteins with unknown function. Since MmpL7 is required for PDIM transport, and MmpL8 is required for SL-1 synthesis, we hypothesized that MmpL proteins may in general be involved in lipid synthesis and transport. We attempted to identify the function of other MmpL proteins by comparing the lipid spectra of *mmpL* mutants to that of wild-type. MmpL and wild-type strains were grown in 7H9 with OADC, glycerol and Tween-

80 (see methods for details) to log phase and whole lipid extracts were analyzed by FT-ICR MS in negative and positive ion mode. Surface-exposed lipids in the various strains were also compared by resuspending cells in hexanes (see methods) and comparing the lipid spectra of the hexanes fractions. Unfortunately, we were unable to identify reproducible differences between *mmpL1*, *mmpL2*, *mmpL4*, *mmpL6*, *mmpL9*, *mmpL10*, *mmpL11*, *mmpL12*, *mmpL13* and wild-type under the conditions tested. We also tested the whole lipid extracts of four strains, JCM118, JCM122, JCM123, and JCM126 containing deletions in *pks1/15*, *pks6*, *pks7,8,9,10,11,17*, and *pks16*, respectively, and were unable to detect any differences when compared to wild-type. It is possible that the lipid substrates of the MmpL and Pks proteins tested above are not synthesized under the growth conditions used here. It will be interesting to see in the future, if perhaps these proteins are involved in lipid transport under conditions of stress.

Our results contradict existing reports that implicate *pks7*, *pks12*, *pks10* and *pks1/15* in PDIM synthesis (Rousseau et al., 2003; Sirakova et al., 2003; Sirakova et al., 2003). We directly tested PDIM synthesis by radio-labeling JCM118, JCM122, JCM123 and JCM126 with ^{14}C-propionate which incorporates into PDIM and analyzing whole lipid extracts by TLC. We found no differences in PDIM synthesis as compared to wild-type (data not shown). Since the mutants in *pks7*, *10*, *12* and *1/15* that were shown to have PDIM synthesis defects were never complemented, and PDIM mutations are known to accumulate in *M. tuberculosis* over time (unpublished observations), it is likely that these strains contain an additional mutation in the PDIM synthetic machinery leading to the observed results.

Discussion

FT-ICR MS methodology.

In these studies we used FT-ICR MS to monitor the global lipid profile of *M. tuberculosis* quantitatively. FT-ICR MS provides a much broader view of the lipid profile by allowing us to monitor hundreds of species simultaneously, aiding in the identification of cellular lipid changes in mutants. FT-ICR MS also offers a highly sensitive way of analyzing lipid virulence factors under different conditions and can easily discriminate between species with varying lengths of lipid chains.

Another advantage of this method is that it allows for the trapping of ions and subsequent CID to elucidate structural information about the molecules. In this way, we were able to show that the phthiocerol portion of PDIM is invariant and all the heterogeneity is in the mycocerosic acids. We propose that the Pps enzymes are precise, but that the increased mass of both PDIM and SL-1 in response to increased concentrations of methyl malonyl CoA is due to increased processivity of Mas and Pks2, respectively.

Metabolic coupling of virulence lipid synthesis

We have gained new insight into the compensatory cellular lipid changes that occur upon genetic perturbation. Our experiments show that interconnections between seemingly disparate pathways can complicate standard genetic analysis of lipid biosynthetic mutants. Using FT-ICR MS, we made the unexpected discovery that the production of two lipid virulence factors of *M. tuberculosis*, PDIM and SL-1, are coupled *via* the metabolic flux of a common precursor, methyl malonyl CoA. We suggest that in the absence of PDIM synthesis there is increased concentration of the methyl malonyl CoA precursor which is utilized in the SL-1 biosynthetic pathway, leading to the observed increase in abundance and mass of SL-1. It is important to note that *mmpL7*$^-$ cells have a comparable virulence phenotype to PDIM biosynthetic mutants (Cox et al., 1999) indicating that SL-1 up-regulation cannot compensate for the loss of PDIM. Exogenous addition of a direct precursor of methyl malonyl CoA, propionate, to wild-type cells results in increased abundance and mass of both PDIM and SL-1. This further supports the idea that increased flux of methyl malonyl CoA through both pathways leads to an increase in PDIM and SL-1 production.

Interestingly, although both *mmpL8*$^-$ and *pks2*$^-$ cells do not make SL-1, *mmpL8*$^-$ cells have attenuated growth in vivo while *pks2*$^-$ mutants do not (Converse et al., 2003). It is possible that compensatory regulation exists in *pks2*$^-$ mutants that is not present in *mmpL8*$^-$ cells. Although there are no significant changes in PDIM in *pks2*$^-$ cells, we observed an increase in abundance of unknown lipid species at m/z 1826.73, 1854.77, 1942.89 and 1970.91 under conditions of high propionate as well as in *pks2*$^-$ cells and PDIM synthesis mutants but not in *mmpL8*$^-$ cells. These are likely to be methyl branched lipids and perhaps play a role in virulence.

Regulation of virulence lipid synthesis during infection.

FT-ICR MS has, for the first time, allowed us to directly analyze *M. tuberculosis* lipids from infected tissue. The high mass of PDIM recovered from infected tissues suggests that high levels of methyl malonyl CoA exist during infection. Although we cannot rule out the possibility that Mas has increased processivity in vivo due to other reasons, the simplest model is that increased levels of methyl malonyl CoA result in increased production of pathogenic lipids by *M. tuberculosis*. Increased levels of methyl malonyl CoA could be due to either increased availability of propionate in animal tissues, up-regulation of methyl malonyl CoA production by the bacteria during growth on fatty acids, or increased propionate due to beta-oxidation of odd-chain fatty acids by the bacteria. We favor the last explanation as PDIM and SL-1 production was stimulated only during growth on valerate, but not on butyrate (Figure 12). Thus we propose that virulence polyketide anabolism is directly regulated by the metabolic shift to growth on fatty acids, including odd-chain fatty acids, during infection.

Propionate released from the catabolism of odd chain fatty acids can also be assimilated into the citric acid cycle via the methyl citrate cycle. A recent study showed that the methyl citrate cycle is dispensable for *M. tuberculosis* virulence in mice and proposed that methyl-branched polyketide production may act as a sink to buffer the increased concentration of propionate in the absence of this pathway in vivo (Munoz-Elias et al., 2006). Our results are certainly consistent with this idea. This raises the interesting possibility that additional control mechanisms exist to regulate the flux of propionyl CoA through catabolic or anabolic pathways.

Materials and Methods

Strains and Plasmids. *M. tuberculosis* cells (Erdman strain) were cultured in 7H9 medium supplemented with 10% OADC, 0.5% glycerol, and 0.05% Tween-80, or on 7H10 solid agar medium with the same supplements plus 50 mg L^{-1} cycloheximide and without Tween-80. Kanamycin, 20 μg ml^{-1} was used where necessary. All strains and plasmids used in this study are described in Table S1.

Biochemical extraction of lipids. Cells were synchronized to an OD_{600} of 0.2 and grown to an OD_{600} of 0.8. Ten ml of cells were harvested by centrifugation and total lipids were extracted by the Bligh-Dyer method (Bligh and Dyer, 1959) (also see Chapter 2 methods for details). For samples analyzed in positive mode, Tween-80 was removed by resuspending extracts in a 1:1 mixture of hexanes and water, mixing thoroughly, and centrifuging. The organic layer was extracted with water five times. Cell wall associated lipids were extracted by resuspension in hexanes as described in the methods for Chapter 2.

Addition of propionate to cultures. Cultures of *M. tuberculosis* were synchronized to an OD_{600} of 0.1 and propionic acid (P1386, Sigma, St. Louis, MO) was added at the indicated concentration daily over the course of three doublings until the cells reached an OD_{600} of 0.8. Ten mls of culture was used to extract lipids as described above. Cells doubled with the same kinetics independent of the propionate concentration used.

Growth of *M. tuberculosis* on fatty acids. Cultures of *M. tuberculosis* were synchronized to an OD_{600} of 0.1 and resuspended in media containing either 0.1% glucose or 10 mM acetate, propionate, butyrate or valeric acid as the sole carbon source, along with 0.47% 7H9, 0.5% albumin, 0.085% NaCl, and 0.05% Tween-80, as described (Munoz-Elias et al., 2006). Cells doubled with the same kinetics independent of the media used and twenty mls of culture was harvested at an OD_{600} of 0.4 for lipid extraction.

Extraction of bacterial lipids from mouse lung tissue. Lungs from infected mice were homogenized in PBS and pelleted by centrifugation. Host lipids were extracted by washing the homogenates three times with 5 ml methanol. The remaining material was extracted with 4 ml 1:1 chloroform:methanol solution and agitated for 8 hours. The organic extracts were clarified by centrifugation and analyzed by FT-ICR MS.

FT-ICR MS Methods. Total lipids extracted from cells as described above, were resuspended in 2:1 chloroform/methanol solution (lipids extracted from 10 mL of culture were resuspended in 1 mL of 2:1 chloroform/methanol) and introduced into the mass spectrometer at a flow rate of 2 $\mu l\ min^{-1}$ by means of an Apollo (Bruker-Daltonics, Billerica, MA) pneumatically-assisted electrospray source operating in positive or negative ion mode. Mass spectra were acquired on a Bruker-Daltonics Apex II FT-ICR mass spectrometer equipped with a 7 Tesla actively-shielded magnet (Cancilla et al., 2000). After ionization, ions were accumulated in an rf-only external hexapole for 2 s before being transferred to the ICR cell for mass analysis. Tandem mass spectrometry experiments for structural analysis of lipid components were performed as described previously (Mougous et al., 2002). Briefly, sustained off-resonance irradiation collision induced dissociation (SORI-CID) (Gauthier et al., 1991) was applied to the PDIM ions to generate structural data. The ions of interest were isolated by a correlated harmonic excitation field (de Koning et al., 1997) prior to fragmentation. A pulse of argon was introduced into the ultrahigh vacuum region of the ICR cell while the ions were excited 1500Hz above their resonance frequency. Following a delay of 3-5 s, to allow the residual argon to pump away, the fragment ions were excited for detection. Spectra are composed of 512 k data points and are an average of between 20 and 32 scans. The spectra were acquired on the FT-ICR data station, operating Xmass version 6.0 (Bruker-Daltonics). Total abundance of lipid species was calculated by summing the peak intensities as measured by FT-ICR and reported by Xmass. Average mass was calculated as a weighted average using peak intensities as weights.

Microarray analysis. Cells were grown to log phase and RNA was harvested as described (Rodriguez et al., 2002). Briefly, pellets were bead-beat in TRIzol reagent (Invitrogen, Carlsbad, CA), chloroform extracted, and aqueous fractions precipitated overnight in isopropanol. RNA samples were then resuspended in water, DNAse treated, purified by Qiagen RNeasy kit (Qiagen, Valencia, CA), and quantified by O.D.$_{260}$ using a Nanodrop ND-1000 spectrophotometer (Nanodrop Technologies, Wilmington DE) . 5μg of RNA from each sample was random-primed with hexamers and reverse transcribed in the presence of amino-allyl dUTP using SuperScript reverse transcriptase (Invitrogen, Carlsbad, CA) to generate cDNA. Residual RNA was then hydrolyzed by addition of 0.2N NaOH / 0.1M EDTA and incubation at 65° for 15 minutes, followed by neutralization with 0.2N HCl. cDNA samples were purified using Zymo binding columns (Zymo, Orange, CA). Erdman cDNA samples were then conjugated to Cy3, while cDNA samples from mutant strains were conjugated to Cy5 for two out of three experiments. For the third experiment, the dye-conjugation was reversed. Dyeconjugated cDNA samples were competitively hybridized on microarray slides containing oligonucleotide spots representing every gene in *M. tuberculosis* (Qiagen, Valencia, CA). After 2 days of hybridization at 65° C, arrays were washed and scanned using a GenePix 3000B scanner (Axon Instruments, Molecular Devices, Sunnyvale, CA). Data analysis was performed using GenePix Pro 4.1 (Molecular Devices, Sunnyvale, CA) and SpotReader 1.2 (Niles Scientific, Portola Valley, CA). Significance Analysis of Microarray (SAM) was used to detect statistically significant differences in gene transcription between strains (Tusher et al., 2001).

Mouse infections. Bacteria were grown to log phase, washed 1x in PBS, cup-sonicated using a Branson Sonifier 250 at 90% for 15 s, spun for 5 minutes at 40xg to remove clumps and diluted to the desired inoculum in PBS. Bacteria were administered to BALB/C mice via nebulization for 15 minutes using a custom built aerosolization chamber (Mechanical Engineering Shops, University of Wisconsin, Madison). For normal dose infections (Figure 7A-C), an OD_{600} of 0.1 and a total volume of 50 mL was used which resulted in an initial seeding of ~250 bacteria per mouse. For high dose infections with the wild-type Erdman strain (Figure 7D), an OD_{600} of 0.8 was used resulting in an initial seeding of ~1400 bacteria per mouse and an average of $8x10^8$ cfu in the lungs at 19 days. BALB/C mice thus infected with a high dose of *M. tuberculosis* Erdman had severely reduced longevity to about 3 weeks. Organs from infected mice were homogenized and plated for cfu as described (Cox et al., 1999). 4-5 mice were used per timepoint. All mice were housed and treated humanely as described in an animal care protocol approved by UCSF IACUC.

Figure 1. Pathways of SL-1 and PDIM biosynthesis.

(A) The structure of SL_{1278} (Converse et al., 2003; Domenech et al., 2004) and SL-1 as proposed by (Goren, 1970) is shown. The trehalose-2-sulfate (T2S) core is esterified with two hydroxy-phthioceranic groups, one phthioceranic group and a palmitate or stearate. **(B)** The structures of phthiocerol, mycocerosic acids and PDIM are shown. Both pathways are described in the introduction. Pps = phthiocerol synthase; Mas = mycocerosic acid synthase.

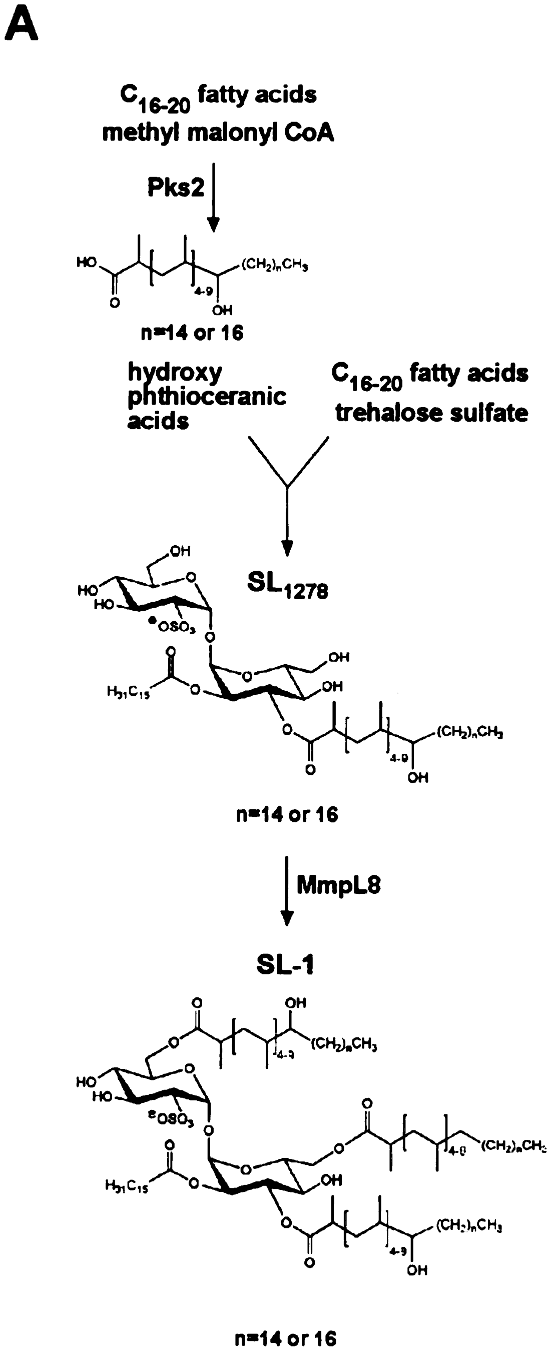
A
C16-20 fatty acids
methyl malonyl CoA
Pks2
n=14 or 16
hydroxy phthioceranic acids
C16-20 fatty acids
trehalose sulfate
SL1278
n=14 or 16
MmpL8
SL-1
n=14 or 16

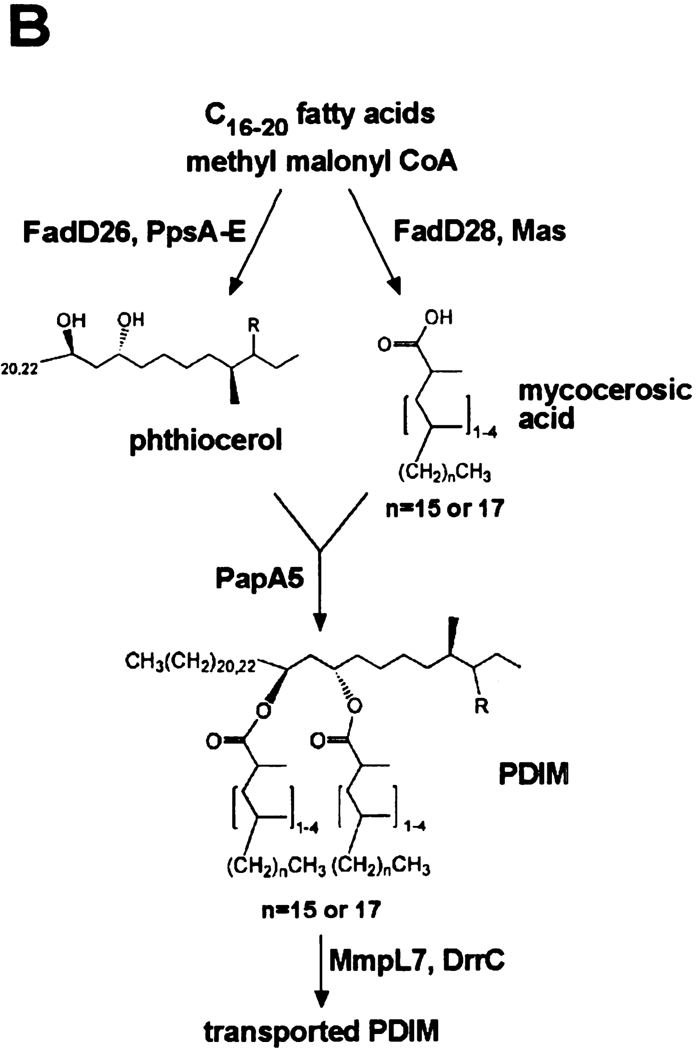
B
C16-20 fatty acids
methyl malonyl CoA
FadD26, PpsA-E
FadD28, Mas
OH
OH
R
CH3(CH2)20,22
phthiocerol
OH
O
1-4
mycocerosic acid
(CH2)nCH3
n=15 or 17
PapA5
CH3(CH2)20,22
O
O
R
O
O
1-4
1-4
PDIM
(CH2)nCH3 (CH2)nCH3
n=15 or 17
MmpL7, DrrC
transported PDIM

Figure 2. Increased abundance and mass of SL-1 in PDIM synthesis mutants.

(A) Crude lipid extracts prepared from *M. tuberculosis* cultures from the indicated strains were analyzed in negative ion mode by FT-ICR MS. SL-1 = sulfolipid-1, PI = phosphatidyl inositol, PIM = phosphatidyl inositol mannoside, Ac = acyl chain. **(B)** The SL-1 regions of the spectra obtained in (A) are shown. SL-1 is observed as a broad set of peaks separated by 14 amu corresponding to differing numbers of CH_2 units. **(C)** Relative SL-1 abundance in the indicated strains was quantified using Xmass 6.0 as the sum of peak intensities of all peaks corresponding to SL-1. **(D)** Average mass of SL-1 in the indicated strains was calculated as the weighted average mass of SL-1 using individual peak intensities as weights. Error bars indicate the standard deviation of the means. Experiments were performed in duplicate and are representative of n>3 experiments.

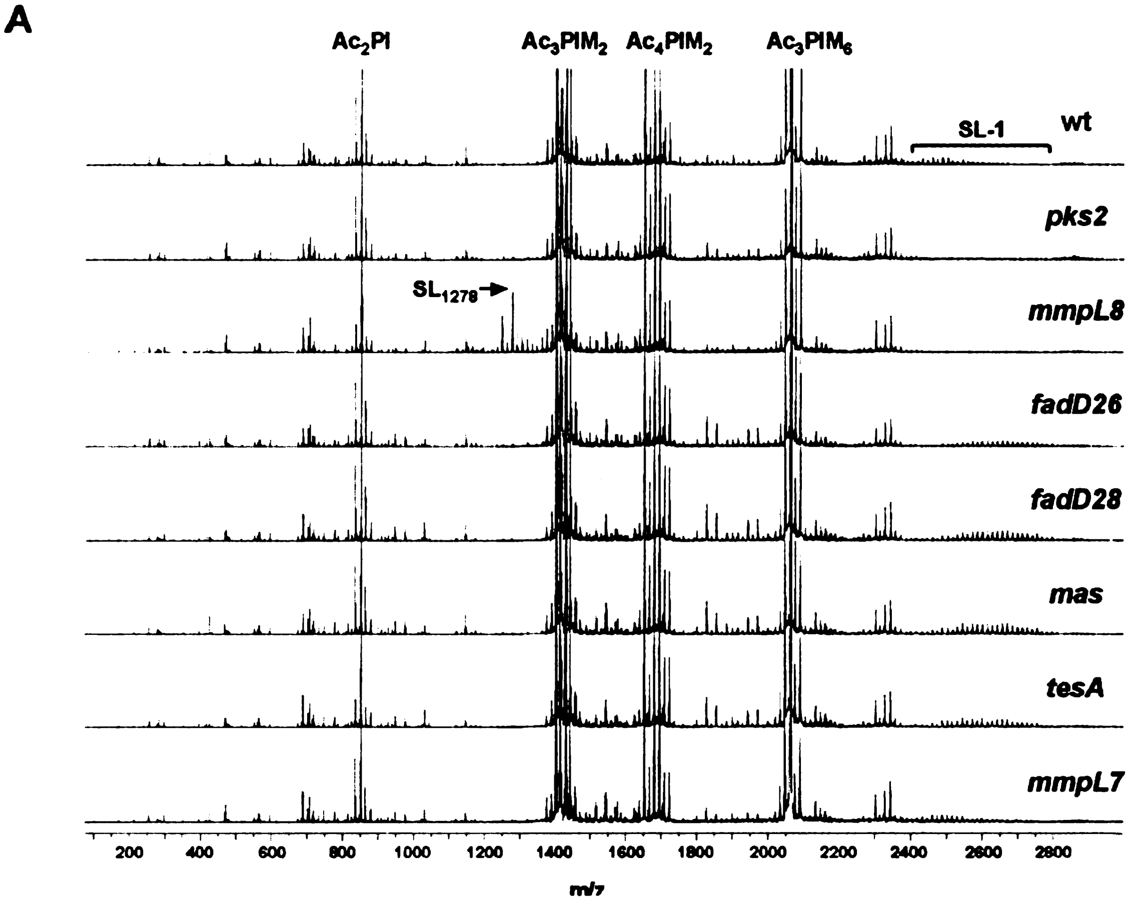
A
Ac2PI
Ac3PIM2
Ac4PIM2
Ac3PIM6
SL-1
wt
pks2
SL1278
mmpL8
fadD26
fadD28
mas
tesA
mmpL7
200
400
600
800
1000
1200
1400
1600
1800
2000
2200
2400
2600
2800
m/z

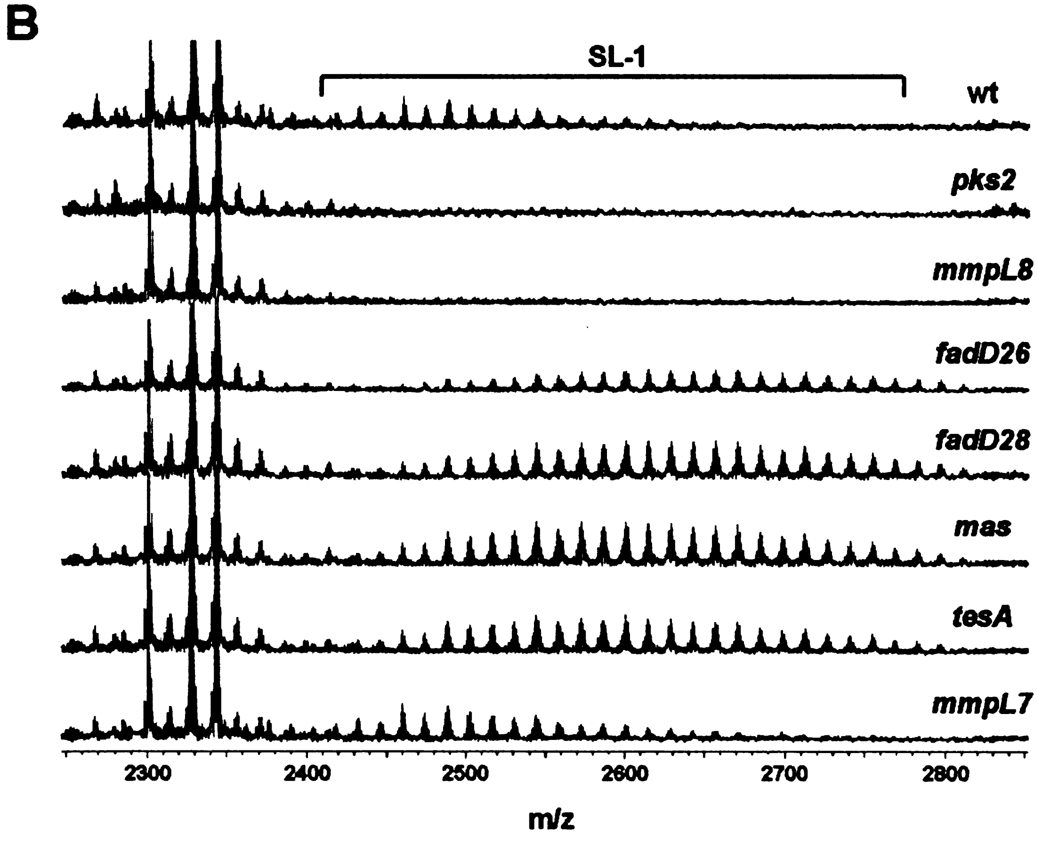
B
SL-1
wt
pks2
mmpL8
fadD26
fadD28
mas
tesA
mmpL7
2300
2400
2500
2600
2700
2800
m/z

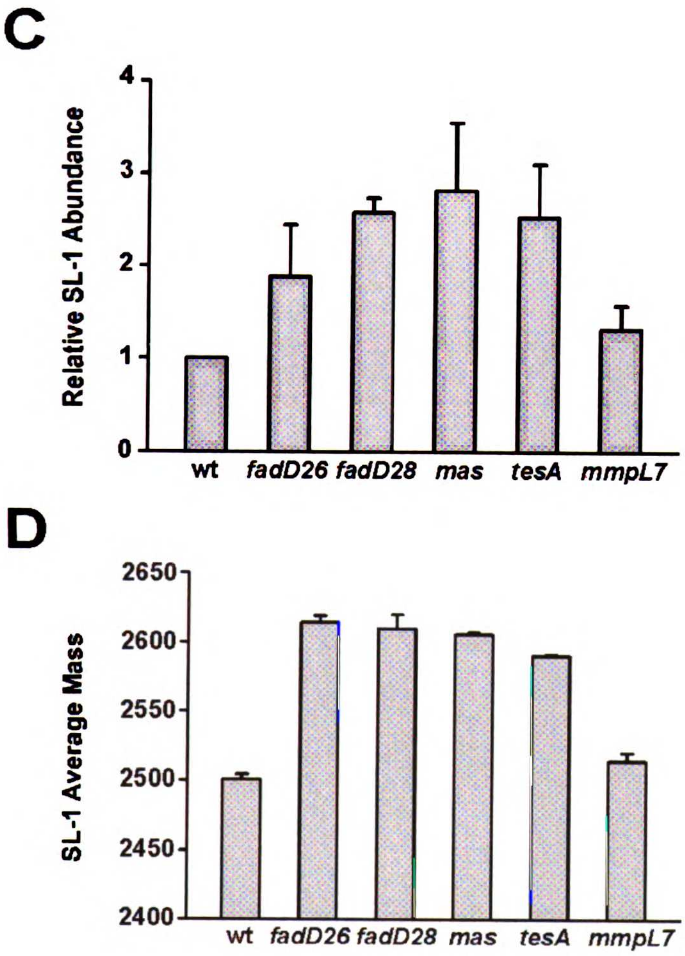
C
Relative SL-1 Abundance
0
1
2
3
4
wt
fadD26
fadD28
mas
tesA
mmpL7
D
SL-1 Average Mass
2400
2450
2500
2550
2600
2650
wt
fadD26
fadD28
mas
tesA
mmpL7

Figure 3. Addition of propionate leads to increased abundance and mass of SL-1.

(A) Increasing concentrations of propionate were added to the indicated *M. tuberculosis* strains over the course of three doublings and SL-1 was monitored using FT-ICR MS. **(B)** Relative SL-1 abundance and **(C)** average mass of SL-1 in wild-type and *mas*$^-$ cultures treated with the indicated amounts of propionate were quantified as in Figure 2C and D respectively.

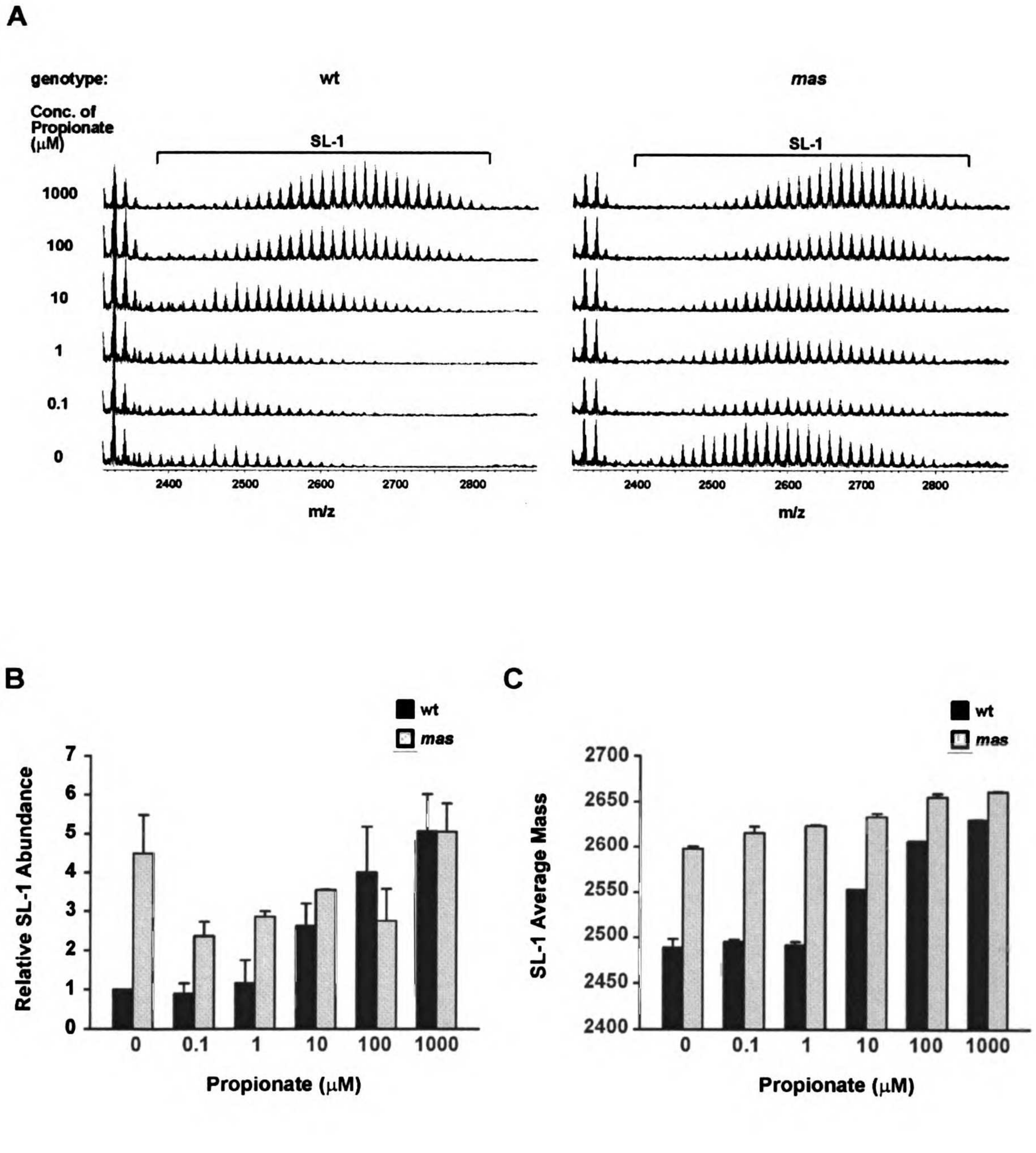
A
genotype:
wt
mas
Conc. of Propionate (μM)
SL-1
SL-1
1000
100
10
1
0.1
0
2400
2500
2600
2700
2800
m/z
2400
2500
2600
2700
2800
m/z
B
wt
mas
Relative SL-1 Abundance
7
6
5
4
3
2
1
0
0
0.1
1
10
100
1000
Propionate (μM)
C
wt
mas
SL-1 Average Mass
2700
2650
2600
2550
2500
2450
2400
0
0.1
1
10
100
1000
Propionate (μM)

Figure 4. Addition of propionate leads to increased abundance and mass of PDIM.

(A) Crude lipid extracts were prepared from the indicated strains of *M. tuberculosis* and PDIM was analyzed by FT-ICR MS in positive mode. PDIM is observed as a broad set of peaks separated by 14 amu corresponding to a variable number of CH_2 units. **(B)** Increasing concentrations of propionate were added to wild-type *M. tuberculosis* as in Figure 3A and PDIM was monitored in crude lipid extracts by FT-ICR MS. **(C)** Relative PDIM abundance and **(D)** average mass of PDIM in wild-type cultures treated with propionate were quantified as in Figure 2C and D respectively.

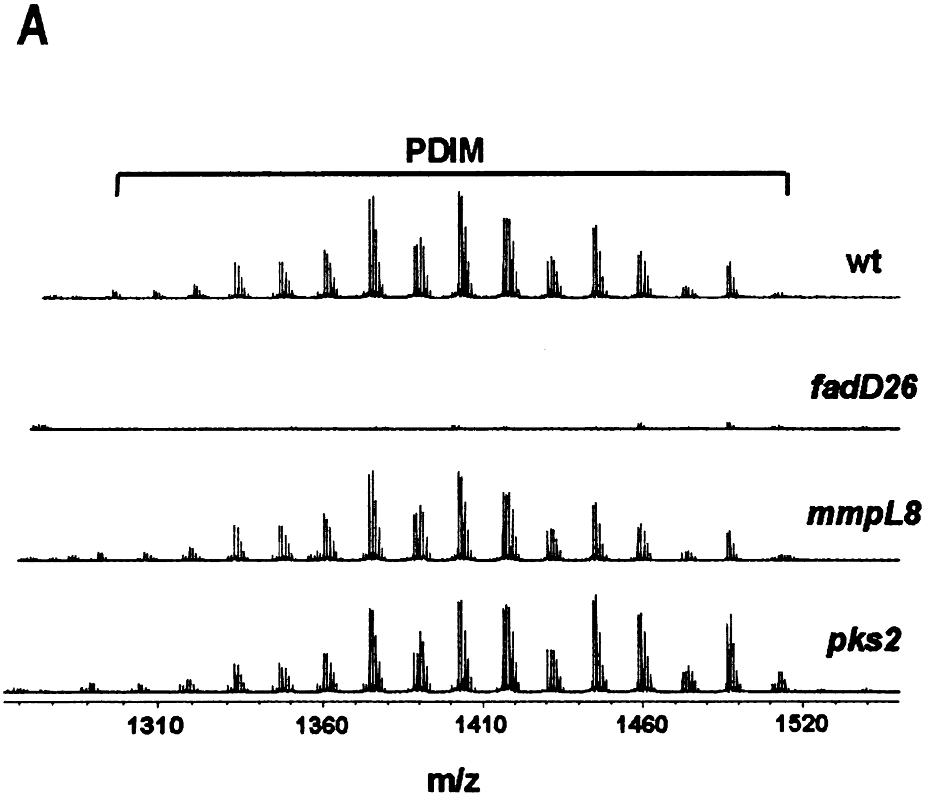
A
PDIM
wt
fadD26
mmpL8
pks2
1310
1360
1410
1460
1520
m/z

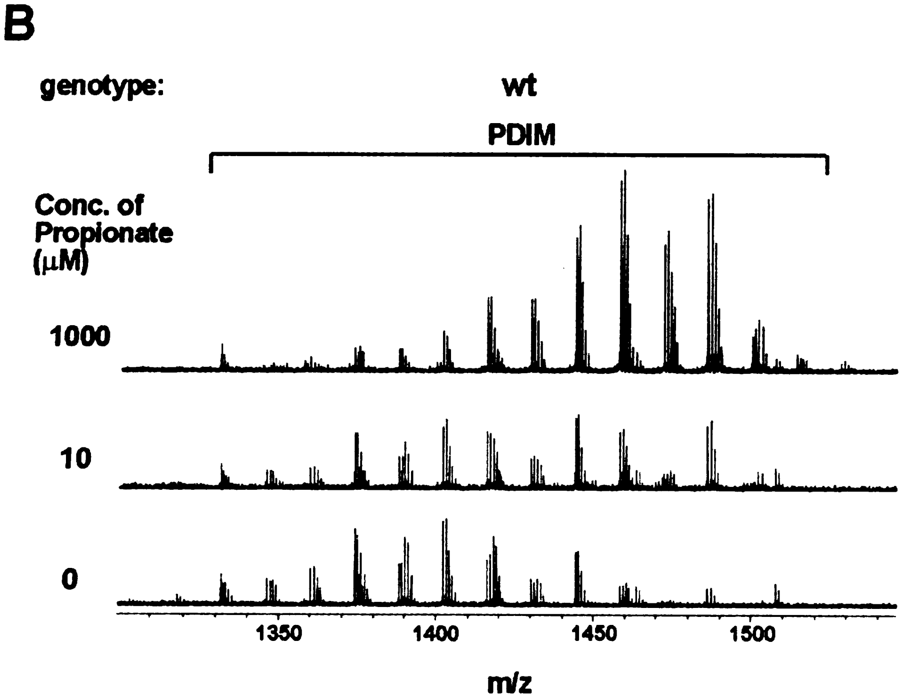
B
genotype:
wt
PDIM
Conc. of Propionate (μM)
1000
10
0
1350
1400
1450
1500
m/z

C

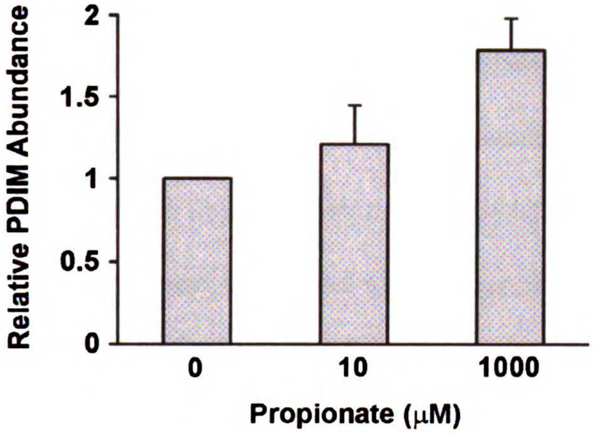
Relative PDIM Abundance
2
1.5
1
0.5
0
0
10
1000
Propionate (μM)

D

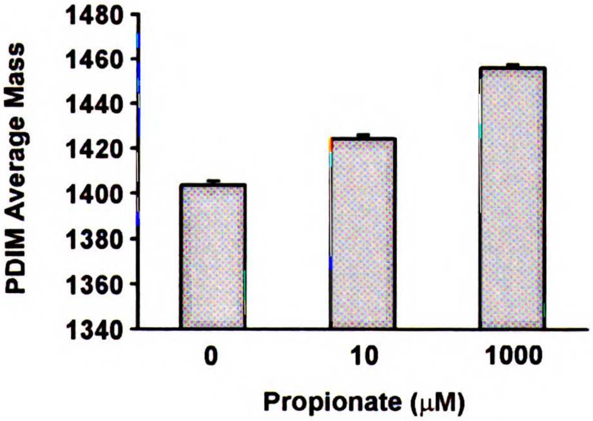
PDIM Average Mass
1480
1460
1440
1420
1400
1380
1360
1340
0
10
1000
Propionate (μM)

Figure 5. Increase in average mass of PDIM is due to the increase in length of mycocerosic acids.

The CID fragmentation patterns of PDIM lipoforms at m/z 1402 (**A**), 1458 (**B**), and 1486 (**C**), are shown. The fragmentation consists of sequential loss of mycocerosic acids from the PDIM moiety resulting in phthiocerol. Two forms of phthiocerol are observed, one at m/z 497.5 and one at m/z 525.5. Structures corresponding to the masses of the lipid fragments are shown and the number of methyl branches is indicated.

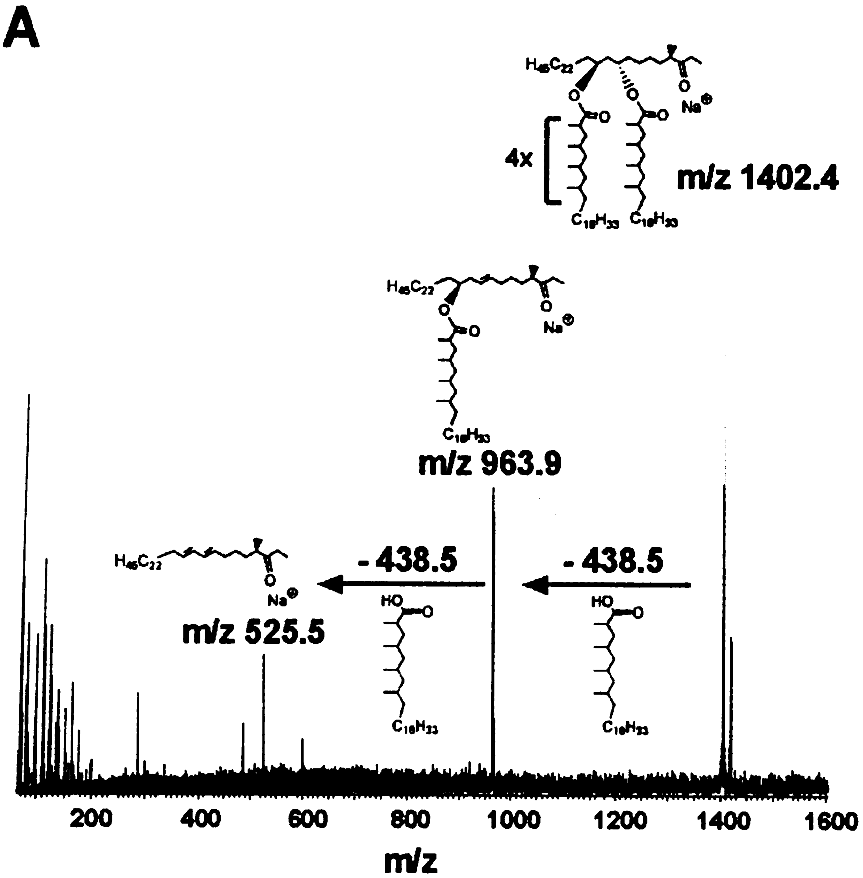
A
H45C22
O
Na⊕
4x
C16H33
m/z 1402.4
m/z 963.9
- 438.5
HO
m/z 525.5
200
400
600
800
1000
1200
1400
1600
m/z

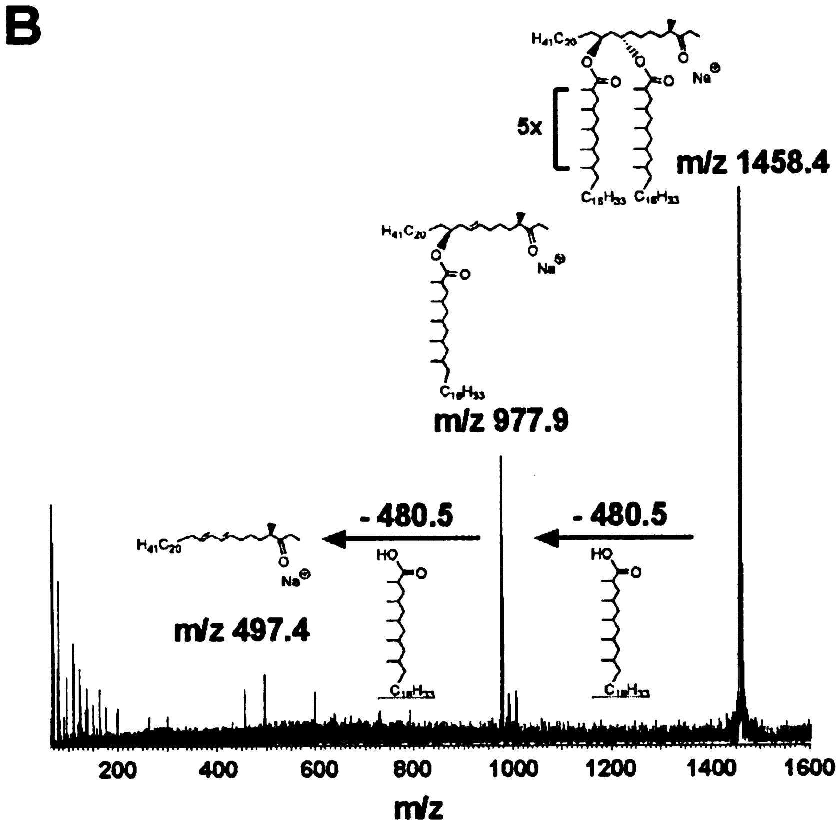
B
H41C20
O
O
Na⊕
5x
C18H33
C18H33
m/z 1458.4
H41C20
O
O
Na⊕
C18H33
m/z 977.9
- 480.5
- 480.5
HO
O
C18H33
HO
O
C18H33
H41C20
O
Na⊕
m/z 497.4
200
400
600
800
1000
1200
1400
1600
m/z

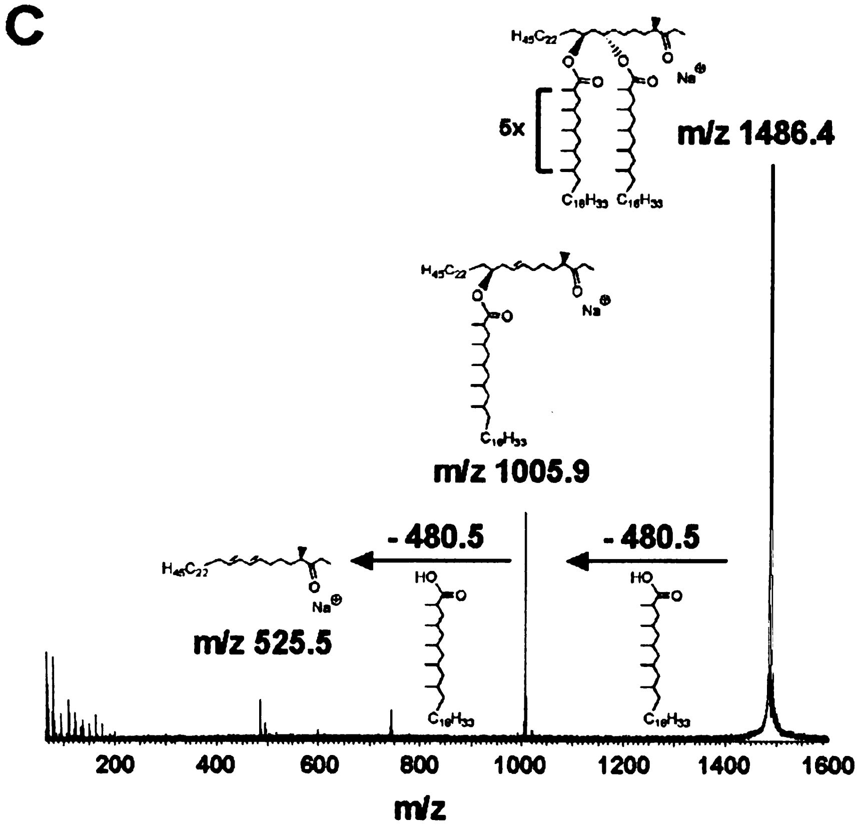C
$H_{45}C_{22}$
O
Na⊕
5x
$C_{16}H_{33}$
m/z 1486.4
m/z 1005.9
- 480.5
- 480.5
HO
m/z 525.5
200
400
600
800
1000
1200
1400
1600
m/z

Figure 6. Over-expression of MutAB leads to changes in PDIM and SL-1 production.

(A) Pathway depicting the production and incorporation of methyl malonyl CoA into PDIM and SL-1 is shown. Methyl malonyl CoA can be synthesized from propionyl CoA or from succinyl CoA via the action of MutAB. **(B)** SL-1 and **(C)** PDIM region of FT-ICR mass spectra of crude extracts from wild-type *M. tuberculosis* containing either the MutAB expression construct or an empty vector as a control is shown. **(D-G)** Relative abundance and average mass of SL-1 and PDIM in the indicated strains were quantified as described in Figure 2C and D.

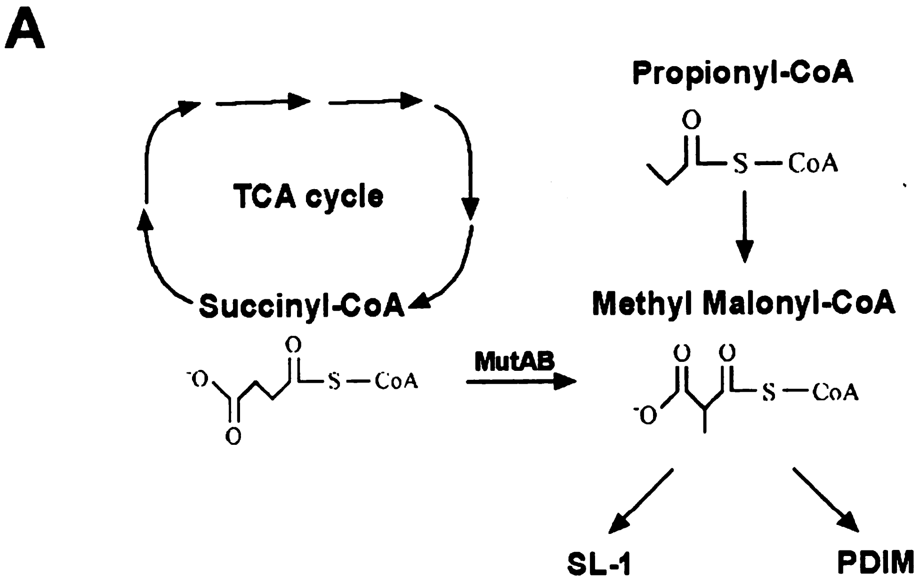
A
TCA cycle
Succinyl-CoA
MutAB
Propionyl-CoA
Methyl Malonyl-CoA
SL-1
PDIM
O
S—CoA
-O

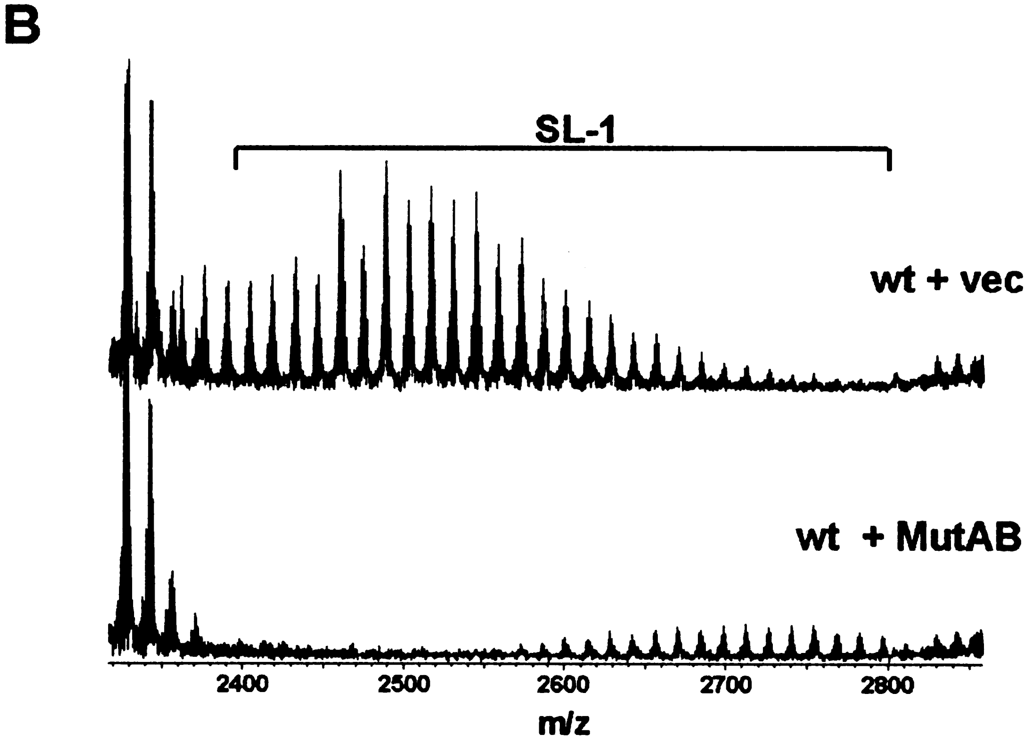
B
SL-1
wt + vec
wt + MutAB
2400
2500
2600
2700
2800
m/z

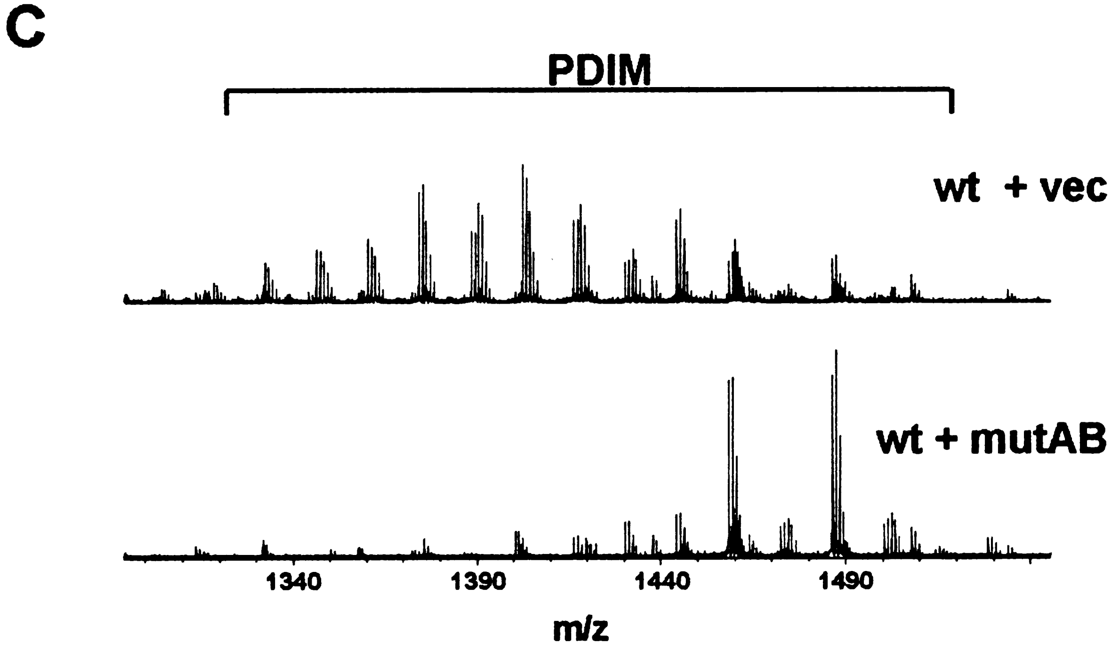
C
PDIM
wt + vec
wt + mutAB
1340
1390
1440
1490
m/z

D

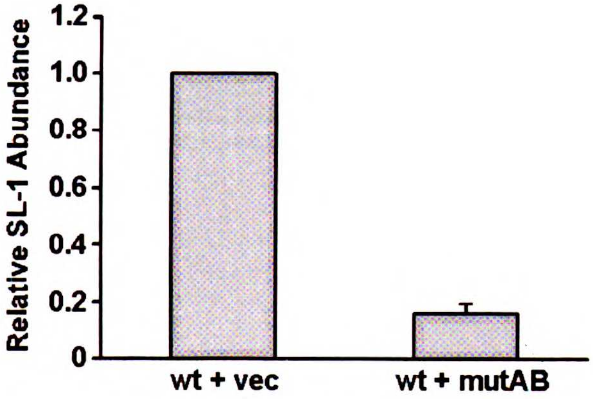
1.2
1.0
0.8
0.6
0.4
0.2
0
Relative SL-1 Abundance
wt + vec
wt + mutAB

E

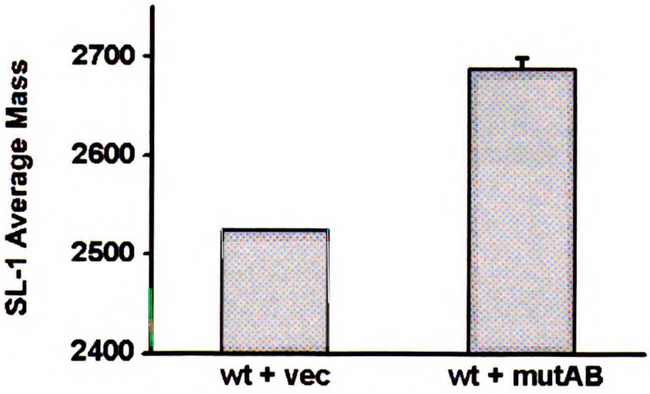
2700
2600
2500
2400
SL-1 Average Mass
wt + vec
wt + mutAB

F

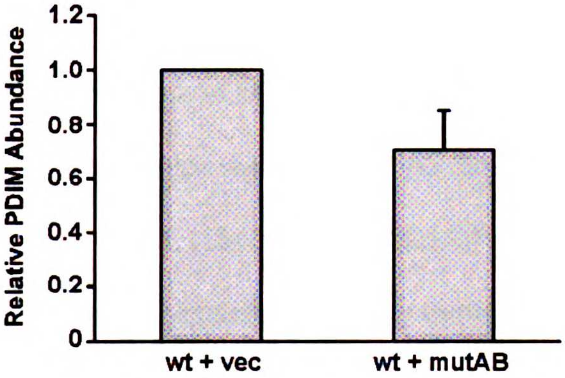
Relative PDIM Abundance
1.2
1.0
0.8
0.6
0.4
0.2
0
wt + vec
wt + mutAB

G

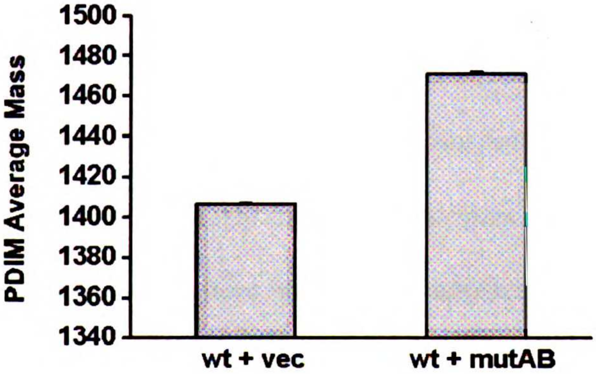
PDIM Average Mass
1500
1480
1460
1440
1420
1400
1380
1360
1340
wt + vec
wt + mutAB

Figure 7. Changes in methyl malonyl CoA regulation lead to attenuated growth in vivo and PDIM is produced in increased mass forms in a mouse model of infection.

(A-C) Over-expression of MutAB leads to attenuated growth in a mouse model of infection. BALB/C mice were infected via the aerosol route with bacteria containing either an empty vector (circles) or the MutAB expression construct (inverted triangles), or *fadD26*$^-$ bacteria containing an empty vector (squares). Growth in the lung (**A**), spleen (**B**), and liver (**C**) was monitored by harvesting organs at the indicated timepoints and plating dilutions on solid media containing kanamycin (open symbols) or without antibiotic (closed symbols). Growth on media without kanamycin revealed the total number of bacteria, while growth on media containing kanamycin revealed the number of bacteria that retained the plasmid. Each data point represents the average colony-forming units (cfu) from 4-5 infected mice and error bars indicate the standard deviation of the means. The data shown here is from one representative experiment of two. **(D)** PDIM is produced in higher mass forms in a mouse model of *M. tuberculosis* infection. BALB/C mice were infected with a high dose (~1400 bacteria) of wild-type *M. tuberculosis* and lungs were harvested 19 days post infection. Bacillary loads in the lung at this timepoint were $8x10^8$ colony-forming units. Lipids were extracted from infected and uninfected lungs and analyzed by FT-ICR MS. The PDIM regions of the mass spectra are shown. The data shown here is from one representative experiment of two. FT-ICR mass spectra from wild-type *M. tuberculosis* cells grown in vitro, with or without propionate, as described in Figure 4B are also shown here for comparison. Average mass of PDIM in vivo is 1430 amu as compared to 1403 amu for cells grown in vitro without propionate and 1456 amu for cells grown in the presence of 1 mM propionate. **(E)** Mortality of mice infected with bacteria containing either an empty vector (filled circles, MJM2) or the MutAB expression construct (open circles, MJM58), or *fadD26*$^-$ bacteria containing an empty vector (inverted triangles, MJM63) as described in (A-C).

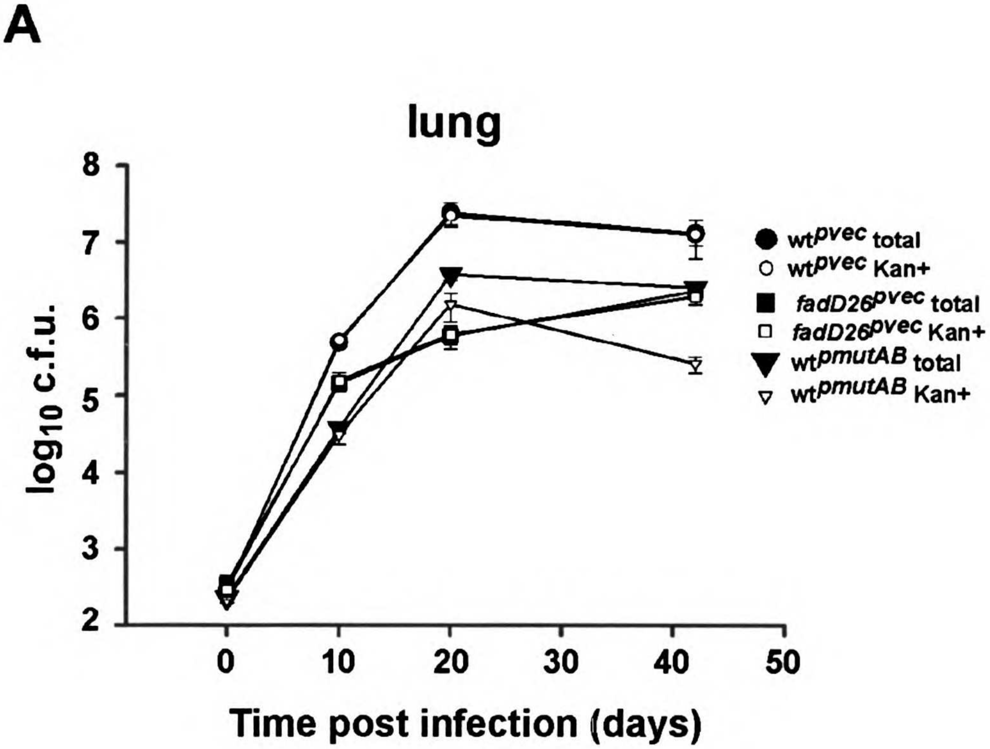
A
lung
8
7
6
5
4
3
2
log10 c.f.u.
0
10
20
30
40
50
Time post infection (days)
● wtpvec total
○ wtpvec Kan+
■ fadD26pvec total
□ fadD26pvec Kan+
▼ wtpmutAB total
▽ wtpmutAB Kan+

B

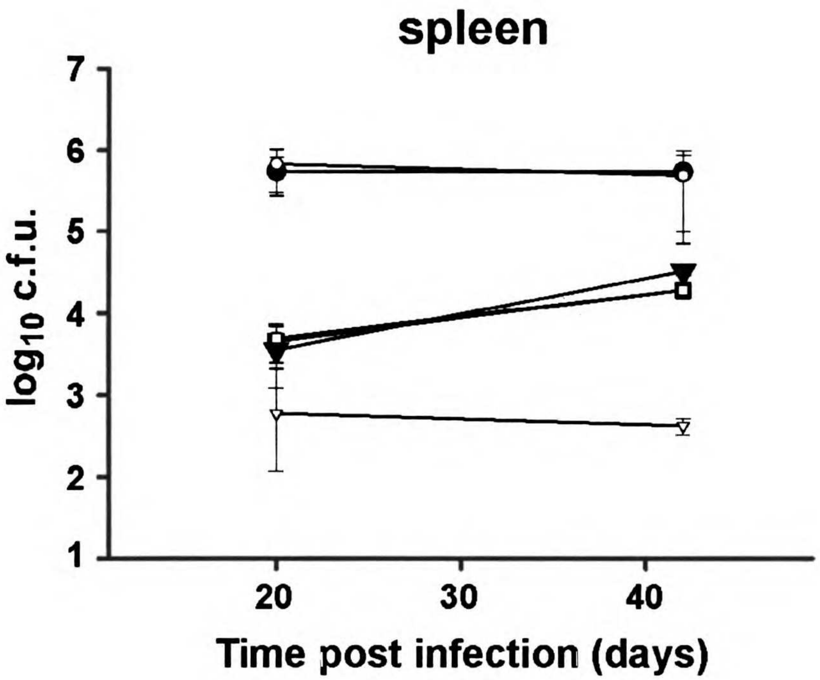

C

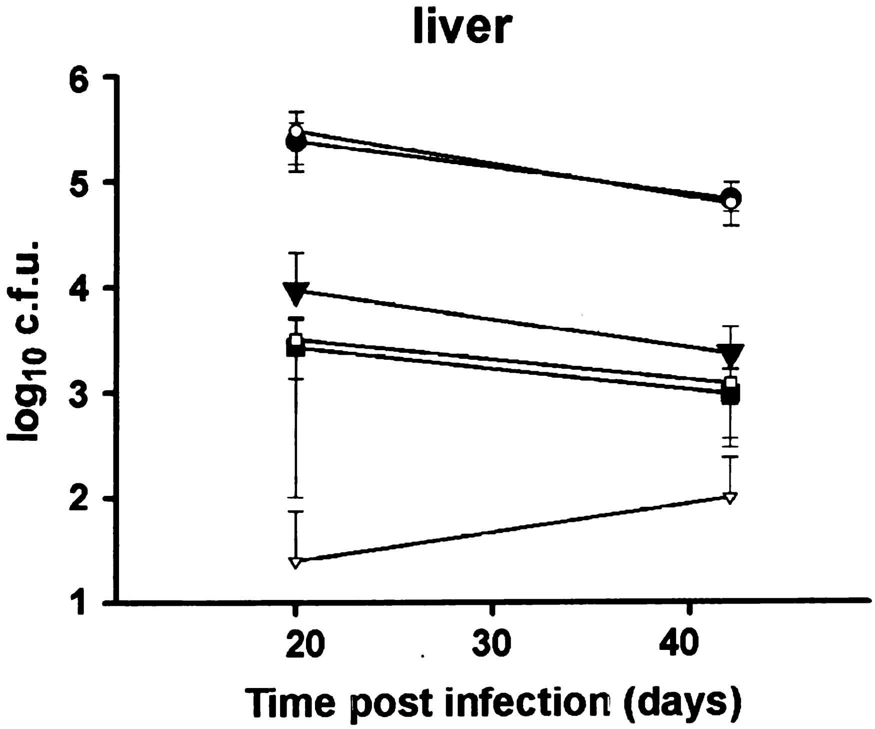

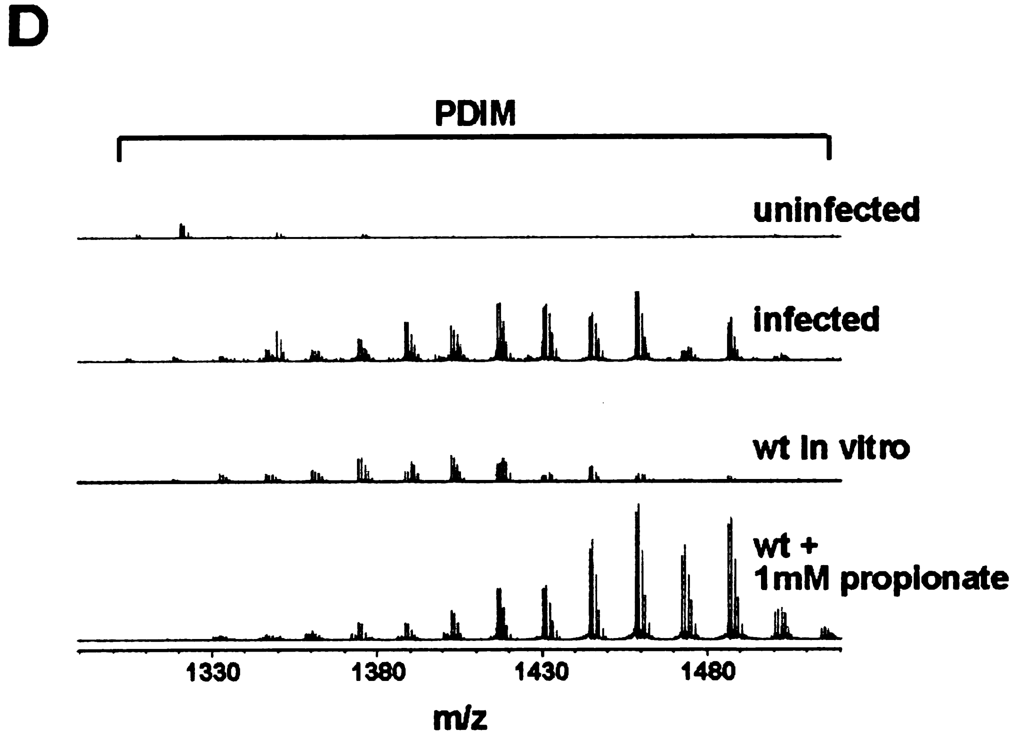
D
PDIM
uninfected
infected
wt in vitro
wt +
1mM propionate
1330
1380
1430
1480
m/z

E

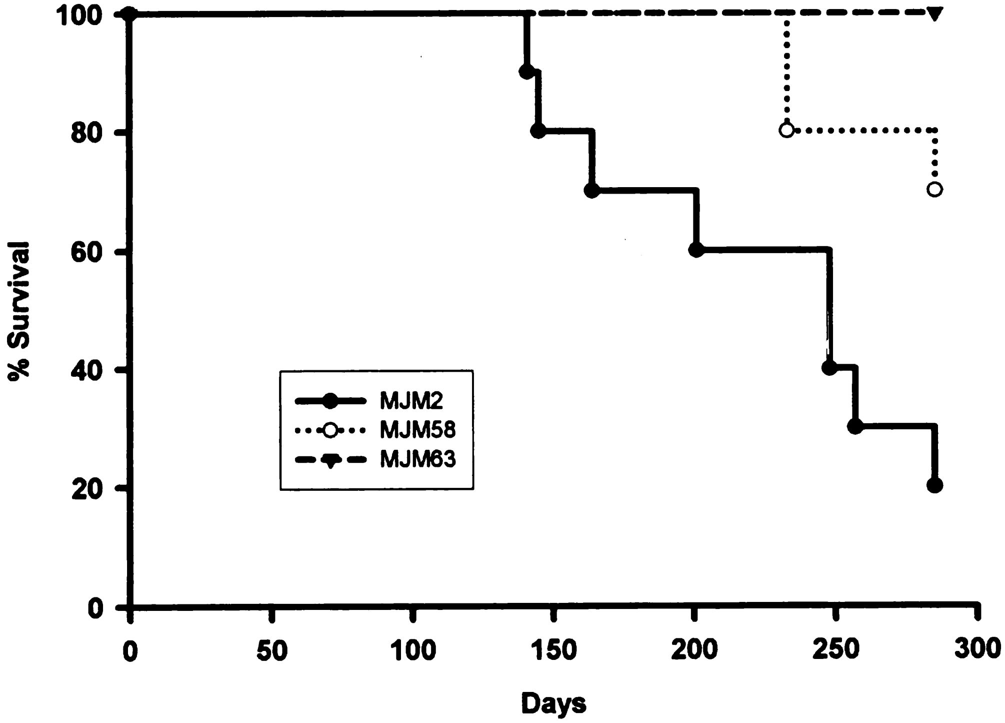
100
80
60
40
20
0
% Survival
0
50
100
150
200
250
300
Days
MJM2
MJM58
MJM63

Figure 8. An SL-1 isotope packet in the FT-ICR mass spectrum obtained from a crude lipid extract of wild-type *M. tuberculosis*.

The peak at m/z 2485 corresponds to the published structure of SL-1 shown in Figure 1 and contains two hydroxy-phthioceranic acids and one phthioceranic acid. The peak at 2487 is a major SL-1 lipoform and is more abundant than would be predicted from the theoretical isotope pattern for SL-1. We propose that the lipoform at m/z 2487 is a mixture of an isotope of the peak at 2485 and an SL-1 lipoform that contains three hydroxy-phthioceranic acids instead of two hydroxy-phthioceranic acids and one phthioceranic acid. The peak at 2487 would also contain one less CH_2 unit than the peak at 2485 resulting in a mass +16 – 14 = 2 amu greater than the peak at 2485.

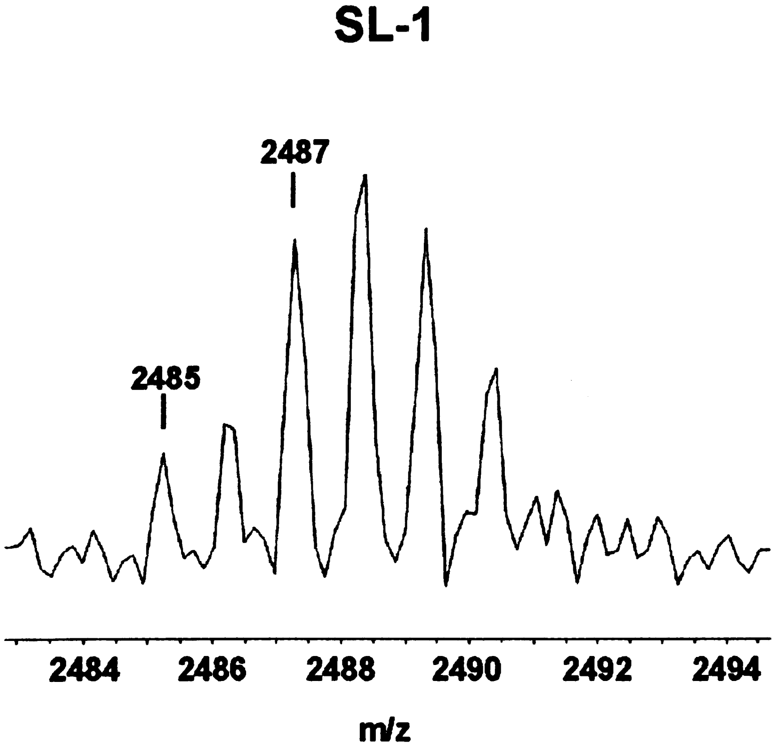
SL-1
2487
2485
2484
2486
2488
2490
2492
2494
m/z

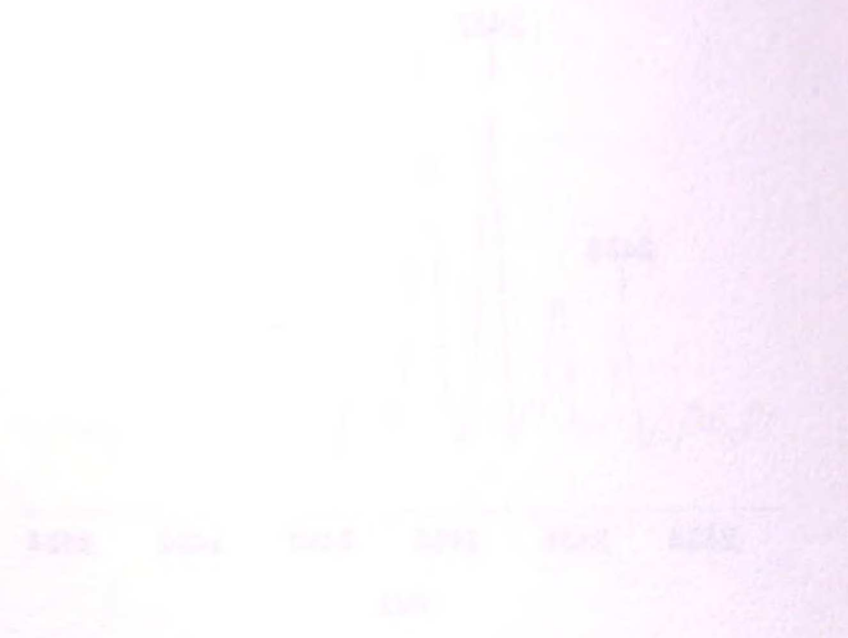

Figure 9. Growth phase dependence of SL-1.

Relative SL-1 abundance was calculated as described in Figure 2C. The experiment was performed in duplicate and is representative of n=3 experiments. Error bars represent standard deviations from the means.

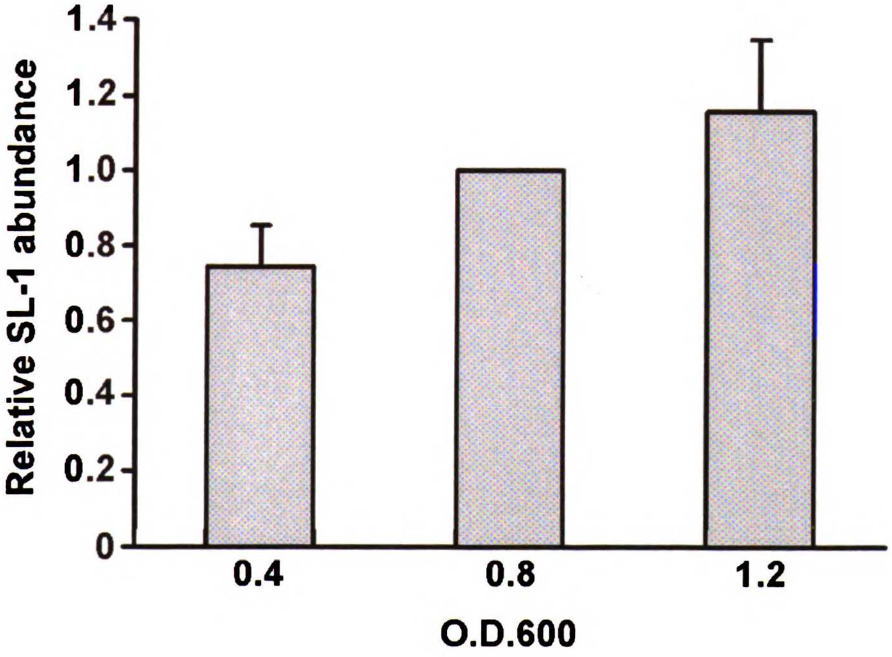
Relative SL-1 abundance
1.4
1.2
1.0
0.8
0.6
0.4
0.2
0
0.4
0.8
1.2
O.D.600

Figure 10. Transcriptional changes do not account for increased SL-1 production in *fadD26⁻* cells.

Wild-type cDNA was conjugated to Cy3 (green) and *fadD26⁻* (**A**) or *pks2⁻* (**B**) cDNA was conjugated to Cy5 (red). The median Cy5 (532 nm) vs. median Cy3 (635 nm) signal for each gene on the microarray in a representative experiment was plotted to generate the scatter plots shown. Genes that were consistently and significantly different across multiple experiments were determined by SAM analysis (Tusher et al., 2001) and are indicated.

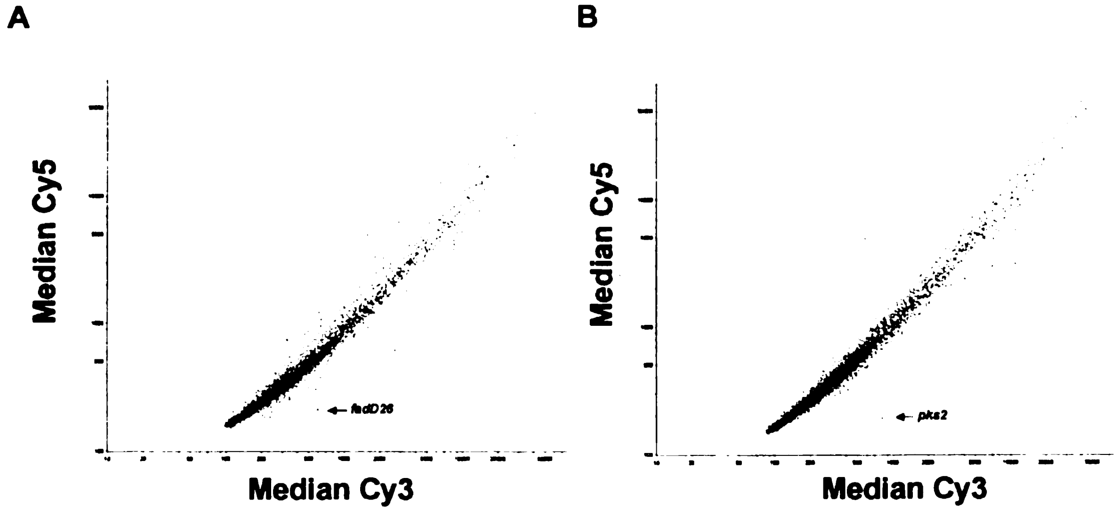
A
Median Cy5
fadD26
Median Cy3
B
Median Cy5
pks2
Median Cy3

Figure 11. Addition of propionate leads to increased abundance and mass of SL_{1278}.

(A) SL_{1278} region of FT-ICR mass spectra of crude extracts from *mmpL8*⁻ cells treated with increasing concentrations of propionate. Propionate was added as described in Figure 3A. **(B)** Relative SL_{1278} abundance and **(C)** average mass of SL_{1278} in *mmpL8*⁻ cells treated with propionate were quantified as in Figure 2C and D respectively.

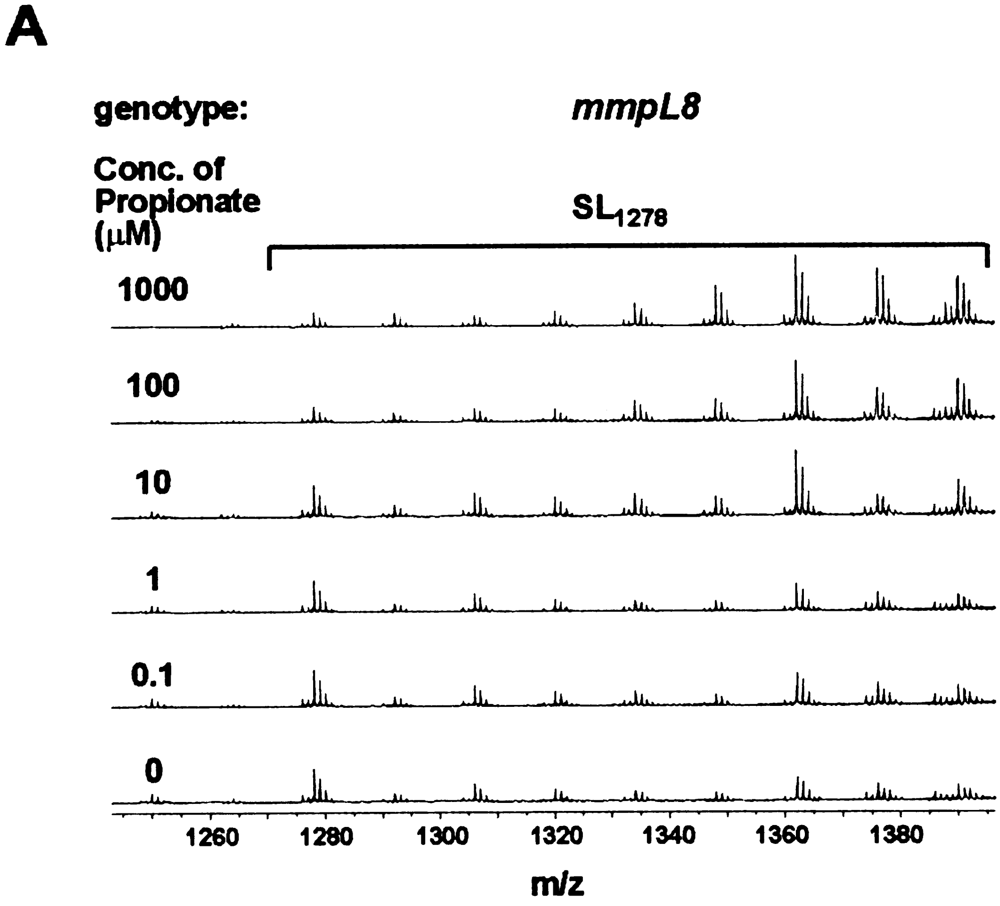
A
genotype:
mmpL8
Conc. of Propionate (μM)
SL1278
1000
100
10
1
0.1
0
1260
1280
1300
1320
1340
1360
1380
m/z

B

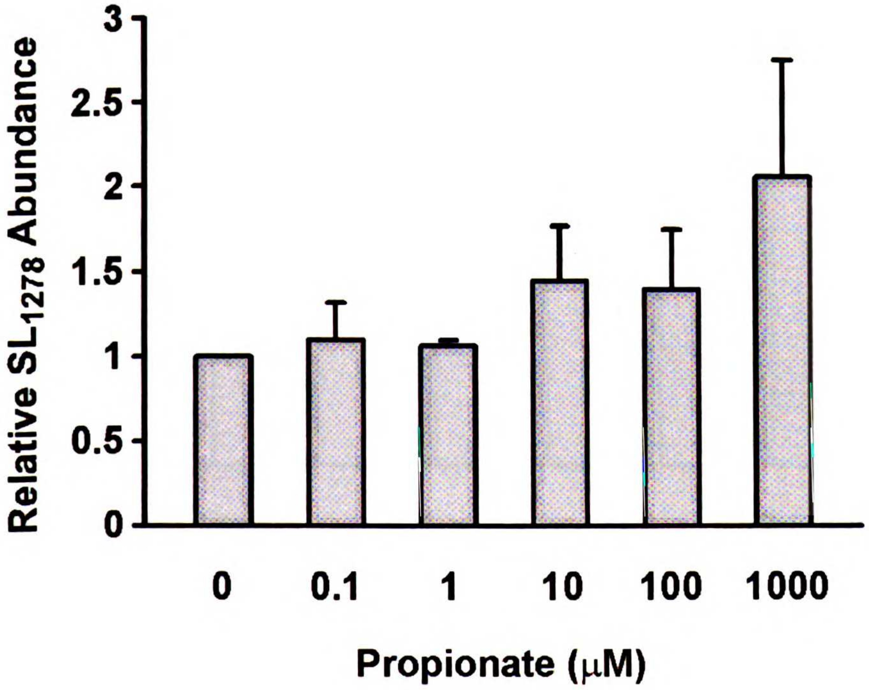
Relative SL_{1278} Abundance
3
2.5
2
1.5
1
0.5
0
0
0.1
1
10
100
1000
Propionate (μM)

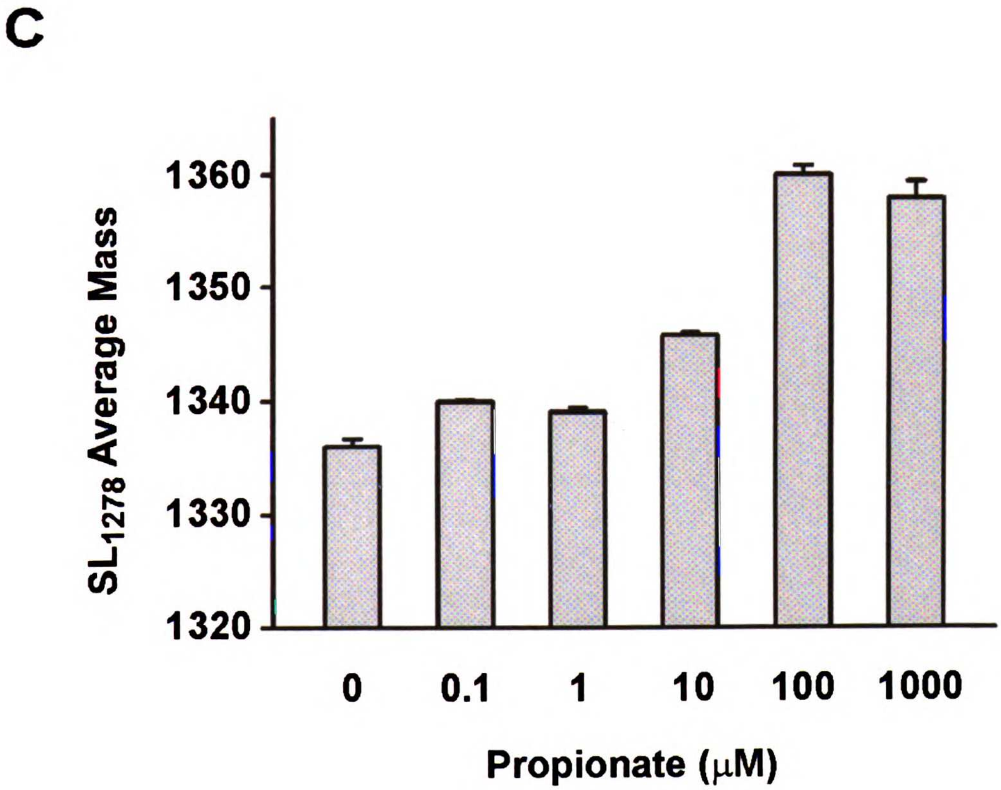
C
SL₁₂₇₈ Average Mass
1360
1350
1340
1330
1320
0
0.1
1
10
100
1000
Propionate (μM)

Figure 12. Growth of *M. tuberculosis* on fatty acids.

(A) PDIM and **(B)** SL-1 region of FT-ICR mass spectra of crude extracts from wild-type cells grown on 0.1% glucose, or 10 mM acetate, propionate, butyrate or valerate as a sole carbon cource. Three contaminating peaks of polyethylene glycol from residual Tween-80 in the sample are marked with an asterisk (*) in the PDIM spectra for cells grown on glucose.

A

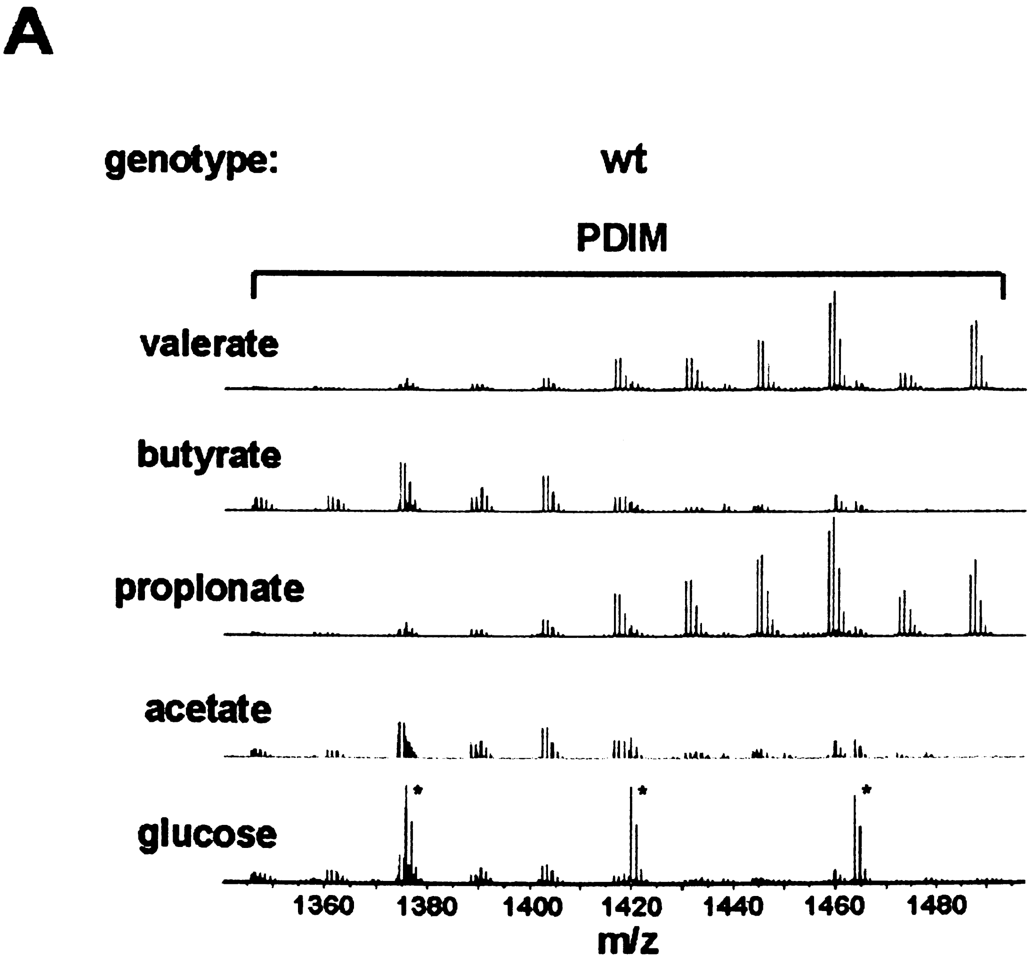
A
genotype:
wt
PDIM
valerate
butyrate
propionate
acetate
glucose
*
*
*
1360
1380
1400
1420
1440
1460
1480
m/z

B

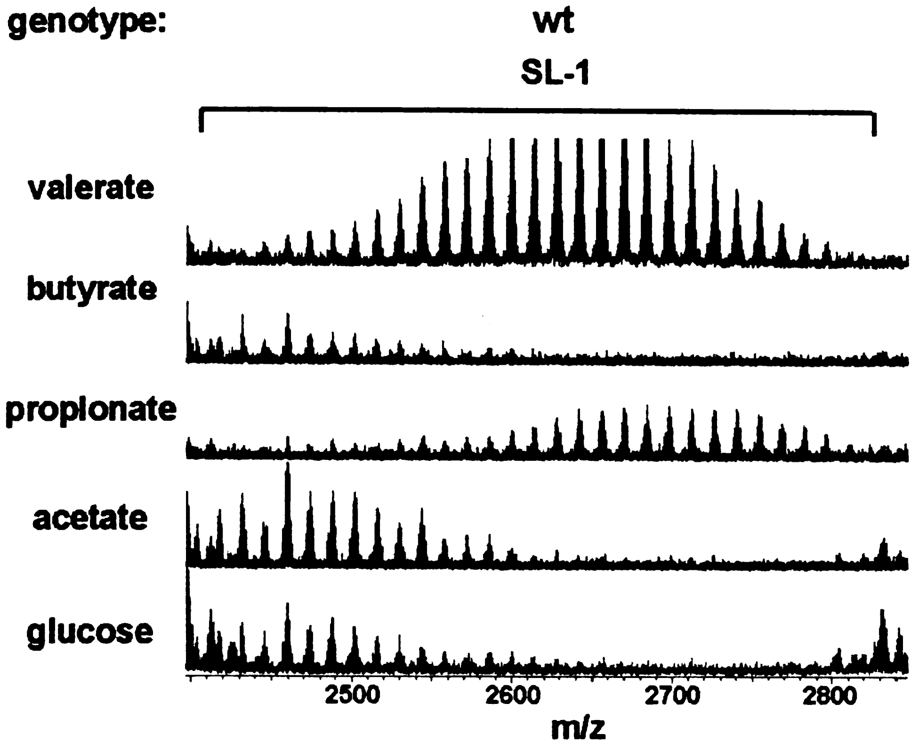
genotype:
wt
SL-1
valerate
butyrate
propionate
acetate
glucose
2500
2600
2700
2800
m/z

Table 1. Strains and Plasmids

Strain or Plasmid	**Genotype/Description**	**Source/ref.**
M. tuberculosis		
Erdman	wild-type	W. R. Jacobs, Jr.
mc^{2}3105	Erdman *fadD26::*Tn*5370*, Hyg^R	(Cox et al., 1999)
mc^{2}3106	Erdman *fadD28::*Tn*5370*, Hyg^R	(Cox et al., 1999)
mc^{2}3107	Erdman *mmpL7::*Tn*5370*, Hyg^R	(Cox et al., 1999)
JCM133	Erdman *mas::*Tn*5370*, Hyg^R	This study
JCM132	Erdman *tesA::*Tn*5370*, Hyg^R	This study
JCM108	Erdman Δ*mmpL8*, Hyg^R	(Converse et al., 2003)
JCM119	Erdman Δ*pks2*, Hyg^R	(Converse et al., 2003)
MJM2	Erdman + pMV261.kan, Kan^R	This study
MJM58	Erdman + pMJ77, Kan^R	This study
MJM63	mc^{2}3105 + pMV261.kan, Kan^R	This study
Plasmids		
pMV261.kan	*oriE*, *oriM*, groEL2 promoter, Kan^R	W. R. Jacobs, Jr.
pMJ77	pMV261.kan + *mutAB*, Kan^R	This study

Chapter 4

Conclusions and Perspectives

The mycobacterial cell wall has long been thought to be important for virulence. Several key structural components including the mycolate layer are crucial for the survival of *M. tuberculosis* in vivo (Brennan and Nikaido, 1995). Surface-exposed lipids associated with the mycobacterial cell wall have also been studied extensively. Over the last several years, the importance of these lipids has been demonstrated rigorously through genetic mutation (Camacho et al., 1999; Converse et al., 2003; Cox et al., 1999). The first part of this thesis describes the coordinate synthesis and secretion of the key lipid virulence factor, PDIM. We show that a domain of the protein MmpL7 interacts with the PDIM biosynthetic enzyme, PpsE. MmpL7 is genetically required for the transport of PDIM, yet appears to participate in synthesis of PDIM by virtue of its interaction with PpsE. To our knowledge, the interaction between MmpL7 and PpsE is the first report of an interaction between a synthase and its cognate transporter. This paradigm is reminiscent of protein secretion where newly synthesized polypeptides are co-translationally translocated across the membrane (Keenan et al., 2001).

MmpL7 is a member of the MmpL family of proteins in *M. tuberculosis*, which are themselves members of the broad class of RND permeases (Tseng et al., 1999). Although most RND family members in gram negative bacteria function as multi-drug efflux pumps, mycobacteria appear to utilize MmpLs as transporters for endogenous lipid substrates. Based on the role of MmpL7 in PDIM transport and the role of MmpL8 in SL-1 biosynthesis (Converse et al., 2003), as well the function of MmpL homologs in other bacteria, it is tempting to speculate that MmpLs may in general be involved in biosynthesis and transport of surface-exposed lipids. However, this remains to be tested and it may well be that other MmpLs will have roles in protein export across the cell

membrane based on the myriad of functions performed by members of the larger RND superfamily (Ma et al., 2002). Although *mmpL* mutants in *M. tuberculosis* do not have increased susceptibility to various drugs tested (Domenech et al., 2005), it is also possible that MmpL family members in other mycobacteria may function as drug efflux pumps.

The mechanism of MmpL function is not clearly understood and whether MmpLs actively participate in the export of lipids across the cell membrane, or act as scaffolds to recruit lipid biosynthetic machinery prior to transport remains to be elucidated. Indeed since MmpLs are required for the transport of specific substrates, MmpLs may function as adapters between their cognate lipid synthases and the transport machinery and not act as transporters at all. The interaction between MmpL7 and PpsE also raises the intriguing possibility that specificity in MmpL transport may be encoded by protein-protein interactions (Jain and Cox, 2005) (Chapter 2). Interestingly, in gram negative bacteria, the specificity for certain substrates in RND family drug efflux pumps is encoded in the two non-transmembrane regions domains 1 and 2 (Figure 1). Domain swaps between the drug efflux pumps AcrB and AcrD in *E. coli* resulted in the switching of their respective drug efflux specificities (Elkins and Nikaido, 2002). Similar experiments with MexB in *Pseudomonas aeruginosa* yielded similar results (Tikhonova et al., 2002). Although preliminary experiments with domain swaps between MmpL7 and MmpL8 yielded non-functional chimeras (Jain and Cox, 2005), it will be interesting to see if these domains contribute to the specificity in MmpL transport.

It is also unclear how energy is provided for the translocation of lipids across the cell membrane. The eukaryotic RND family member, Niemann-Pick C1 (NPC1) has been shown to utilize the proton motive force to translocate cholesterol across the cell

membrane (Davies et al., 2000) and it is widely thought that RND family members use proton antiport or symport as a mechanism of facilitated transport of their substrates. Surprisingly, it has also been shown that an ABC transporter LmrA in *Lactococcus lactis* can catalyze drug transport by a proton symport mechanism even when the ATP hydrolyzing domain is removed (Venter et al., 2003), leading to the hypothesis that LmrA may have evolved from an RND like transporter to an ABC transporter via acquisition of the ATP-hydrolysis domain (Kim et al., 2004). Thus RND transporters may function as passive transporters and export their substrates by facilitated diffusion or be coupled to ABC transporters that provide energy for active translocation across the membrane. Interestingly, the PDIM locus contains an ABC transporter, drrABC, which may use ATP to provide energy for PDIM translocation. DrrC has been shown to be required for PDIM export (Camacho et al., 1999) suggesting perhaps that active transport via ATP hydrolysis is required for PDIM transport.

The mechanism of transport of surface-exposed lipids from the cell membrane to the outer layers of the cell wall is also poorly understood. After translocation across the cell membrane, the lipids need to be transported to the outer layers of the cell wall. This may occur simply through the process of diffusion, or perhaps there exist accessory proteins to aid in the transport of these hydrophobic lipids across the periplasm to the mycolate layer. In gram negative bacteria, transport across the outer membrane is accomplished by outer membrane factors that associate with RND transporters. In fact, the RND drug efflux pump AcrB interacts with an outer membrane factor TolC and the drug substrates are presumably expelled through successive export via AcrB and TolC (Tikhonova and Zgurskaya, 2004; Touze et al., 2004). There exist cell wall porins in

mycobacteria but their function in lipid export remains unexplored. The yeast two-hyrbid analysis presented in Chapter 2 yielded some MmpL7-interaction partners that contain a putative signal sequence. These proteins may interact with MmpLs and participate in the transport of lipids to the outer layers of the cell wall.

One candidate for such a protein is Lppx which is encoded in the PDIM locus and has recently been shown to be required for PDIM export to the cell wall (Sulzenbacher et al., 2006). Lppx is a lipoprotein, has a signal sequence, and is an attractive candidate for a perplasmic or cell wall transporter that shuttles PDIM to the outer layers of the cell wall. Interestingly, Lppx is homologous to the lipoproteins LolA and LolB which are found in the periplasm and the outer membrane respectively of *E. coli*. The Lol system functions to export lipoproteins across the periplasm of *E. coli* to the inner leaflet of the outer membrane (Sulzenbacher et al., 2006). LolCDE bind specifically to lipoproteins destined for the outer membrane and export them across the cell membrane where they bind the periplasmic shuttle LolA. LolA in turn transfers the lipoproteins to LolB which is located in the outer membrane. From LolB the lipoproteins are released to the outer membrane where they remain anchored. Interestingly, Lppx shares a similar beta half barrel structure to LolA and LolB but has a larger substrate binding pocket that could accommodate a PDIM molecule (Sulzenbacher et al., 2006). Thus Lppx may function in a similar manner to export PDIM to the outer layer of the cell wall (Figure 4).

Since many MmpL family members play a role in *M. tuberculosis* virulence, MmpLs may be excellent drug targets. They might be especially tractable drug targets as they reside in the membrane and are likely more accessible to drugs than key lipid synthesis and modification enzymes located inside the cell. However, the role of MmpLs

during the chronic phase of infection is unclear and if MmpLs are not required in the persistent state of mycobacteria, they may not represent a substantial improvement over existing cell wall targets.

In the second part part of this thesis, we employ a powerful mass-spectrometric method to study lipid synthesis and secretion under different conditions. We discovered that the synthesis of virulence lipids PDIM and SL-1 is controlled by the availability of metabolites and that this regulation occurs in vivo during infection. Since *M. tuberculosis* is thought to grow on fatty acids during infection, we propose that the catabolism of odd-chain fatty acids leads to an increase in methyl malonyl CoA, which in turn leads to increased mass of virulence lipids in vivo. These results marry the two fields of host lipid catabolism and virulence polyketide anabolism by *M. tuberculosis* and raise a number of interesting questions about the way in which *M. tuberculosis* adapts to its host.

It is known that *M. tuberculosis* transcriptionally upregulates the genes *icl1* and *icl2* during infection and that these genes are required for the production of succinate via the glyoxylate shunt pathway. While our results show that *M. tuberculosis* metabolically shifts the production of PDIM and SL-1 to increased mass forms only during growth on odd-chain fatty acids but not on even-chain fatty acids in culture (Chapter 3), it is still possible that, in vivo, increased flux through the citric acid cycle and upregulation of Icl1 and Icl2 leads to an increase in methyl malonyl CoA via the action of MutAB and thus contributes to the increased mass PDIM and SL-1 observed in vivo. It will be interesting to test both mutants in the *icl* genes as well as Icl over-expressing cells for PDIM and SL-1 production. Furthermore, in addition to the post-transcriptional metabolic control we describe for PDIM and SL-1 synthesis, upregulation of MutAB genes in vivo could also

result in increased mass PDIM and SL-1. Finally, propionate released from the catabolism of odd chain fatty acids can also be assimilated into the citric acid cycle via the methyl citrate cycle. A recent study showed that the methyl citrate cycle is dispensable for *M. tuberculosis* virulence in mice and proposed that methyl-branched polyketide production may act as a sink to buffer the increased concentration of propionate in the absence of this pathway in vivo (Munoz-Elias et al., 2006). This idea could be easily tested by monitoring PDIM and SL-1 production in the existing methyl citrate cycle mutants.

A complete understanding of the flux of various metabolites through the different metabolic pathways in *M. tuberculosis* during infection awaits elucidation of the exact in vivo environment in the host. What are the concentrations of the various metabolites in vivo? What is the distribution of fatty acids catabolized by *M. tuberculosis* during infection? And, finally, how does the availability of these metabolites influence the virulence lipid profile? With FT-ICR MS, we can begin to answer these questions by monitoring host lipids in infected tissue. This method also has limitless potential in understanding the host-pathogen biology of *M. tuberculosis*, as it permits the study of TB lipid production in different environments and in different host genetic backgrounds.

References

Alexander, D. C., Jones, J. R., Tan, T., Chen, J. M., and Liu, J. (2004). PimF, a mannosyltransferase of mycobacteria, is involved in the biosynthesis of phosphatidylinositol mannosides and lipoarabinomannan. J Biol Chem *279*, 18824-18833.

Azad, A. K., Sirakova, T. D., Fernandes, N. D., and Kolattukudy, P. E. (1997). Gene knockout reveals a novel gene cluster for the synthesis of a class of cell wall lipids unique to pathogenic mycobacteria. Journal of Biological Chemistry *272*, 16741-16745.

Azad, A. K., Sirakova, T. D., Rogers, L. M., and Kolattukudy, P. E. (1996). Targeted replacement of the mycocerosic acid synthase gene in Mycobacterium bovis BCG produces a mutant that lacks mycosides. Proc Natl Acad Sci U S A *93*, 4787-4792.

Banerjee, A., Dubnau, E., Quemard, A., Balasubramanian, V., Um, K. S., Wilson, T., Collins, D., de Lisle, G., and Jacobs, W. R., Jr. (1994). inhA, a gene encoding a target for isoniazid and ethionamide in Mycobacterium tuberculosis. Science *263*, 227-230.

Bennett, M. A., Shern, J. F., and Kahn, R. A. (2004). Reverse two-hybrid techniques in the yeast Saccharomyces cerevisiae. Methods Mol Biol *261*, 313-326.

Bligh, E. G., and Dyer, W. J. (1959). A rapid method of total lipid extraction and purification. Can J Biochem Physiol *37*, 911-917.

Brennan, P. J., and Nikaido, H. (1995). The envelope of mycobacteria. Annual Review of Biochemistry *64*, 29-63.

Bystrykh, L. V., Fernandez-Moreno, M. A., Herrema, J. K., Malpartida, F., Hopwood, D. A., and Dijkhuizen, L. (1996). Production of actinorhodin-related "blue pigments" by Streptomyces coelicolor A3(2). J Bacteriol *178*, 2238-2244.

Camacho, L. R., Constant, P., Raynaud, C., Laneelle, M. A., Triccas, J. A., Gicquel, B., Daffe, M., and Guilhot, C. (2001). Analysis of the phthiocerol dimycocerosate locus of Mycobacterium tuberculosis. Evidence that this lipid is involved in the cell wall permeability barrier. J Biol Chem *276*, 19845-19854.

Camacho, L. R., Ensergueix, D., Perez, E., Gicquel, B., and Guilhot, C. (1999). Identification of a virulence gene cluster of Mycobacterium tuberculosis by signature-tagged transposon mutagenesis. Mol Microbiol *34*, 257-267.

Cancilla, M. T., Gaucher, S. P., Desaire, H., and Leary, J. A. (2000). Combined partial acid hydrolysis and electrospray ionization-mass spectrometry for the structural determination of oligosaccharides. Anal Chem *72*, 2901-2907.

Chan, J., Fan, X. D., Hunter, S. W., Brennan, P. J., and Bloom, B. R. (1991). Lipoarabinomannan, a possible virulence factor involved in persistence of Mycobacterium tuberculosis within macrophages. Infection & Immunity *59*, 1755-1761.

Cole, S. T., Brosch, R., Parkhill, J., Garnier, T., Churcher, C., Harris, D., Gordon, S. V., Eiglmeier, K., Gas, S., Barry, C. E., 3rd, *et al.* (1998). Deciphering the biology of Mycobacterium tuberculosis from the complete genome sequence [see comments]. Nature *393*, 537-544.

[illegible]

[illegible]

[illegible]

[illegible] and [illegible] for Development and [illegible]

[illegible] involved in [illegible] Infection & Immunity 67, [illegible]

[illegible] Deciphering the biology of [illegible] from the complete genome sequence [illegible]

Nature [illegible]

Converse, S. E., and Cox, J. S. (2005). A protein secretion pathway critical for Mycobacterium tuberculosis virulence is conserved and functional in Mycobacterium smegmatis. J Bacteriol *187*, 1238-1245.

Converse, S. E., Mougous, J. D., Leavell, M. D., Leary, J. A., Bertozzi, C. R., and Cox, J. S. (2003). MmpL8 is required for sulfolipid-1 biosynthesis and Mycobacterium tuberculosis virulence. Proc Natl Acad Sci U S A *100*, 6121-6126.

Cox, J. S., Chen, B., McNeil, M., and Jacobs, W. R., Jr. (1999). Complex lipid determines tissue-specific replication of Mycobacterium tuberculosis in mice. Nature *402*, 79-83.

Davies, J. P., Chen, F. W., and Ioannou, Y. A. (2000). Transmembrane molecular pump activity of Niemann-Pick C1 protein. Science *290*, 2295-2298.

Dayem, L. C., Carney, J. R., Santi, D. V., Pfeifer, B. A., Khosla, C., and Kealey, J. T. (2002). Metabolic engineering of a methylmalonyl-CoA mutase-epimerase pathway for complex polyketide biosynthesis in Escherichia coli. Biochemistry *41*, 5193-5201.

de Koning, L. J., Nibbering, N. M. M., van Orden, S. L., and Laukien, F. H. (1997). Mass selection of ions in a Fourier transform ion cyclotron resonance trap using correlated harmonic excitation fields (CHEF). Int J Mass Spectrom Ion Proc *165*, 209-219.

de la Salle, H., Mariotti, S., Angenieux, C., Gilleron, M., Garcia-Alles, L. F., Malm, D., Berg, T., Paoletti, S., Maitre, B., Mourey, L., *et al.* (2005). Assistance of microbial glycolipid antigen processing by CD1e. Science *310*, 1321-1324.

Coronado, [illegible] Pond [illegible] A. [illegible]
lipoprotein [illegible]
[illegible] J. Biochem [illegible]

Cornwall, G. [illegible]
[illegible]
[illegible]

Dan, A. S., Chen, H., [illegible]
[illegible]
263, 79-85

Chacko, J. R., Chen, J. W., and [illegible] using
[illegible]

Davis, L. C., [illegible], J. E., [illegible] and [illegible], J.
(2001). [illegible] pathway for
[illegible] Biochemistry 41, 4195-4202

de Koning, L. J., [illegible] (1999). [illegible]
[illegible]
[illegible]

de la [illegible], R., [illegible], S., [illegible], C., [illegible], M., [illegible], L. F., [illegible], D.,
[illegible], P., [illegible], S., [illegible], H., [illegible], L., et al. (1998). [illegible]
[illegible] (CD) [illegible] 1321-1328

Domenech, P., Reed, M. B., and Barry, C. E., 3rd (2005). Contribution of the Mycobacterium tuberculosis MmpL protein family to virulence and drug resistance. Infect Immun *73*, 3492-3501.

Domenech, P., Reed, M. B., Dowd, C. S., Manca, C., Kaplan, G., and Barry, C. E., 3rd (2004). The role of MmpL8 in sulfatide biogenesis and virulence of Mycobacterium tuberculosis. J Biol Chem *279*, 21257-21265.

Dubnau, E., Chan, J., Mohan, V. P., and Smith, I. (2005). Responses of Mycobacterium tuberculosis to growth in the mouse lung. Infect Immun *73*, 3754-3757.

Elkins, C. A., and Nikaido, H. (2002). Substrate specificity of the RND-type multidrug efflux pumps AcrB and AcrD of Escherichia coli is determined predominantly by two large periplasmic loops. J Bacteriol *184*, 6490-6498.

Gauthier, J. W., Trautman, T. R., and Jacobson, D. B. (1991). Sustained off-resonance irradiation for collision-activated dissociation involving Fourier transform mass spectrometry. Collision-activated dissociation technique that emulates infrared multiphoton dissociation. Anal Chim Acta *246*, 211-225.

Gilleron, M., Stenger, S., Mazorra, Z., Wittke, F., Mariotti, S., Bohmer, G., Prandi, J., Mori, L., Puzo, G., and De Libero, G. (2004). Diacylated sulfoglycolipids are novel mycobacterial antigens stimulating CD1-restricted T cells during infection with Mycobacterium tuberculosis. J Exp Med *199*, 649-659.

Glickman, M. S., Cox, J. S., and Jacobs, W. R., Jr. (2000). A novel mycolic acid cyclopropane synthetase is required for coding, persistence, and virulence of Mycobacterium tuberculosis. Mol Cell *5*, 717-727.

Glickman, M. S., and Jacobs, W. R., Jr. (2001). Microbial pathogenesis of Mycobacterium tuberculosis: dawn of a discipline. Cell *104*, 477-485.

Golemis, E., Serebriiskii, I., Finley, R. L. J., Kolonin, M. G., Gyuris, J., and Brent, R. (1999). Interaction trap/two-hybrid system to identify interacting proteins, In Current Protocols in Molecular Biology, F. M. Ausubel, R. Brent, R. E. Kingston, D. D. Moore, J. G. Seidman, J. A. Smith, and K. Struhl, eds. (New York: John Wiley & Sons).

Goren, M. B. (1970). Sulfolipid I of Mycobacterium tuberculosis, strain H37Rv. II. Structural studies. Biochim Biophys Acta *210*, 127-138.

Goren, M. B., Brokl, O., and Das, B. C. (1976). Sulfatides of Mycobacterium tuberculosis: the structure of the principal sulfatide (SL-I). Biochemistry *15*, 2728-2735.

Goren, M. B., Brokl, O., Das, B. C., and Lederer, E. (1971). Sulfolipid I of Mycobacterium tuberculosis, strain H37RV. Nature of the acyl substituents. Biochemistry *10*, 72-81.

Goren, M. B., Brokl, O., and Schaefer, W. B. (1974). Lipids of putative relevance to virulence in Mycobacterium tuberculosis: correlation of virulence with elaboration of sulfatides and strongly acidic lipids. Infect Immun *9*, 142-149.

Goren, M. B., Brokl, O., and Schaefer, W. B. (1974). Lipids of putative relevance to virulence in Mycobacterium tuberculosis: phthiocerol dimycocerosate and the attenuation indicator lipid. Infection & Immunity *9*, 150-158.

Graham, J. E., and Clark-Curtiss, J. E. (1999). Identification of Mycobacterium tuberculosis RNAs synthesized in response to phagocytosis by human macrophages by selective capture of transcribed sequences (SCOTS). Proc Natl Acad Sci U S A *96*, 11554-11559.

Guarente, L., and Ptashne, M. (1981). Fusion of Escherichia coli lacZ to the cytochrome c gene of Saccharomyces cerevisiae. Proc Natl Acad Sci U S A *78*, 2199-2203.

Honer Zu Bentrup, K., Miczak, A., Swenson, D. L., and Russell, D. G. (1999). Characterization of activity and expression of isocitrate lyase in Mycobacterium avium and Mycobacterium tuberculosis. J Bacteriol *181*, 7161-7167.

Jain, M., and Cox, J. S. (2005). Interaction between Polyketide Synthase and Transporter Suggests Coupled Synthesis and Export of Virulence Lipid in M. tuberculosis. PLoS Pathog *1*, e2.

Keenan, R. J., Freymann, D. M., Stroud, R. M., and Walter, P. (2001). The signal recognition particle. Annu Rev Biochem *70*, 755-775.

Kim, S. H., Chang, A. B., and Saier, M. H., Jr. (2004). Sequence similarity between multidrug resistance efflux pumps of the ABC and RND superfamilies. Microbiology *150*, 2493-2495.

Kolattukudy, P. E., Fernandes, N. D., Azad, A. K., Fitzmaurice, A. M., and Sirakova, T. D. (1997). Biochemistry and molecular genetics of cell-wall lipid biosynthesis in mycobacteria. Molecular Microbiology *24*, 263-270.

Ma, Y., Erkner, A., Gong, R., Yao, S., Taipale, J., Basler, K., and Beachy, P. A. (2002). Hedgehog-mediated patterning of the mammalian embryo requires transporter-like function of dispatched. Cell *111*, 63-75.

Makinoshima, H., and Glickman, M. S. (2005). Regulation of Mycobacterium tuberculosis cell envelope composition and virulence by intramembrane proteolysis. Nature *436*, 406-409.

Marshall, A. G., Hendrickson, C. L., and Jackson, G. S. (1998). Fourier transform ion cyclotron resonance mass spectrometry: a primer. Mass Spectrom Rev *17*, 1-35.

McKinney, J. D., Honer zu Bentrup, K., Munoz-Elias, E. J., Miczak, A., Chen, B., Chan, W. T., Swenson, D., Sacchettini, J. C., Jacobs, W. R., Jr., and Russell, D. G. (2000). Persistence of Mycobacterium tuberculosis in macrophages and mice requires the glyoxylate shunt enzyme isocitrate lyase [see comments]. Nature *406*, 735-738.

McKinney, J. D., Jacobs, J., W.R., and Bloom, B. R. (1998). Persisting Problems in Tuberculosis, In Emerging Infections, A. Fauci, and R. Krause, eds. (London: Academic Press), pp. 51-146.

Minnikin, D. E., Kremer, L., Dover, L. G., and Besra, G. S. (2002). The methyl-branched fortifications of Mycobacterium tuberculosis. Chem Biol *9*, 545-553.

Moody, D. B., Guy, M. R., Grant, E., Cheng, T. Y., Brenner, M. B., Besra, G. S., and Porcelli, S. A. (2000). CD1b-mediated T cell recognition of a glycolipid antigen generated from mycobacterial lipid and host carbohydrate during infection. J Exp Med *192*, 965-976.

Moody, D. B., Ulrichs, T., Muhlecker, W., Young, D. C., Gurcha, S. S., Grant, E., Rosat, J. P., Brenner, M. B., Costello, C. E., Besra, G. S., and Porcelli, S. A. (2000). CD1c-mediated T-cell recognition of isoprenoid glycolipids in Mycobacterium tuberculosis infection. Nature *404*, 884-888.

Mougous, J. D., Leavell, M. D., Senaratne, R. H., Leigh, C. D., Williams, S. J., Riley, L. W., Leary, J. A., and Bertozzi, C. R. (2002). Discovery of sulfated metabolites in mycobacteria with a genetic and mass spectrometric approach. Proc Natl Acad Sci U S A *13*, 13.

Munoz-Elias, E. J., and McKinney, J. D. (2005). Mycobacterium tuberculosis isocitrate lyases 1 and 2 are jointly required for in vivo growth and virulence. Nat Med *11*, 638-644.

Munoz-Elias, E. J., and McKinney, J. D. (2006). Carbon metabolism of intracellular bacteria. Cell Microbiol *8*, 10-22.

Munoz-Elias, E. J., Upton, A. M., Cherian, J., and McKinney, J. D. (2006). Role of the methylcitrate cycle in Mycobacterium tuberculosis metabolism, intracellular growth, and virulence. Mol Microbiol *60*, 1109-1122.

Murakami, S., Nakashima, R., Yamashita, E., and Yamaguchi, A. (2002). Crystal structure of bacterial multidrug efflux transporter AcrB. Nature *419*, 587-593.

Ng, V., Zanazzi, G., Timpl, R., Talts, J. F., Salzer, J. L., Brennan, P. J., and Rambukkana, A. (2000). Role of the cell wall phenolic glycolipid-1 in the peripheral nerve predilection of Mycobacterium leprae. Cell *103*, 511-524.

Nigou, J., Gilleron, M., and Puzo, G. (2003). Lipoarabinomannans: from structure to biosynthesis. Biochimie *85*, 153-166.

Noll, H. (1957). The chemistry of some native constituents of the purified wax of Mycobacterium tuberculosis. J Biol Chem *224*, 149-164.

Ogata, H., Goto, S., Sato, K., Fujibuchi, W., Bono, H., and Kanehisa, M. (1999). KEGG: Kyoto Encyclopedia of Genes and Genomes. Nucleic Acids Res *27*, 29-34. http://www.genome.jp/kegg/pathway/map/map00640.html.

Onwueme, K. C., Ferreras, J. A., Buglino, J., Lima, C. D., and Quadri, L. E. (2004). Mycobacterial polyketide-associated proteins are acyltransferases: proof of principle with Mycobacterium tuberculosis PapA5. Proc Natl Acad Sci U S A *101*, 4608-4613.

Rainwater, D. L., and Kolattukudy, P. E. (1985). Fatty acid biosynthesis in Mycobacterium tuberculosis var. bovis Bacillus Calmette-Guerin. Purification and characterization of a novel fatty acid synthase, mycocerosic acid synthase, which elongates n-fatty acyl-CoA with methylmalonyl-CoA. Journal of Biological Chemistry *260*, 616-623.

Rao, V., Fujiwara, N., Porcelli, S. A., and Glickman, M. S. (2005). Mycobacterium tuberculosis controls host innate immune activation through cyclopropane modification of a glycolipid effector molecule. J Exp Med *201*, 535-543.

Reed, M. B., Domenech, P., Manca, C., Su, H., Barczak, A. K., Kreiswirth, B. N., Kaplan, G., and Barry, C. E., 3rd (2004). A glycolipid of hypervirulent tuberculosis strains that inhibits the innate immune response. Nature *431*, 84-87.

Rodriguez, G. M., Voskuil, M. I., Gold, B., Schoolnik, G. K., and Smith, I. (2002). ideR, An essential gene in mycobacterium tuberculosis: role of IdeR in iron-dependent gene expression, iron metabolism, and oxidative stress response. Infect Immun *70*, 3371-3381.

Rousseau, C., Sirakova, T. D., Dubey, V. S., Bordat, Y., Kolattukudy, P. E., Gicquel, B., and Jackson, M. (2003). Virulence attenuation of two Mas-like polyketide synthase mutants of Mycobacterium tuberculosis. Microbiology *149*, 1837-1847.

Rousseau, C., Winter, N., Pivert, E., Bordat, Y., Neyrolles, O., Ave, P., Huerre, M., Gicquel, B., and Jackson, M. (2004). Production of phthiocerol dimycocerosates protects Mycobacterium tuberculosis from the cidal activity of reactive nitrogen intermediates produced by macrophages and modulates the early immune response to infection. Cell Microbiol *6*, 277-287.

Saier, M. H., Jr. (2003). Tracing pathways of transport protein evolution. Mol Microbiol *48*, 1145-1156.

Schnappinger, D., Ehrt, S., Voskuil, M. I., Liu, Y., Mangan, J. A., Monahan, I. M., Dolganov, G., Efron, B., Butcher, P. D., Nathan, C., and Schoolnik, G. K. (2003).

Transcriptional Adaptation of Mycobacterium tuberculosis within Macrophages: Insights into the Phagosomal Environment. J Exp Med *198*, 693-704.

Seal, R. P., and Amara, S. G. (1998). A reentrant loop domain in the glutamate carrier EAAT1 participates in substrate binding and translocation. Neuron *21*, 1487-1498.

Segal, W., and Bloch, H. (1956). Biochemical differentiation of Mycobacterium tuberculosis grown in vivo and in vitro. J Bacteriol *72*, 132-141.

Sirakova, T. D., Dubey, V. S., Cynamon, M. H., and Kolattukudy, P. E. (2003). Attenuation of Mycobacterium tuberculosis by disruption of a mas-like gene or a chalcone synthase-like gene, which causes deficiency in dimycocerosyl phthiocerol synthesis. J Bacteriol *185*, 2999-3008.

Sirakova, T. D., Dubey, V. S., Kim, H. J., Cynamon, M. H., and Kolattukudy, P. E. (2003). The largest open reading frame (pks12) in the Mycobacterium tuberculosis genome is involved in pathogenesis and dimycocerosyl phthiocerol synthesis. Infect Immun *71*, 3794-3801.

Sirakova, T. D., Thirumala, A. K., Dubey, V. S., Sprecher, H., and Kolattukudy, P. E. (2001). The Mycobacterium tuberculosis pks2 gene encodes the synthase for the hepta- and octamethyl-branched fatty acids required for sulfolipid synthesis. J Biol Chem *276*, 16833-16839.

Stanley, S. A., Raghavan, S., Hwang, W. W., and Cox, J. S. (2003). Acute infection and macrophage subversion by Mycobacterium tuberculosis requires a novel specialized secretion system. Proc Natl Acad Sci USA *100*, 13001-13006.

Sturgill-Koszycki, S., Haddix, P. L., and Russell, D. G. (1997). The interaction between Mycobacterium and the macrophage analyzed by two-dimensional polyacrylamide gel electrophoresis. Electrophoresis *18*, 2558-2565.

Sulzenbacher, G., Canaan, S., Bordat, Y., Neyrolles, O., Stadthagen, G., Roig-Zamboni, V., Rauzier, J., Maurin, D., Laval, F., Daffe, M., *et al.* (2006). LppX is a lipoprotein required for the translocation of phthiocerol dimycocerosates to the surface of Mycobacterium tuberculosis. Embo J *25*, 1436-1444.

Tikhonova, E. B., Wang, Q., and Zgurskaya, H. I. (2002). Chimeric analysis of the multicomponent multidrug efflux transporters from gram-negative bacteria. J Bacteriol *184*, 6499-6507.

Tikhonova, E. B., and Zgurskaya, H. I. (2004). AcrA, AcrB, and TolC of Escherichia coli Form a Stable Intermembrane Multidrug Efflux Complex. J Biol Chem *279*, 32116-32124.

Timm, J., Post, F. A., Bekker, L. G., Walther, G. B., Wainwright, H. C., Manganelli, R., Chan, W. T., Tsenova, L., Gold, B., Smith, I., *et al.* (2003). Differential expression of iron-, carbon-, and oxygen-responsive mycobacterial genes in the lungs of chronically infected mice and tuberculosis patients. Proc Natl Acad Sci U S A *100*, 14321-14326.

Touze, T., Eswaran, J., Bokma, E., Koronakis, E., Hughes, C., and Koronakis, V. (2004). Interactions underlying assembly of the Escherichia coli AcrAB-TolC multidrug efflux system. Mol Microbiol *53*, 697-706.

Trivedi, O. A., Arora, P., Sridharan, V., Tickoo, R., Mohanty, D., and Gokhale, R. S. (2004). Enzymic activation and transfer of fatty acids as acyl-adenylates in mycobacteria. Nature *428*, 441-445.

Trivedi, O. A., Arora, P., Vats, A., Ansari, M. Z., Tickoo, R., Sridharan, V., Mohanty, D., and Gokhale, R. S. (2005). Dissecting the mechanism and assembly of a complex virulence mycobacterial lipid. Mol Cell *17*, 631-643.

Tseng, T. T., Gratwick, K. S., Kollman, J., Park, D., Nies, D. H., Goffeau, A., and Saier, M. H., Jr. (1999). The RND permease superfamily: an ancient, ubiquitous and diverse family that includes human disease and development proteins. J Mol Microbiol Biotechnol *1*, 107-125.

Tusher, V. G., Tibshirani, R., and Chu, G. (2001). Significance analysis of microarrays applied to the ionizing radiation response. Proc Natl Acad Sci U S A *98*, 5116-5121.

Venter, H., Shilling, R. A., Velamakanni, S., Balakrishnan, L., and Van Veen, H. W. (2003). An ABC transporter with a secondary-active multidrug translocator domain. Nature *426*, 866-870.

Yu, E. W., McDermott, G., Zgurskaya, H. I., Nikaido, H., and Koshland, D. E., Jr. (2003). Structural basis of multiple drug-binding capacity of the AcrB multidrug efflux pump. Science *300*, 976-980.

Trivedi, O. A., Arora, P., Sridharan, V., Tickoo, R., Mohanty, D., and Gokhale, R. S. (2004). Enzymic activation and transfer of fatty acids as acyl-adenylates in mycobacteria. Nature *428*, 441-445.

Trivedi, O. A., Arora, P., Vats, A., Ansari, M. Z., Tickoo, R., Sridharan, V., Mohanty, D., and Gokhale, R. S. (2005). Dissecting the mechanism and assembly of a complex virulence mycobacterial lipid. Mol Cell *17*, 631-643.

Tseng, T. T., Gratwick, K. S., Kollman, J., Park, D., Nies, D. H., Goffeau, A., and Saier, M. H., Jr. (1999). The RND permease superfamily: an ancient, ubiquitous and diverse family that includes human disease and development proteins. J Mol Microbiol Biotechnol *1*, 107-125.

Tusher, V. G., Tibshirani, R., and Chu, G. (2001). Significance analysis of microarrays applied to the ionizing radiation response. Proc Natl Acad Sci U S A *98*, 5116-5121.

Venter, H., Shilling, R. A., Velamakanni, S., Balakrishnan, L., and Van Veen, H. W. (2003). An ABC transporter with a secondary-active multidrug translocator domain. Nature *426*, 866-870.

Yu, E. W., McDermott, G., Zgurskaya, H. I., Nikaido, H., and Koshland, D. E., Jr. (2003). Structural basis of multiple drug-binding capacity of the AcrB multidrug efflux pump. Science *300*, 976-980.

[illegible] Turrell, G. A., Avise [illegible]
[illegible] (2004). Glucose [illegible]
[illegible] Nature 408, 651–655.

[illegible] Trivedi, O. [illegible]
[illegible] and Gotham, R. R. (2000). [illegible]
[illegible] synthetic [illegible]

[illegible] Twigg, T. T., [illegible]
[illegible] M. H., [illegible] (2000). [illegible]
[illegible] family for [illegible]
[illegible] Biotechnol. [illegible]

Tsuda, V. O., [illegible] approaches,
Applied to the [illegible] USA 96, 3111–3116.

Venter, H., Shilling, R. A., [illegible] and Van Veen, H. W.
(2003). An ABC [illegible] multidrug translocator domain.
Nature 426, 866–870.

Yu, E. W., McDermott, G., Zgurskaya, H. I., Nikaido, H., and Koshland, D. E., Jr.
(2003). Structural basis of multiple drug-binding capacity of the AcrB multidrug efflux
pump. Science 300, 976–980.

6942 R

UCSF LIBRARY

UC
San Francisco
LIBRARY
UNIVERSITY OF CALIFORNIA

7541090
3 1378 00754 1090

UC
San Francisco
LIBRARY